UNIVERSITÀ DEGLI STUDI DI CATANIA
Dipartimento di fisica e astronomia
Dottorato di Ricerca in Fisica

Jessica Ilaria Bellone

DETERMINATION OF THE LINK BETWEEN HEAVY ION CHARGE EXCHANGE REACTIONS AND SINGLE AND DOUBLE BETA DECAY MATRIX ELEMENTS

PhD thesis

PhD Coordinator:
Prof. Vincenzo Bellini

Tutors:
Prof. Vincenzo Greco
Dr. Maria Colonna

XXXI ciclo 2015 - 2018

CONTENTS

INTRODUCTION

Nuclear charge exchange transitions are one of the most versatile research tool, because they are involved in many processes underlying variuos physical phenomena, from astrophysics to particle physics, so that their study allow to gain relevant information on a wide range of physics. Such transitions can be "spontaneous" processes (weak decays) or can be induced by weak or strong external fields, like lepton-nucleus and meson/nucleon/nucleus-nucleus scatterings, respectively.

In the last decades, particular interest has been turning towards heavy ion nuclear charge exchange transitions for studying new possible nuclear states, such as the double Gamow-Teller giant resonance, the formation and properties of exotic nuclei, high multipolarity transitions and, above all, the investigation of physics beyond the Standard Model.

The latter topic is of most "transversal" nature than the others.

One of the main probes of physics beyond the Standard Model is represented by the theorized Neutrinoless Double Beta decay process ($0\nu\beta\beta$), not experimentally observed, yet. This decay is forbidden by the Standard Model and can happen only if neutrinos are Majorana particles. $0\nu\beta\beta$ represents the only process with physical observables directly related to Majorana phases and so the only process able to distinguish

between Dirac and Majorana neutrinos.

The main physical observable is represented by $0\nu\beta\beta$ half-life; indeed, the inverse of the half-life of nuclei which could undergo $0\nu\beta\beta$ is proportional to the Nuclear Matrix Element (NME) square modulus, the phase-space factor and a function that embodies all particle physics information, including also the neutrino effective mass, which contains Majorana phases.

In order to gain information on Majorana effective mass from half-life measurements with high precision, it is necessary to determine NME with high accuracy. Unfortunately, present different nuclear structure models calculations give values of the latter quantity differing up to a factor of 3; hence, it is desirable to proceed in another way. One of the most promising tools, in this direction, is just represented by heavy ion double charge exchange (DCE) nuclear reactions. Indeed, one can note that there are a lot of analogies between $0\nu\beta\beta$ and heavy ion "direct" DCE nuclear reactions [1], in particular initial and final states involved in both processes and the spin -isospin operators describing both transitions are the same, although the first one is a weak process, while the second one proceeds via nuclear strong interaction. While the relation between light [2] or heavy ions (part of this work) "direct" SCE forward angular distribution and β decay nuclear matrix element is well established, through the factorization of such cross section into the product of a nuclear structure term and a reaction term, unfortunately this is not the case for heavy ion "direct" DCE processes, even if one would be able to factorize the cross section. Indeed, DCE processes can be described as a one step process or as a second order charge exchange reaction, in terms of a convolution of two SCE processes, according to perturbation theory. In the latter case, the nuclear matrix element involved in the strong field - induced process exhibits a structure similar to the one describing $2\nu\beta\beta$ decay (intermediate states and the momentum

transferred to the intermediate states can be different), which represents the huge irreducible background of the experiments looking for $0\nu\beta\beta$ decay. The former description of DCE reactions deals with a strong process which diagrammatically resembles the wanted $0\nu\beta\beta$ decay; in fact, different nuclear structure models calculations [3, 4] show a nearly linear proportionality relation between heavy ion DCE Double Gamow - Teller (DGT) transition and $0\nu\beta\beta$ decay nuclear matrix elements, but the different nature of the propagators involved in the two (weak and strong) processes makes the determination of an analytical relation between the two nuclear matrix elements not trivial [5], thus questioning the direct extraction of the $0\nu\beta\beta$ NME from heavy ion "direct" DCE Cross Sections measurements.

Nowadays the latter topic is representing the main goal of the NUMEN experiment at INFN/LNS in Catania.

The present PhD work focuses on the investigation on low and intermediate energy heavy ion charge exchange processes induced by strong external fields, looking at the study of the role of the different ingredients of the cross section of such reactions, within DWBA framework:

- kinematical factors in which the dependence on the $Q-$value of the reaction is encoded;
- nuclear structure components, calculated within Quasiparticle Random Phase Approximation (QRPA);
- initial and final state reactions, dealing with elastic processes, accounted for by microscopic optical potentials.

with the aim to provide for the first time an extention to heavy ions [6], in low and intermediate energy regime, of the theoretical description of "direct" single charge exchange reactions given by Taddeucci et al. for light ions [2].

Moreover, while it has been widely tested [2, 7, 8] the proportionality relation between the zero degree "direct" single charge exchange (SCE) cross section and single β decay strength, proposed by Goodman and co-workers [7] and theoretically described by Taddeucci [2], since '80s, the present PhD thesis aims at investigating Single and Double Charge Exchange Cross Section factorization at low and intermediate energies, in particular for heavy ion reactions studied within the NUMEN collaboration, by using the Distorted Wave Born Approximation (DWBA), justified by the direct nature of such nuclear reactions.

This PhD thesis is organized in 6 chapters treating the above topics as follows:

1. The first chapter starts with a rapid overview on nuclear charge changing transitions. Then, the main features of single beta decay are described, together with a brief review on neutrino mass and on the problem of its smallness and its Dirac or Majorana nature, hinting at the see-saw meachanism as the one most naturally explaining the smallness of neutrino mass. Then, $0\nu\beta\beta$ and $2\nu\beta\beta$ decays are introduced, stressing how the former represents the main tool allowing to distinguish between Dirac and Majorana neutrinos. Moreover, this chapter briefly shows the problems in experimentally extracting information on neutrino Majorana effective mass, in this regard pointing to the study of heavy ion double charge exchange nuclear reactions as a smart tool to overcome these challenges. In this way, the attention is turned to light and heavy ion "direct" single and double charge exchange, due to meson (mainly pion) exchange, and to single and double charge changing processes originating by a sequence of nucleon transfer processes. The chapter ends with a review on these three types of charge exchange nuclear reactions.

2. The second chapter presents a review on the basic concepts of nu-

clear reaction theory, describing the different kind of possible nuclear reactions, from compound nucleus to direct reactions, focusing on the latter ones, in view of a deeper treatement of "direct" single and double charge exchange processes, then giving an overview of the most important approximation used in such context and on nuclear structure models used to describe heavy ion (single) charge exchange reactions.

3. The third chapter starts with a brief overview on the theoretical fomalism on light ion single charge exchange at high energies, by Taddeucci in '80s, and then provides the theoretical formalism developed within the present PhD work for the description of heavy ion single charge exchange reactions at low and intermediate energies, moreover showing the existence of a proportionality relation between beta decay nuclear matrix element and heavy ion SCE angular distribution at forward angles, thus extending the previous work to heavy nuclear systems.

4. The fourth chapter shows the formalism developed within the present PhD thesis for heavy ion double charge exchange reactions at low and intermediate energies, together with the possibility to factorize the cross section for such processes, following just the same procedure as for SCE case, and in particular focusing on the analogy with $2\nu\beta\beta$ decay, thus giving the chance of gaining information on the main process competing with the theorized $0\nu\beta\beta$ decay.

5. The fifth chapter illustrates the main numerical codes used in performing simulations both on single and double charge exchange reactions. Among these codes, the one simulating heavy ion DCE reactions, in the case of close analogy with $2\nu\beta\beta$ decay, has been developed within the present PhD work.

6. The sixth chapter presents the results of the simulations performed with the formalism and the codes discussed in the previous chapters, together with a preliminary comparison with the experimental results by the NUMEN experiment.

In the end, conclusions about this work are drawn.

CHAPTER 1

NUCLEAR CHARGE CHANGING TRANSITIONS

The term Nuclear Charge Changing transitions refers to all nuclear processes characterized by the only change of the charge of the initial nucleus, by one or more units, in one or more steps.

These kind of processes can be of different nature: they can be nuclear weak processes, like beta, double beta decays, charged lepton capture and neutrino - nucleus scattering, or strong ones, induced by nuclear reactions. They represent very important tools towards an understanding of a very wide range of Physics, e. g. they can give information on both single particle and collective features of nuclear structure (e. g. isobaric analog and Gamow-Teller giant resonances [8–10]), on stellar evolution (Standard Solar Model) and on the production of secondary nuclei in the interstellar medium [11] and hence on the relative abundances of the elements in the universe, on Physics beyond the Standard Model (e. g. the search of the theorized $0\nu\beta\beta$ decay [1, 12]) and so on [13].

The present work deals with the study of nuclear reaction induced charge changing transitions in order to gain information on the behaviour of nucleons within the nuclear medium, paying particular attention on

spin - isospin components of the effective nucleon - nucleon interaction in nuclear medium and on their possible relation with the operators describing single and double beta decays (both with and without neutrinos).

1.1 Nuclear Weak Decays

Nuclear weak decays are spontaneous charge changing processes, characterized by the exchange of the massive bosons $W^{\pm}$ and Z^0, with masses $m_W \simeq 80.38\,GeV$ and $m_{Z^0} = 91.19\,GeV$, respectively. Due to the large mass of the weak bosons, i. e. the very short range of weak interactions, weak processes at energy scales characteristic of nuclear reactions can be well described as effective point-like interactions, as confirmed by the huge success of Fermi's theory of beta decay in describing experimental results [14].

Nuclear weak decays can change the charge of the parent nucleus by one unit (single beta decay and electron capture) or by two units (double beta decay), as discussed in the following sections.

1.1.1 Single beta decay

Within the Standard Model, the single beta decay is a nuclear process characterized by the decay of a neutron into a proton (third component of the isospin changes by one unit, $\Delta T_z = -1$), an electron and an electronic antineutrino (β^- decay)

$$(A, Z) \rightarrow (A, Z+1) + e^- + \overline{\nu_e} \tag{1.1}$$

or by the transition of a proton, inside the nuclear medium, into a neutron (third component of the isospin changes by one unit, $\Delta T_z = +1$), a

positron and an electronic neutrino (β^+ decay)[1]

$$(A, Z) \rightarrow (A, Z-1) + e^+ + \nu_e \tag{1.2}$$

In both cases the charge of the parent nucleus is changed by one unit and orbital angular momentum does not change, $\Delta L = 0$.

A Feynman diagram representation of both β^- and β^+ decays is represented in fig. 1.1.

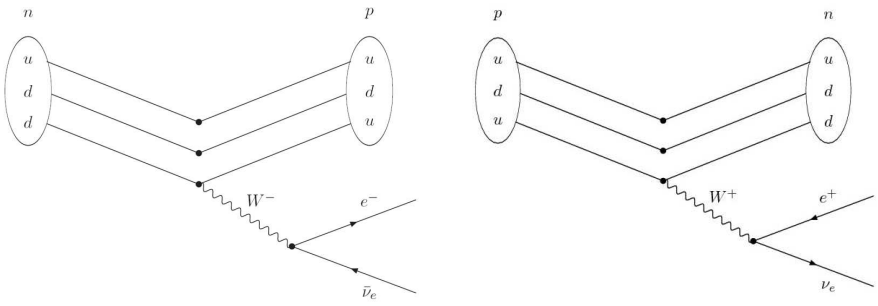

Figure 1.1: Feynman diagram of β^- (left panel) and β^+ (right panel) decay.

In the final channel, the energy of the system is divided among the daughter nucleus and the charged (e^-/e^+) and neutral ($\overline{\nu}_e/\nu_e$) leptons, so that charged lepton energy (or momentum) spectrum is given by a continuum distribution, as shown in fig. 1.2 both for the β^- (upper panel) and β^+ (lower panel) particles emitted by ^{64}Cu [15].

β^+ energy (momentum) spectrum of a given nucleus is peaked at an energy (momentum) value higher than that for β^- decay of the same nucleus, due to Coulomb repulsion between the positron and the positively charged (daugther) nucleus.

According to Fermi's theory of beta decay, formulated in 1934 [14], the decay rate per energy interval can be obtained through Fermi's Golden

[1]Another nuclear weak process characterized by the change of a proton into a neutron is represented by the Electron Capture (EC), $(A, Z)+e^{\pm} \rightarrow (A, Z \pm 1)+\overline{\nu}_e/\nu_e$, not treated in this work.

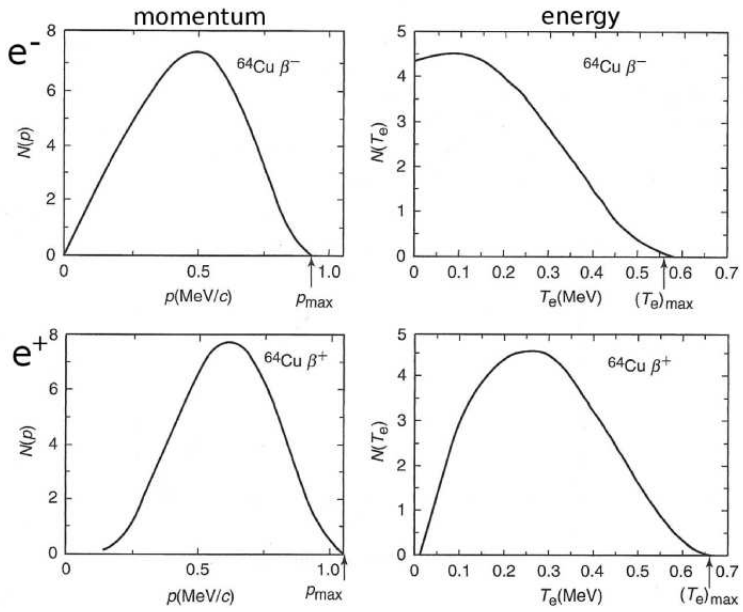

Figure 1.2: Momentum (left column) and energy spectrum (right column) of electrons (upper panel) and positrons (lower panel) from beta decay of ^{64}Cu.

rule and is given by

$$\frac{d\Gamma}{dE_e} = \frac{G_F^2 m_e^5}{2\pi^3} \cos^2\theta_C |\mathcal{M}_\beta|^2 F(Z, E_e) E_e p_e E_\nu p_\nu \tag{1.3}$$

where G_F is Fermi coupling constant, θ_C is Cabibbo's angle, E_e (E_ν) and p_e (p_ν) are the electron (neutrino) energy and momentum, respectively, $F(Z, E_e)$ is Fermi's function, which describes the final state electron−nucleus electromagnetic interaction (taking into account the presence of the electrons surrounding the nucleus in the final channel), the factors $E_i p_i$ ($i = e, \nu$) in eq. (1.3) come from final channel phase space factor $d^3p_i = p_i^2 dp_i d\cos\theta_i d\phi_i = p_i E_i dE_i d\cos\theta_i d\phi_i$, and $\mathcal{M}_\beta$ is the nuclear matrix element, given by

$$\mathcal{M}_\beta = g\langle\psi_B| \sum_i \mathcal{O}_i |\psi_A\rangle \tag{1.4}$$

where the sum $\sum_i$ is over all the nucleons of the decaying nucleus, ψ_A (ψ_B) represents the total wave function of the parent (daughter) nucleus and $\mathcal{O}$ is the operator describing the transitions in spin and isospin space.

For "superallowed" beta decays, characterized by no change both in total angular momentum and parity of the nucleus ($\Delta J = 0$, $\Delta\pi = 0$), called Fermi transitions, the coupling constant g identifies the weak vector coupling constant (often named g_V) and the transition operator, e. g. for β^- decay, is $\mathcal{O} = \tau^+$, being τ^+ the isospin raising operator, that increase the isospin of the system by one unit, thus accounting for the transition of a neutron into a proton[2]; for "allowed" beta decays, characterized by a change of the total angular momentum of the decaying isotope by one unit, leaving unchanged its parity ($\Delta J = 0, \pm 1$ and $\Delta\pi = 0$), called Gamow-Teller transitions, this operator can be expressed as $\mathcal{O} = \boldsymbol{\sigma}\tau^+$, where $\boldsymbol{\sigma} \equiv (\sigma_1, \sigma_2, \sigma_3)$ the vector of Pauli spin matrices, and in this case the constant g is identified with the axial weak coupling constant (often indicated as g_A) associated to the weak process.

The hypothesis about the existence of neutrino was formulated by Pauli in 1930 and then borrowed by Fermi in order to justify the continuum energy spectrum of electrons produced in beta decay processes, thus ensuring energy conservation. Indeed, experimentally a two−body decay was observed, $(A, Z) \rightarrow (A, Z + 1) + e^-$; in a two−body problem the energy of each of the two objects is determined uniquely, through energy−momentum conservation laws, which in turn means that the electrons energy spectrum should have been characterized by a peak at the energy corresponding to the Q−value of the process. Instead, from beta decay experiments a continuum energy spectrum is found, as shown in fig. 1.2, which can be explained by supposing a 3−body, instead of a 2−body, decay process, because the energy is not divided uniquely among the objects, in a 3−body process. This means that the "missing" electron energy is carried by a third particle, which cannot be detected: the *neutrino*. Because the latter particle is not directly detected, it was

[2]In particle physics, the isospin associated to neutrons is $-\frac{1}{2}$ and that for protons is $+\frac{1}{2}$, while in nuclear physics the inverse convention is used. In this thesis, the latter convention is adopted.

supposed that this new particle must have zero electromagnetic charge (in order to preserve charge conservation), it must have a mass smaller than that of the electron and it must not interact via strong interaction. Moreover, to preserve the angular momentum conservation and the statistics, the neutrino must be $\frac{1}{2}$-spin fermion.

1.1.1.1 Neutrino mass

One of the most debated neutrino features is its mass: are neutrinos massless or massive particles?

The experimental observation of neutrinos flavour oscillations (Super-Kamiokande and Subdury Neutrino Observatory [16, 17]) made it possible to establish that the neutrino is not a massless particle. Unfortunately, from these kind of experiments it is not possible to gain information on the absolute value of neutrino mass, but only on the differences between the squared masses of the different neutrino species.

The main observable sensible to the absolute value of neutrino mass[3] is just represented by the measurement of energy spectrum of the charged leptons emitted in beta decays [18].

Observing that the daughter nucleus mass is greater than that of the two leptons emitted, its kinetic energy can be neglected, and thus neutrino energy can be expressed in terms of energy and masses of the charged beta particle and of the daugther nucleus, from energy conservation, as follows

$$E_\nu = Q_\beta - T \tag{1.5}$$

where $T = E_e - m_e$ is electron kinetic energy and Q_β represents the Q-value of the process, defined as (neglecting neutrino mass, m_ν)

$$Q_\beta = M_A - M_B - m_e \tag{1.6}$$

[3]Properly speaking, it is the effective neutrino mass, defined in footnote 11.

being M_A and M_B parent and daughter nuclei masses (including excitation energy, if an excited nuclear state is populated), respectively. Hence, using $m_\nu \simeq 0$ approximation, the Q-value represents the maximum possible value of electron kinetic energy; instead, if neutrino mass is taken into account, then the maximum electron energy will be

$$T_{max} = Q_\beta - m_\nu \tag{1.7}$$

Neutrino momentum is given by

$$p_\nu = \sqrt{E_\nu^2 - m_\nu^2} = \sqrt{(Q_\beta - T)^2 - m_\nu^2} \tag{1.8}$$

By using eq. (1.8), the decay rate, in eq. (1.3), becomes

$$\frac{d\Gamma}{dT} = \frac{G_F^2 m_e^5}{2\pi^3} \cos^2\theta_C |\mathcal{M}_\beta|^2 F(Z, E_e) E_e p_e (Q_\beta - T)\sqrt{(Q_\beta - T)^2 - m_\nu^2} \tag{1.9}$$

knowing that $dT = dE_e$.[4]

Thus, if neutrino mass is very small, but non zero, its effect is maximum, i. e. perceptible, near the end−point of the electron energy spectrum, i. e. when $T \simeq T_{max}$, which implies $E_\nu = Q_\beta - T \simeq m_\nu$. The problem is that it's hard to make measurements of the end−point of the electron energy spectrum, because of very low statistics in this energy range.

[4]Sometimes, instead of the decay rate, it is convenient to consider beta decay half-life

$$T_{1/2}^{(\beta)} = \frac{ln(2)}{\lambda} = \frac{ln(2)}{\frac{G_F^2 m_e^5}{2\pi^3} \cos^2\theta_C |\mathcal{M}_\beta|^2 \int_0^\infty dT\, F(Z, E_e) E_e p_e (Q_\beta - T)\sqrt{(Q_\beta - T)^2 - m_\nu^2}}$$
$$= \frac{ln(2)}{\frac{G_F^2 m_e^5}{2\pi^3} \cos^2\theta_C |\mathcal{M}_\beta|^2 f(Z, Q_\beta)}$$

where in the last line Fermi's integral function, $f(Z, Q_\beta)$, has been introduced, which represents the integrated number of states available for both charged and neutral leptons, sharing the energy equal to the Q−value of the decay. In order to directly gain information both on nuclear structure and on weak interaction, the product $f(Z, Q_\beta)T_{1/2}^{(\beta)}$, called ft−product, or *comparative half-life*, is often used, being this product inversely proportional to the square modulus of the nuclear matrix element and to the second power (fourth power for double beta decay, described in the following sections) weak coupling constant, respectively.

In order to estimate the relative number of events in an energy range ΔT near the end-point spectrum, one can proceed in the following way:

neglecting neutrino mass, the total number of events is

$$n_{tot} = \int_0^{Q_\beta} \frac{d\Gamma}{dT}\, dT \propto \int_0^{Q_\beta} E_e p_e (Q_\beta - T)^2\, dT \tag{1.10}$$

$$= \int_0^{Q_\beta} (T + m_e)\sqrt{T(T + 2m_e)}(Q_\beta - T)^2\, dT \tag{1.11}$$

which, in the $Q_\beta \gg m_e$ limit, becomes

$$\int_0^{Q_\beta} \frac{d\Gamma}{dT}\, dT \propto Q_\beta^5 \tag{1.12}$$

The number of events in a small range near the end−point, i. e. for $T \simeq Q_\beta$, is given by

$$n(\Delta T) = \int_{Q_\beta - \Delta T}^{Q_\beta} \frac{d\Gamma}{dT}\, dT \propto \tag{1.13}$$

$$\int_{Q_\beta - \Delta T}^{Q_\beta} dT\, (Q_\beta + m_e)\sqrt{Q_\beta(Q_\beta + 2m_e)}(Q_\beta - T)^2 \propto \tag{1.14}$$

$$(Q_\beta + m_e)\sqrt{Q_\beta(Q_\beta + 2m_e)}(\Delta T)^3 \tag{1.15}$$

that, in the $Q_\beta \gg m_e$ limit, is $\propto Q_\beta^2 (\Delta T)^3$. Hence, the relative number of events is obtained from the ratio

$$\frac{n(\Delta T)}{n_{tot}} \propto \left(\frac{\Delta T}{Q_\beta}\right)^3 \tag{1.16}$$

Eq. (1.16) shows that the smaller the Q-value is, the greater is the number of events near the end−point energy [18].

Indeed, the most stringent upper limit on the absolute value of neutrino mass comes from the end-point of β^- energy spectrum obtained from ^{3}H β - decay measurements ($Q_\beta(^3\mathrm{H}) = 18.574\, keV$) [19]. The main reason why tritium β-decay experiments are the most sensitive to the electron neutrino mass is that tritium β-decay has one of the smallest

Q-values among all known β-decays. Moreover, tritium β-decay is a superallowed transition between mirror nuclei with a relatively short half-life (about 12.3 years), which implies an acceptable number of observed events during the experiment lifetime. Another advantage of tritium β-decay is that the atomic structure is less complicated than those of heavier atoms, leading to a more accurate calculation of atomic effects [18]. If $m_\nu \neq 0$, then the β^- end$-$point energy spectrum would be shifted from $T_{max} = Q_\beta$ to $T_{max} = Q_\beta - m_\nu$.

To determine neutrino mass from the end$-$point shift, it is convenient to define *Kurie 's function* (or *Fermi - Kurie's function*)

$$K(T) \equiv \sqrt{\frac{\frac{d\Gamma}{dT}}{\frac{G_F^2 m_e^5}{2\pi^3}\cos^2\theta_C |\mathcal{M}_\beta|^2 F(Z,E_e) E_e p_e}}$$

$$= \left[(Q_\beta - T)\sqrt{(Q_\beta - T)^2 - m_\nu^2}\right]^{\frac{1}{2}} = \sqrt{E_\nu p_\nu} \tag{1.17}$$

Hence, if $m_\nu = 0$, Kurie's function would depend linearly from electron kinetic energy T

$$K(T)|_{m_\nu=0} = Q_\beta - T \tag{1.18}$$

Thus a neutrino mass different from zero implies a deviation of $K(T)$ from linear behaviour.

In fact, what is done in experiments based on the study of the energy spectrum of the electrons (positrons) emitted in a β^- (β^+) decay, is just to catch such $K(T)$ deviations from linearity. In this way, Mainz e Troitzk experiments, studying tritium beta decay established the first upper limit for neutrino mass [20], [21]

$$m_\nu < 2.3\, eV \;\; (95\% C.L.) \tag{1.19}$$

$$m_\nu < 2.5\, eV \;\; (95\% C.L.) \tag{1.20}$$

respectively. The most recent KATRIN experiment, based on the analisys of such $K(T)$ deviations, lowers the neutrino mass upper limit to $0.35\, eV$ [22].

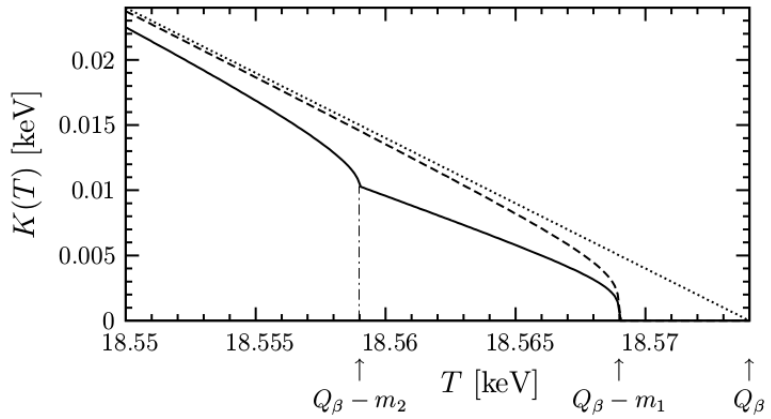

Figure 1.3: Kurie function vs electron kinetic energy (Kurie plot), for tritium β decay. The plot illustrates the zero neutrino mass case (dotted curve), the case of non - zero mass, $m_{\nu_e} = 5\,eV$ (dashed line) and the two neutrino mixing case, considering the two mass eigenstates $m_1 = 5\,eV$ and $m_2 = 15\,eV$ (solid curve).

1.1.1.1.1 Dirac and Majorana Neutrinos: main differences

Before the discovery of neutrino flavour oscillations, i. e. $m_\nu \neq 0$, due to the experimental observation of only left neutrinos and right antineutrinos (if neutrino does not coincide with its own antiparticle), these leptonic fields were initially treated in terms of left (neutrino), ψ_L, and right (antineutrino), ψ_R, Weyl spinors[5], respectively characterized by the following Lagrangian densities

$$\mathcal{L}_\mathcal{L} = i\psi_L^\dagger \overline{\sigma^\mu}\partial_\mu \psi_L \tag{1.21}$$

$$\mathcal{L}_\mathcal{R} = i\psi_R^\dagger \sigma^\mu \partial_\mu \psi_R \tag{1.22}$$

from which the following equations of motion are obtained

$$\overline{\sigma^\mu}\partial_\mu \psi_L = 0 \tag{1.23}$$

$$\sigma^\mu \partial_\mu \psi_R = 0 \tag{1.24}$$

[5]Weyl spinors are spinors with two components, which are elicity eigenstates, i. e. they are solutions of an equation, Weyl's equation, characterized by an Hamiltonian that commutates with the elicity operator.

both describing particles with zero mass, $m = 0$ (in fact, by multiplying each equation by its own complex conjugated, one finds Klein Gordon equation for massless particles); in the above equations, $\sigma_\mu \equiv (\mathbb{I}, \vec{\sigma})$ and $\overline{\sigma}_\mu \equiv (\mathbb{I}, -\vec{\sigma})$, being $\vec{\sigma} \equiv (\sigma^1, \sigma^2, \sigma^3)$ the vector of Pauli spin matrices[6]. Moreover, considering, for example, a positive energy solution of eq.(1.23)

$$\psi_L(x) = u_L e^{-ipx}|_{p^0=E_p} = u_L e^{(-iEt+i\vec{p}\cdot\vec{x})}|_{E=\sqrt{\vec{p}^2}} \tag{1.25}$$

where u_L is a constant spinor, and substituting this expression to $\psi_L(x)$ in eq.(1.23) one finds

$$\left(\vec{S}\cdot\hat{p}\right) u_L = -\frac{1}{2} u_L \tag{1.26}$$

which means that u_L spinor is an eigenstate of the elicity operator, $\left(\vec{S}\cdot\hat{p}\right)$, being $\vec{S} \equiv \frac{1}{2}\vec{\sigma}$, with eigenvalue $-\frac{1}{2}$ (in the same way it is possible to show that u_R is an elicity eigenstate with eigenvalue $+\frac{1}{2}$).

A left field can be transformed into a right field (and viceversa) through Charge Conjugation operator $\mathcal{C}$, defined as

$$\mathcal{C}\psi_L = i\sigma^2\psi_L^* \tag{1.27}$$

where the right hand side of eq. (1.27) is a right spinor (because it is possible to show that it's a solution of the eq. (1.24)). The problem of neutrinos description in terms of Weyl spinors is that the latter ones do not provide a representation of parity transformation group, because under parity transformation a left spinor is changed into a right one and viceversa (this comes just from parity operator definition), thus coming out of the initial left, or right, Weyl spinors space. Because electromagnetic and strong interactions are parity conserving, it is convenient working with fields which give a parity transformation representation. Just for this reason, Weyl spinors were abandoned in place of Dirac fields; indeed, the latter ones allow to describe massive $\frac{1}{2}-$spin fermions, in terms

[6]For particle physics arguments relativistic notation is used.

of 4−components spinors (bispinors or Dirac spinors), which evolve according to the following equation of motion

$$(i\gamma_\mu \partial^\mu - m)\psi = 0 \tag{1.28}$$

A Dirac spinor can be expressed in terms of Weyl spinors (*chiral representation*)

$$\psi = \begin{pmatrix} \psi_L \\ \psi_R \end{pmatrix} \tag{1.29}$$

where ψ_L and ψ_R are spinors indipendent of each other, i. e. they are not linked to each other by a charge conjugation transformation. Dirac equation in terms of Weyl spinors becomes

$$\begin{cases} i\overline{\sigma^\mu}\partial_\mu \psi_L = m\psi_R \\ i\sigma^\mu \partial_\mu \psi_R = m\psi_L \end{cases} \tag{1.30}$$

whose corresponding Lagrangian density is

$$\mathcal{L}_D = i\psi_L^\dagger \overline{\sigma^\mu}\partial_\mu \psi_L + i\psi_R^\dagger \sigma^\mu \partial_\mu \psi_R - m(\psi_L^\dagger \psi_R + \psi_R^\dagger \psi_L) \tag{1.31}$$

which is just invariant under parity transformation. It is important to note that the mass term (Dirac mass) mixes left and right states, which in turn implies that Dirac spinors are not elicity eigenstates (as it must be for massive particles). Defining γ^5 matrix (*chirality operator*)

$$\gamma^5 = i\gamma^0\gamma^1\gamma^2\gamma^3 = \begin{pmatrix} -\mathbf{1} & 0 \\ 0 & \mathbf{1} \end{pmatrix} \tag{1.32}$$

it is possible to define the left and right Weyl spinor space projection operators as follows

$$P_L\psi \equiv \frac{1-\gamma^5}{2}\psi = \frac{1-\gamma^5}{2}\begin{pmatrix} \psi_L \\ \psi_R \end{pmatrix} = \begin{pmatrix} \psi_L \\ 0 \end{pmatrix} \tag{1.33}$$

$$P_R\psi \equiv \frac{1+\gamma^5}{2}\psi = \frac{1+\gamma^5}{2}\begin{pmatrix} \psi_L \\ \psi_R \end{pmatrix} = \begin{pmatrix} 0 \\ \psi_R \end{pmatrix} \tag{1.34}$$

respectively.

All weak charged current[7] experiments show the "$(V-A)$ nature" of weak interactions, i. e. only left chirality projection of particle (e. g. neutrino) fields (and right projection of antiparticle fields) take part to the interaction[8]; this behaviour is formalized, within the Standard Model framework, through the following formalism for the charged current (CC) interaction

$$J^{\mu}_{CC} = \frac{1}{\sqrt{2}}\overline{\psi}_e\gamma^{\mu}\left[\frac{(1-\gamma^5)}{2}\psi_{\nu}\right] + h.c. \tag{1.35}$$

Majorana found that it is also possible to describe massive particles just through one Weyl spinor, by taking ψ_L e ψ_R, within the Dirac spinor, not indipendent of each other, but related by charge conjugation transformation [18, 23, 24]; e. g.,

$$\psi_R = \psi^C_L = i\gamma^2\psi^*_L \tag{1.36}$$

By using the right field given by eq. (1.36), the two equations in (1.30) reduces to the same equation; this implies a reduction of the degrees of freedom of the system, from 4 to 2. Moreover, $\psi_R = \psi^C_L$ is a solution of Klein Gordon equation for massive particles, too. Hence, in this way one can describe a massive, $\frac{1}{2}$ - spin fermion by using only one Weyl spinor. The bispinor with chiral components satisfying the relation in (1.36) is called *Majorana spinor*

$$\psi_M = \begin{pmatrix} \psi_L \\ i\gamma^2\psi^*_L \end{pmatrix} \tag{1.37}$$

With this new spinor, the equation of motion becomes

$$(i\gamma_{\mu}\partial^{\mu} - m)\psi_M = 0$$

or

$$(i\partial\!\!\!/ - m)\psi_M = 0 \tag{1.38}$$

[7] Weak charged current is a weak interaction mediated by charged bosons $W^{\pm}$.

[8] Another possibility is to mantain right neutrino components under the hypothesis that the latter ones interact only gravitationally (*sterile neutrino* hypothesis).

which is identical to Dirac equation only formally, because if we could write the Lagrangian density for Majorana fields like the Dirac Lagrangian density, then we would have the following mass term (à la Dirac)

$$\begin{aligned}
&\overline{\psi}_M \psi_M = (-i\psi_L\sigma^2, \psi_L^*) \begin{pmatrix} \psi_L \\ i\sigma^2\psi_L^* \end{pmatrix} = -i\psi_L^T\sigma^2\psi_L + i\psi_L^{*T}\sigma^2\psi_L^* \\
&= -i\psi_L^T\sigma^2\psi_L + c.c. \\
&= -i(\psi_L)_a(\sigma^2)_{ab}(\psi_L)_b + c.c. \\
&= -i \underbrace{(\sigma^2)_{ab}}_{antisymm.} \underbrace{(\psi_L)_a(\psi_L)_b}_{symm.} + c.c. = 0
\end{aligned} \tag{1.39}$$

which would imply that we are using classical anticommuting fields, in order to ensure that the product $(\psi_L)_a(\psi_L)_b$ is antisymmetric, instead of symmetric. This is just a first signal of the differences between Majorana and Dirac fields. In quantum field theory (QFT) it is possible to derive Majorana fermions equation of motion starting from a Lagrangian density formally Dirac - like, because spinor fields can be represented through anticommuting operators.

$$\mathcal{L}^M = \frac{1}{2}\overline{\nu}\,(i\partial\!\!\!/ - m)\,\nu \quad (Majorana) \tag{1.40}$$

$$\mathcal{L} = \overline{\psi}\,(i\partial\!\!\!/ - m)\,\psi \quad (Dirac) \tag{1.41}$$

The $\frac{1}{2}$ factor in eq. (1.40) is inserted to avoid double counting, due to the halving of the spinor field degrees of freedom, because we are using Majorana fields; the definition of the latter fields implies that eq. (1.40) is no more $U(1)$ - symmetric, differently from the Dirac case, meaning that only neutral fermions can be described by Majorana fields. Moreover, Majorana condition, $\nu = \nu^C$, implies that Majorana particles coincide with their own antiparticles. All these features suggest that the only possible Majorana particle candidate is the neutrino[9].

[9]Other neutral fermions, like the neutron together with other Standard Model neutral barions, cannot be Majorana particles, i. e. they do not coincide with their own antiparticle, because they can be distinguished by their non zero magnetic moment [25].

1.1.1.1.2 How to explain the small neutrino mass: see-saw mechanism

The discovery of neutrino flavour oscillations, allowed only for massive neutrinos, confirmed that neutrinos have non - zero mass. Direct experiments (e.g. tritium beta particle energy spectrum measurements) give upper limits showing that neutrinos should have a very small mass.

It is very tricky to explain the smallness of neutrino mass, as one can guess from the plethora of mechanisms, within and beyond the Standard Model, proposed up to now [26–32]; the simplest and most convincing one is represented by the so called *see-saw* mechanism.

There are 3 kinds of see - saw mechanisms, all giving a light neutrino mass inversely proportional to a huge mass, setting the energy scale of physics beyond the Standard Model. The most important one is the type I see - saw, based on the use of Standard Model fields, while type II and type III See - Saw mechanisms use fields not accounted for within the Standard Model [33] [34]. In type I see - saw [18] [35], right neutrinos, ν_R, are introduced as fields which transform like $SU(3)_C \times SU(2)_L \times U(1)_Y$ singlets, meaning that right neutrinos would be sterile, i. e. they do not interact with any field, but with the Higgs one. According to type I see - saw mechanism, neutrino mass is given by

$$m_\nu = \frac{m_D^2}{m_R} \tag{1.42}$$

where m_D is a Dirac mass (like quarks and charged leptons masses), generated by the Higgs mechanism allowed by the Standard Model.

Eq. (1.42) implies that the larger right neutrino (not observed, because sterile) mass m_R is, the smaller is light neutrino mass m_ν (the one which is "observed").

Hence, this mechanism provides "spontaneously" the many orders of magnitude among neutrino mass and that of the other Standard Model fermions.

1.1.1.1.3 Consequences of neutrino mass nature

If neutrinos have Majorana mass, then they would be low - energy manifestation of physics beyond the Standard Model. Moreover, in supersymmetric theories, fotino and neutralino are Majorana particles and the latter would be one of the possible candidates of Dark Matter.

Finally, a Majorana mass would support the leptogenesis theory, in which it is supposed that in the early Universe, due to the high energies, there should exist a lot of heavy neutrinos; in thermal non-equilibrium conditions, the CP - violating phases[10] [37] would lead to different decay rates for heavy neutrinos and this, in turn, would generate the asymmetry between leptons and anti-leptons, which would be converted into barion anti-barion asymmetry [38, 39] through the "sphaleron" fields. The latter are non-perturbative time-independent solutions of the electro-weak equations of motion; because of their non-pertubative nature, sphalerons cannot be represented within Feynman diagram framework. Therefore, sphalerons would violate barion (B) and lepton number (L) conservation, but would preserve their difference, $B - L$ [39].

1.1.2 Double beta decay

From experiments on neutrino flavour oscillations it is possible to get information only on the differences between squared neutrino masses, through the determination of flavour oscillation probability

$$P_{\nu_\alpha \to \nu_\beta}(E, L) = \sum_{k,j} U^*_{\alpha k} U_{\beta k} U_{\alpha j} U^*_{\beta j} e^{-i \frac{\Delta m^2_{kj} L}{2E}} \tag{1.43}$$

where $\alpha, \beta = e, \mu, \tau$ are the flavour indices and $k, j = 1, 2, 3$ identify the mass eigenstates, $U_{\beta k}$ are the neutrino mixing matrix elements, L is the distance between neutrinos source and the detector, E represents

[10] In 1967 Sakharov suggested that it is possible to provide the actual Universe barion-antibarion asymmetry, starting from a symmetric condition, i. e. zero net barion number, $\Delta B = 0$, thanks to CP violation in non equilibrium conditions, so that the CP violating processes do not compensate each other.

neutrino energy and $\Delta m^2_{kj} = m^2_k - m^2_j$ is the difference between the square of neutrino masses; the latter ones are the eigenvalues of neutrino mass eigenstates, which combine each other through the mixing angles so as to "reproduce" flavour eigenstates, that correspond to the observed neutrinos.

Such experiments allow to indentify two neutrino mass hierarchies:

- Normal: 2 "heavy" neutrinos, characterized by a difference between squared masses $\sim \Delta m^2_{sun} \simeq 7.92(1 \pm 0.09)\text{x}10^{-5}\, eV^2$ and one light neutrino, with a difference of squared masses with respect to the two heavy neutrinos, equal to $\Delta m^2_{atm} \simeq 2.4\left(1^{+0.21}_{-0.26}\right)\, eV^2$.

- Inverted: 2 light and one heavy neutrinos, with the same prescription as for the normal hierarchy.

An experiment which could give information both on the value and the nature of (effective) neutrino mass (Dirac or Majorana), is the neutrinoless double beta decay ($0\nu\beta\beta$), which is indeed sensible to Majorana phases.

The double beta decay is a nuclear process that can occur only in those nuclei for which the single beta decay is energetically forbidden, i. e. when ground state (g. s.) energy of the parent nucleus (A, Z) is lower than g. s. energy of the daughter nucleus $(A, Z \pm 1)$ plus electron mass. Indeed, if a nucleus can decay both β and $\beta\beta$, then the latter process is practically hidden at all by the former, because it is characterized by a half-life longer than that of single β decay, being the double beta decay a second order (and so one order higher than the single beta decay) process. Moreover, double beta decay is characterized by the emission of two charged leptons (e^+/e^-) together with two neutral leptons (neutrinos/antineutrinos) or without any emission of neutral leptons. The former case, known as two neutrino double beta decay ($2\nu\beta\beta$), is allowed by the Standard Model (see sect. 1.1.2.2), while the latter case refers to

the not yet observed $0\nu\beta\beta$ [40](see sect. below).

There exist three experimental methods to study double beta decaying nuclei, all based on half - life determination:

- **geochemical**: the abundance of the final nucleus in a ore sample containing the candidate isotope is monitored;
- **radiochemical**: the procedure is like the geochemical case, but using artificial samples;
- **direct**: study of the energy spectrum of electrons/positrons emetted by the candidate nucleus.

The first two methods are of indirect kind and do not allow to distinguish between 0 and $2\nu\beta\beta$, while the last does, even if it requires very precise and clean measurements, which up to now led to the discovery of most of $2\nu\beta\beta$ decaying nuclei, but no $0\nu\beta\beta$ decaying ones.

1.1.2.1 $0\nu\beta\beta$

If neutrinos are Majorana particles, then the double beta decay can proceed both with and without two neutrinos emission, so that the latter process

$$(A, Z) \rightarrow (A, Z \pm 2) + 2e^{\pm}$$

would represent a good tool to discriminate between Dirac and Majorana neutrinos. $0\nu\beta\beta$, proposed by Furry in 1939 [41], has not been observed, yet. The spectrum of the couple of charged leptons emitted in this case should be discrete, peaked at the Q-value of the process, $Q_{\beta\beta}$, but however it would be hidden by the tale of the continuous energy spectrum of the two charged leptons from $2\nu\beta\beta$ decay. Neutrinoless double beta decay is forbidden by the Standard Model, because it would violate total lepton number conservation by 2 units. The experimental observable

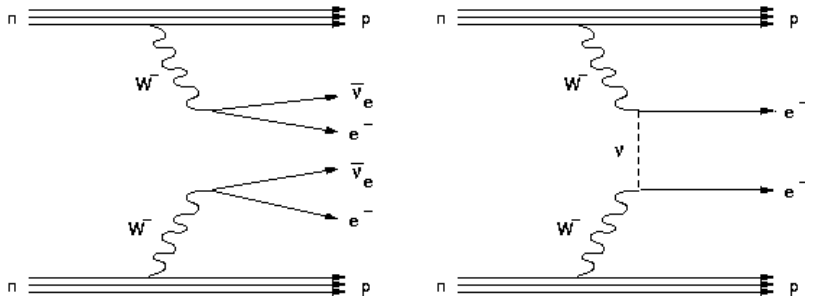

Figure 1.4: Feynman diagrams for $2\nu\beta\beta$ (left panel) and for $0\nu\beta\beta$ (right panel) [24].

checked is the half-life of the given candidate nucleus,

$$T^{0\nu}_{1/2} = \left[G^{0\nu}|\mathcal{M}^{0\nu}|^2|f(m_{\beta\beta}, m)|^2\right]^{-1} \tag{1.44}$$

which depends on the phase space element, $G^{0\nu} \propto Q^5_{\beta\beta}$, and on the nuclear matrix element (NME), $M^{0\nu}$. At first, Furry estimated a $0\nu\beta\beta$ half-life shorter than that of the competing $2\nu\beta\beta$ decay, because He didn't take into account that if neutrinos are massive particles, then they are no more helicity eigenstates and so there is a mixing between big and small components of neutrino field; indeed, this mixing leads to a factor $\sim (m_{\nu_i}/E_{\nu_i})^{-2}$ in $0\nu\beta\beta$ half-life, thus increasing the latter by about $5-6$ orders of magnitude with respect to $2\nu\beta\beta$ decay half - life [42]. Eq. (1.44) also shows the $T^{0\nu}_{1/2}$ dependence on neutrino effective mass[11]

$$m_{\beta\beta} = |\sum_k U^2_{ek} m_k| = |m_1 U^2_{e1} + m_2 U^2_{e2} + m_3 U^2_{e3}| \tag{1.45}$$

[11]The main sources of information on neutrino mass are three:

1) the high energy tale of beta particles spectrum, which is very sensitive to the electron neutrino effective mass $m_\beta = \sqrt{c^2_{13}c^2_{12}m^2_1 + c^2_{13}s^2_{12}m^2_2 + s^2_{13}m^2_3}$ (in this case there is no destructive interference, because m_β is the sum of positive quantities);

2) the double beta decay experiments, probing the effective *Majorana mass*, $m_{\beta\beta} = |c^2_{13}c^2_{12}m_1 + c^2_{13}s^2_{12}m_2 e^{2i\lambda_2} + s^2_{13}m_3 e^{2i(\lambda_3 - \delta_{13})}|$ (in this case destructive interference could happen);

3) the cosmological observable given by the sum of the 3 neutrino masses, $\Sigma = m_1 + m_2 + m_3 \simeq 0.61\, eV$, which can influence the formation of large - scale structures.

where $c_{ij} = \cos\theta_{ij}$ and $s_{ij} = \sin\theta_{ij}$, being θ_{ij} the mixing angle between the two species i and j $(i, j = 1, 2, 3)$; m_i $(i = 1, 2, 3)$ are the three neutrino mass eigenvalues.

and on m in eq. (1.44), whose value depends on the scenarios considered [43–45]:

1. **light neutrino ($m_\nu \ll 1\,MeV$) exchange scenario**: m corresponds to the electron mass;
2. **heavy neutrino ($m_\nu \gg 1\,GeV$) exchange scenario**: m is equal to the proton mass;
3. **Majoron emission scenario**: m represents the Majoron mass;
4. **Sterile neutrino exchange scenario**: m is the sterile neutrino mass.

It can be shown that $0\nu\beta\beta$ NME can be written, in momentum space, as

$$\begin{aligned}\mathcal{M}_{0\nu}(p) &= R\langle B, J_f^\pi | \sum_{i,j} \{\tau_i^+ \tau_j^+ \left[-h^F(p) + h^{GT}(p)\boldsymbol{\sigma}_i \cdot \boldsymbol{\sigma}_j + h^t(p) S_{ij}^p\right]\} | A, 0^+\rangle \\ &= R\left(g_A^2 \mathcal{M}_{0\nu}^{(GT)} - g_V^2 \mathcal{M}_{0\nu}^{(F)} + g_A^2 \mathcal{M}_{0\nu}^{(t)}\right)\end{aligned} \tag{1.46}$$

where A and B denote the parent and daughter nuclei with total angular momentum and parity 0^+ and J_f^π, respectively; $R = 1.2A^{1/3}$ is the nuclear radius in femtometers, introduced to make $\mathcal{M}_{0\nu}(p)$ dimensionless [46]; p is the momentum transfer, viz. the difference between initial and final nuclear linear momenta, $S_{ij}^p = 3\,(\boldsymbol{\sigma}_i \cdot \hat{p})\,(\boldsymbol{\sigma}_j \cdot \hat{p}) - \boldsymbol{\sigma}_i \cdot \boldsymbol{\sigma}_j$ is the rank-2 tensor in momentum space and the sum is over the nucleons involved in the transition. $h^{(i)}(p)$, $i = F, GT, t$, represent Fermi (F), Gamow-Teller (GT) and tensor (t) contributions, which can be further factorized into the product $h^{(i)}(p) = \nu(p)\tilde{h}^{(i)}(p)$, where $\nu(p)$ is called "neutrino potential" and $\tilde{h}^{(i)}(p)$ represents the form factor. Gamow-Teller and tensor contributions for the latter term can in turn be expressed as the following sums [45]

$$\begin{aligned}\tilde{h}^{GT}(p) &= \tilde{h}_{AA}^{GT}(p) + \tilde{h}_{AP}^{GT}(p) + \tilde{h}_{PP}^{GT}(p) + \tilde{h}_{MM}^{GT}(p) \\ \tilde{h}^{t}(p) &= \tilde{h}_{AP}^{t}(p) + \tilde{h}_{PP}^{t}(p) + \tilde{h}_{MM}^{t}(p)\end{aligned} \tag{1.47}$$

where the expressions of all the terms in the sums are given in tab. 1.1. The form factors contain all the information relative to the weak interaction, because they are functions of the weak vector (g_V) and axial (g_A) coupling constants, as shown in tab. 1.1.

The tensor term can be neglected, because it has been provided that it affects the total $0\nu\beta\beta$ NME only by a few percent [49–51]. The expressions of neutrino potential and of the function $f(m_{\beta\beta}, m)$ depend on the "scenario" considered[12], i. e. they depend on the particle exchanged between the two decaying nucleons, as shown in table 1.2 [52], and on the approximations used in the calculations. The expressions of neutrino potential in tab. 1.2 have been obtained by using closure approximation, i. e. by neglecting the denominator dependence on the energy of the intermediate nuclear states (which is approximated with a proper average value, called *closure energy*), so that the completeness of the (virtual) nuclear intermediate states can be exploited to give the unitary operator of Hilbert space of such nuclear states; in this way, the NME of a 2−body nuclear transition operator must be evaluated. Closure approximation turns out to be very useful, because it eliminates the need of calculating a very large number of nuclear states in the intermediate channel, which could be computationally challenging, especially for heavy systems [53].

Actually, different nuclear structure models give $M^{0\nu}$ values differing by about a factor of 3 [52, 54], as shown in fig. 1.5, unlike $G^{0\nu}$, which is totally under control.

The large differences in the values of the $0\nu\beta\beta$ nuclear matrix element, determined by using different nuclear structure models, lead to an even greater uncertainty in $m_{\beta\beta}$ determination. For this reason, alternative methods for NME determination have been explored: the first attempts were made by studying the ($\pi^{\pm}$,$\pi^{\mp}$) double charge exchange

[12]Of course, for $2\nu\beta\beta$ decay there are no scenarios and so there is a unic expression for neutrino potential, $\nu(p) = \frac{\delta(p)}{p^2}$.

terms	$\tilde{h}(p)$
$\tilde{h}^F(p)$	$\frac{g_V^2}{\left(1+p^2/M_V^2\right)^4}$
$\tilde{h}^{GT}_{AA}(p)$	$\frac{g_A^2}{\left(1+p^2/M_A^2\right)^4}$
$\tilde{h}^{GT}_{AP}(p)$	$g_A^2\left[-\frac{2}{3}\frac{1}{\left(1+p^2/M_A^2\right)^4}\frac{p^2}{p^2+m_\pi^2}\left(1-\frac{m_\pi^2}{M_A^2}\right)\right]$
$\tilde{h}^{GT}_{PP}(p)$	$g_A^2\left[\frac{1}{\sqrt{3}}\frac{1}{\left(1+p^2/M_A^2\right)^2}\frac{p^2}{p^2+m_\pi^2}\left(1-\frac{m_\pi^2}{M_A^2}\right)\right]^2$
$\tilde{h}^{GT}_{MM}(p)$	$\frac{2}{3}\tilde{h}^F(p)\frac{\kappa_\beta^2 p^2}{4m_p^2}$
$\tilde{h}^t_{AP}(p)$	$-\tilde{h}^{GT}_{AP}(p)$
$\tilde{h}^t_{PP}(p)$	$-\tilde{h}^{GT}_{PP}(p)$
$\tilde{h}^t_{MM}(p)$	$\frac{1}{2}\tilde{h}^{GT}_{MM}(p)$

Table 1.1: Fermi, Gamow-Teller and tensor terms appearing in the corresponding form factors, according to Šimkovic's formulation [45]. m_p is proton mass, m_π is pion mass, $M_A^2 = 1.09\,GeV^2$ [47], $M_V^2 = 0.71\,GeV^2$ [48] and $\kappa_\beta = 3.70$ is the isovector anomalous magnetic moment of the nucleon.

scenarios	$f(m_{\beta\beta}, m)$	$\nu(p)$
1	$\frac{m_{\beta\beta}}{m_e}$	$\frac{2}{\pi}\frac{1}{p(p+\tilde{A})}$
2	$m_p\langle\frac{1}{m_{\nu_h}}\rangle$ $\langle\frac{1}{m_{\nu_h}}\rangle = \sum_{k=heavy} \lvert U_{ek}\rvert^2 m_{\nu_k}$	$\frac{2}{\pi}\frac{1}{m_p m_e}$
3	$\langle g \rangle$	$\frac{2}{\pi}\frac{1}{p(p+\tilde{A})}$
4	$\frac{m_N}{m_e}$	$\frac{2}{\pi}\frac{1}{\sqrt{p^2+m_N^2}\left(\sqrt{p^2+m_N^2}+\tilde{A}\right)}$

Table 1.2: Expressions for $f(m_{\beta\beta}, m)$ and neutrino potential for the different neutrino exchange scenarios in $0\nu\beta\beta$. $\tilde{A} = 1.12A^{1/2}\,MeV$ is the closure energy, g is the effective Majoron coupling constant and m_N is the sterile neutrino mass, which can vary on a wide mass range ($eV - TeV$).

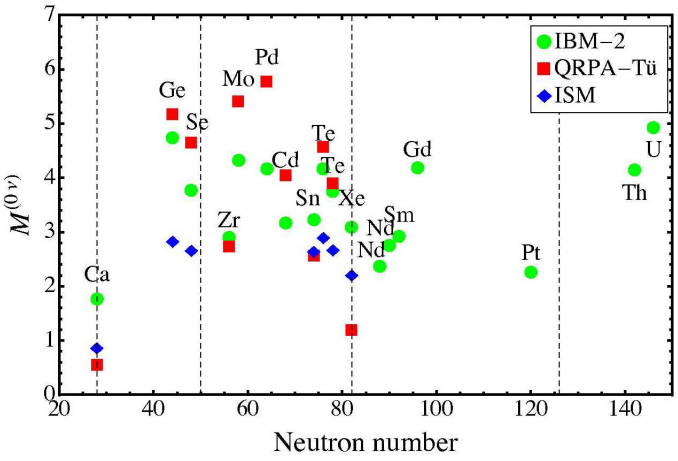

Figure 1.5: Nuclear matrix element for $0\nu\beta\beta$, for different candidate nuclei, in case of light neutrino exchange. Calculations are performed through different nuclear structure models [52].

(DCE) pion-nucleus ($\pi - N$) reactions, but such processes are described by different kind of spin-isospin operators [55–57], so that they do not give information about $0\nu\beta\beta$ NMEs; recentely, increasing interest is reversed in heavy ion double charge exchange nuclear reactions, because of several analogies between such process and neutrinoless double beta decay weak process [1], as will be shown in the next sections.

1.1.2.2 $2\nu\beta\beta$

If neutrinos are Dirac particles, then double beta decay can occur only with the emission of two neutrinos, together with the two charged leptons.

$$(A, Z) \rightarrow (A, Z \pm 2) + 2e^{\pm} + 2\nu_e(\overline{\nu_e})$$

This decay mode was proposed by M. Goeppert-Meyer in 1935 [58] and was first recorded in 1950 in a geochemical experiment with ^{130}Te [59]; then, in 1967 $2\nu\beta\beta$ was observed for ^{82}Se also in a geochemical experiment [60] and has been observed through direct experiments only in 1987 [61]. In the next few years, direct experiments were able to detect such decay in many other nuclei [62]. Nowadays, $2\nu\beta^-\beta^-$ decay has been

observed in 10 nuclei (while $2\nu\beta^+\beta^+$, $2\nu\beta^+EC$ and $2\nu ECEC$ processes have been observed only in ^{130}Ba isotope, from geochemical experiments) [63]: ^{48}Ca, ^{76}Ge, ^{82}Se, ^{96}Zr, ^{100}Mo, ^{116}Cd, ^{128}Te, ^{130}Te, ^{150}Nd and ^{238}U (from radiochemical experiments [64]). Double beta decay half-lives depend on the axial coupling constant to the fourth power, so that they are extremely sensible to g_A value; since $2\nu\beta\beta$ has been measured in several nuclei, it provides a tool, much powerful than single beta decay, for estimating the effects of the nuclear medium on g_A, i. e. its effective value, g_A^{eff}, or the quenching factor $q \equiv g_A^{eff}/g_A = \mathcal{M}_{exp}^{(GT)}/\mathcal{M}_{theo}^{(GT)}$, given by the ratio of experimental to theoretical GT nuclear matrix elements [46].

Because $2\nu\beta\beta$ is a 5-body decay, the energy spectrum of the two electrons/positrons emitted is continuous, with end-point energy equal to the maximum energy available for the couple of charged leptons, $Q_{\beta\beta} = M_A - M_B - 2m_e$, as shown in fig. 1.6.

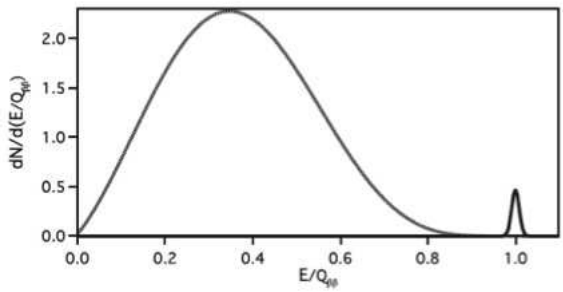

Figure 1.6: Example of an energy spectrum of the couple of charged leptons emitted in double beta decay process with the emission of 2 neutrinos (continuous spectrum) and without neutrinos emission (a quite sharp peak at the Q-value of the process, zoomed of many orders of magnitude), if the latter were observed.

The calculation of $2\nu\beta\beta$ nuclear matrix element, $\mathcal{M}^{(2\nu)}$, turns out to be more complex than for $0\nu\beta\beta$ [46]. Indeed, in general, the inverse of $2\nu\beta\beta$ half-life cannot be factorized into the product of the phase space factor, $G^{2\nu}$, and the square modulus of $\mathcal{M}^{(2\nu)}$, because both these terms depend on the states of the odd-odd nucleus involved in the intermediate

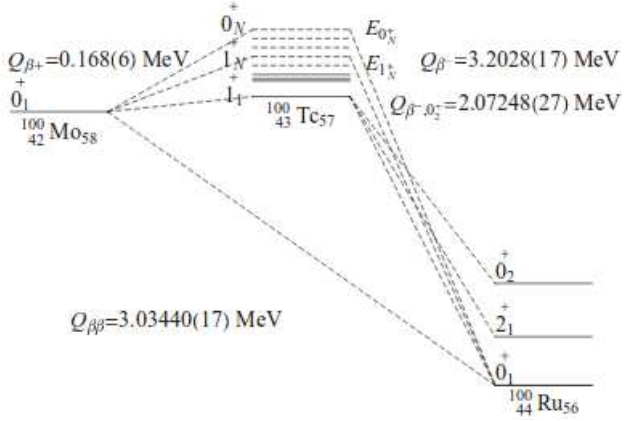

Figure 1.7: Nuclear energy level scheme for $2\nu\beta\beta$ decay of ^{100}Mo [46].

channel, as shown in fig. 1.7 and in eq. (1.48), e. g. for $2\nu\beta^+\beta^+$ decay,

$$\begin{aligned}
&\left[T^{(2\nu)}_{1/2}\right]^{-1} = \sum_n G^{(2\nu)}_n |\mathcal{M}^{(2\nu)}_n|^2 \\
&= \sum_n G^{(2\nu)}_n | \left(g_V^2 \mathcal{M}^{(2\nu)}_{(F)n} - g_A^2 \mathcal{M}^{(2\nu)}_{(GT)n} \right) |^2 \\
&= \sum_n G^{(2\nu)}_n \left(|g_V^2 \frac{\langle \psi_B | \sum_i \tau_i^+ |n\rangle\langle n| \sum_j \tau_j^+ |\psi_A\rangle}{E_n - \frac{1}{2}(M_A + M_B)} \right. \\
&\left. - g_A^2 \frac{\langle \psi_B | \sum_i \boldsymbol{\sigma}_i \tau_i^+ |n\rangle\langle n| \sum_j \boldsymbol{\sigma}_j \tau_j^+ |\psi_A\rangle}{E_n - \frac{1}{2}(M_A + M_B)} |^2 \right)
\end{aligned} \tag{1.48}$$

where the indices i and j run over all nucleons of the decaying nucleus, n runs over all intermediate nuclear states, each with energy E_n, which for allowed or superallowed beta decays can be only 1^+ or 0^+ states, starting from a nucleus with 0^+ ground state. Thus, $2\nu\beta\beta$ decay half-life cannot generally be factorized, because on the one side it is necessary to sum the contributions calculated for each intermediate 0^+ and 1^+ nuclear state, and on the other side closure approximation should not be good, due to the small momentum transfer (of the order of few MeV) characterizing $2\nu\beta\beta$. However, the closure approximation is still valid if a proper average value of the intermediate state energy (closure energy) is chosen, so that phase-space factor can be separated from $2\nu\beta\beta$ nuclear

matrix element, given by the following expression [46]

$$\begin{aligned}\mathcal{M}^{(2\nu)} &= g_V^2 \left(\langle B, 0^+ | \frac{\sum_{i,j} \tau_i^+ \tau_j^+}{\langle E_{0_n^+} \rangle - \frac{1}{2}(M_A + M_B)} | A, 0^+ \rangle \right) \\ &- g_A^2 \left(\langle B, 0^+ | \frac{\sum_{i,j} \boldsymbol{\sigma}_i \boldsymbol{\sigma}_j \tau_i^+ \tau_j^+}{\langle E_{1_n^+} \rangle - \frac{1}{2}(M_A + M_B)} | A, 0^+ \rangle \right) \\ &= g_V^2 \mathcal{M}_F^{(2\nu)} - g_A^2 \mathcal{M}_{GT}^{(2\nu)}\end{aligned} \tag{1.49}$$

taking into account that the closure energies $\langle E_{0_n^+} \rangle$ and $\langle E_{1_n^+} \rangle$, respectively for double Fermi and double GT transitions, are different. However, $2\nu\beta\beta$ decay matrix elements involving only Fermi transitions can often be neglected [46, 51].

Another approximation allowing to separate phase-space factor from $\mathcal{M}^{(2\nu)}$ is the single state dominance (SSD) [65–69], through which nuclear matrix element becomes

$$\begin{aligned}\mathcal{M}^{(2\nu)} &= g_V^2 \left(\langle B, 0^+ | \frac{\sum_{i,j} \tau_i^+ \tau_j^+}{E_{0^+} - \frac{1}{2}(M_A + M_B)} | A, 0^+ \rangle \right) \\ &- g_A^2 \left(\langle B, 0^+ | \frac{\sum_{i,j} \boldsymbol{\sigma}_i \boldsymbol{\sigma}_j \tau_i^+ \tau_j^+}{E_{1^+} - \frac{1}{2}(M_A + M_B)} | A, 0^+ \rangle \right)\end{aligned} \tag{1.50}$$

Hence, $2\nu\beta\beta$ decay half-life can be expressed, both in closure approximation and in SSD, as

$$T_{1/2}^{(2\nu)} = \left[G^{(2\nu)} |\mathcal{M}^{(2\nu)}|^2 \right]^{-1} \tag{1.51}$$

$2\nu\beta\beta$ half-life measurements give directly the value of $2\nu\beta\beta$ nuclear matrix element through eq. (1.51), thus offering a sensitive test of nuclear structure calculations, but from the particle physics point of view, no information on Dirac or Majorana nature of neutrino mass can be gained, because it can be shown that $2\nu\beta\beta$ half-life is free of unknown particle physics parameters [70] (like neutrino effective mass).

Moreover, the existence of a proportionality relation between $2\nu\beta\beta$ and $0\nu\beta\beta$ nuclear matrix elements would represent a lifeline for determining the latter, but unfortunately the state - of - art calculations, within

Quasiparticle Random Phase Approximation (QRPA), lead to results disfavouring such proportionality relation [71].

1.2 Charge Exchange Nuclear Reactions

Together with the weak processes shown above, there exist many other different tools to gain information on the organization of nucleons inside the nucleus, from photon beams off nuclei and charged-lepton nucleus scattering, giving information on charge distribution, magnetic moment and other electromagnetic properties of nuclei, to meson-nucleus, nucleon-nucleus and nucleus-nucleus scattering, carrying information on nuclear mass distribution and on a plethora of other nuclear structure properties, both of collective and of single particle nature.

Since several decades, a special interest has been reversed on the study of *charge exchange* (CE) nuclear reactions induced by the strong interaction, which can be studied through pion-nucleus, nucleon-nucleus or nucleus-nucleus scattering. These reactions can take place in a unic step ("direct" charge exchange) or in more steps (multi - nucleon transfer). All these processes are characterized by the change of the charge of both projectile and target nuclei by one or more units, leaving unchanged their mass number

$$A(Z_A, N_A) + a(Z_a, N_a) \rightarrow B(Z_A \pm n, N_A \mp n) + b(Z_a \mp n, N_a \pm n)$$

or

$$A(Z_A, N_A) + \pi^{\pm} \rightarrow B(Z_A \pm k, N_A \mp k) + \pi^{\mp(k-1)} \tag{1.52}$$

where $n = 1, 2 \cdots \min\{Z_A, N_A, Z_a, N_a\}$ represents the number of nucleons exchanged, while $k = 1, 2$ indicates the change in charge of both pion and nucleus. The first line of eq. (1.52) refers both to direct and multi - nucleon transfer processes, because only initial and final channels are indicated, omitting possible intermediate states, leading to the same

final nuclear system, while the second line of course refers only to direct charge changing nuclear reactions. These kind of processes could help in further constraining the existing plethora of nuclear structure models, that offer discrepant descriptions of many properties of nuclei (magnetic moments, energy levels in odd - odd nuclei and spin - isospin resonances [9]). Particular interest has been reversing on direct single ($n = 1, k = 1$) and double ($n = 2, k = 2$) charge exchange reactions due to their wide range of exploration about the properties of nucleons within the nuclear medium, as shown in the next two sections.

1.2.1 Single Charge Exchange Reactions

After the first pioneering explorations [72, 73], the study of "direct" single charge exchange (SCE) reactions, both pion [74, 75] and light ion induced, was soon extended to transitions associated to spin degrees of freedom [76, 77]. High energy light ion SCE reactions, like high energy (p, n) and (n, p) processess, have been widely studied [2, 9, 78, 79], giving important information on charge exchange resonances (e. g. Isobaric analog resonance and Gamow-Teller giant resonance) and on spin - isospin effective interactions. In particular, considerable interest has been reversed on the monopole component, $\Delta L = 0$, of light ion induced SCE reactions, since the operator describing such transitions in spin - isospin space is analogous to the one describing GT β decays [80].

Heavy ion SCE reactions carry informations complemetary to light ion ones, allowing the study higher multipolarity transitions, thus extending the investigation to the nuclear structure of the so called forbidden transitions, not accessible through β decays.

The theoretical formalism of SCE reactions was developed in '80s by Taddeucci et al. [2] for high energy (p, n) reactions, while a theory for heavy ion charge exchange reactions at low and intermediate energies is for the first time provided by the present PhD work together with an

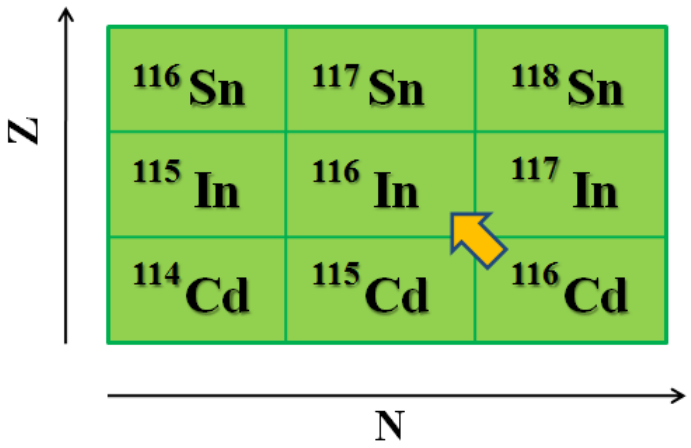

Figure 1.8: Example of "direct" single charge exchange reaction, for ^{116}Cd $\rightarrow^{116}$ In transition, as indicated by the arrow.

extension to heavy ions of the proportionality relation found between the forward angular distribution for (p, n) reactions and beta decay nuclear matrix element [2, 7], as shown in chapter 3.

1.2.2 Double Charge Exchange Reactions

"Direct" double charge exchange (DCE) nuclear reactions consist in the simultaneous exchange of two nucleons ($\Delta T_z = \pm 2$) between projectile and target nuclei

$$A(N_A, Z_A) + a(N_a, Z_a) \rightarrow B(N_A, Z_A \pm 2) + b(N_a, Z_a \mp 2) \qquad (1.53)$$

While SCE processes can be studied both with light and heavy ions, DCE reactions with light nuclei present difficulties like dealing with the measurement and reconstruction of the trajectory of three different final projectile particles, problems avoided by using heavy ions both for projectile and target [81]; however, light ions represent an interesting tool for searching of exotic systems, e. g. the tetra-neutron system through the reaction ^{4}He(^{8}He,^{8} Be)$4n$ [82].

Heavy ion DCE processes can be regarded as multipurpose probes,

further constraining nuclear structure models, because such reactions allow to:

- probe spin - isospin terms of nuclear effective interaction;
- probe high multipolarity collective modes;
- probe new nuclear physics phenomena, like double Gamow-Teller resonance [83];
- probe nucleon - nucleon pairing correlations inside nuclei;
- get information on double beta decay nuclear matrix element.

In the present work main attention is turned to the latter point.

As shown in the next chapters, heavy ion DCE processes are mainly direct (i. e. surface) nuclear reactions, so that a perturbative approach allows to describe such processes in terms of two SCE reactions, by two different mechanisms:

1. DCE processes can be interpreted as a sequence of two independent SCE reactions, i. e. the two nucleons are exchanged incoherently, thus revealing the analogy with $2\nu\beta\beta$, both for zero angular and (also small) linear momentum transfer.
2. In DCE reactions, the two nucleons are exchanged coherently (coherent sum of two SCE processes), thus allowing to obtain a diagrammatical structure strongly resembling the one describing $0\nu\beta\beta$ decay. The different nature of the off - shell propagators describing the two processes made the determination of a proportionality relation between DCE cross section and $0\nu\beta\beta$ decay strength quite difficult, in that it is first of all necessary to be sure of the analogy between the nuclear matrix elements of the two processes; very recently, different nuclear structure calculations (non - relativistic

energy density functional model, shell - model [3] and interacting boson model [4]) reveal the existence of a nearly linear proportionality relation between heavy ion DCE - DGT and $0\nu\beta\beta$ nuclear matrix elements, even if an analytical determination of such relation is anything but straightforward and is still a subject under study [5].

The above different DCE mechanisms are shown in fig. 1.9, together with the weak decay processes they look like, and an example of the

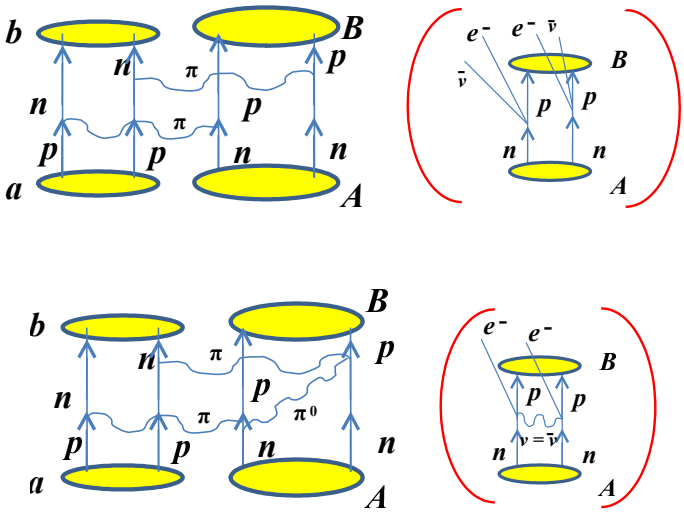

Figure 1.9: In the upper part, a scheme of $2\nu\beta\beta$-like DCE process (left panel) and the analog weak $2\nu\beta\beta$ process (right panel) is shown; in the lower part of the figure, $0\nu\beta\beta$-like DCE process, i. e. two correlated SCE nuclear reactions, (left panel) and the analog $0\nu\beta\beta$ decay (right panel) are illustrated.

corresponding patterns crossed in the nuclear chart are illustrated in fig. 1.10.

However, it is anything but straightforward to extract information on $0\nu\beta\beta$ decay strength, because of the competition between the two DCE mechanisms listed above. Nevertheless, it is pleasing that the second mechanism strongly depends on nuclear correlations, which become more

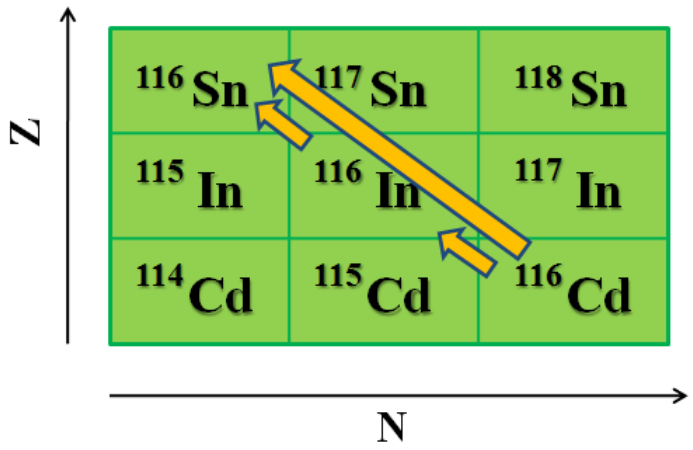

Figure 1.10: Example of "direct" double charge exchange nuclear reaction, leading to the transition ^{116}Cd $\rightarrow^{116}$ Sn. The first mechanism, described in the text, is the one given by the reactions indicated by the two short arrows, while the second mechanism in the text is represented by the long arrow, directly linking initial and final nuclei.

and more important as energy decreases [84], so that the low - energy range would be a promising research tool.

In this thesis main attention has been focused on the point 1, described below in the present chapter, in order to understand to what extent this "competing" process dominates or is dominated by the "golden" one.

As stated in the previous sections, the reason why a lot of interest is turning toward the determination of a relation between the nuclear matrix elements of DCE reaction and of $0\nu\beta\beta$ decay lies in the large differences among $0\nu\beta\beta$ NME values determined by using different nuclear structure models [52].

The first alternative attempt for $0\nu\beta\beta$ NME determination was made by studying the $(\pi^{\pm},\pi^{\mp})$ DCE pion-nucleus $(\pi - N)$ reactions [83, 85–87], but such processes are described by different kind of operators [55, 56, 88], so that they do not give information on $0\nu\beta\beta$ NMEs. Early studies of heavy-ion induced DCE reactions didn't lead to significant results, because of the lack of zero degree data and the poor yields in the

measured energy spectra and angular distributions, due to the very low cross sections observed [80], ranging from about $5 - 40\,nb/sr$ [89, 90] to $10\,\mu b/sr$ [91, 92].

Recently, high resolution and large acceptance spectrometers are available, allowing to overcome the main experimental challenges of heavy ion DCE reactions. This has been leading to a renewed increasing interest on the study of the latter nuclear reactions, guided by the analogies between heavy ion DCE processes and $0\nu\beta\beta$ decays [1], despite the former is mediated by the nuclear strong interaction (charged meson exchange) and the latter by weak interaction (weak charged boson exchange):

1. the same initial and final nuclei are involved;

2. both processes can be described by the same Gamow-Teller, Fermi and rank-2 tensor operators, but combined through different coefficients, whose weight varies changing beam energy;

3. in the intermediate off-shell states, large angular and linear momentum ($\sim 100\,MeV/c$) are involved;

4. both processes are non-local and characterized by 2 vertices localized in the same pair of valence nucleons;

5. the same nuclear medium is involved, so that in medium effects are expected to influence the system in both cases (giving the possibility to extract information on g_A quenching);

6. both processes are characterized by an off-shell propagator.

Moreover, "direct" DCE processes can be mimicked by different competing mechanisms, which do not give any information on $0\nu\beta\beta$ strength (for example all combinations of two two-nucleon transfer processes and the combination of two-nucleon transfer with single charge exchange processes), so that their effect must be minimized.

Nowadays there are three main experiments on heavy ion DCE reactions:

1. NUMEN at INFN − LNS (Italy), looking for a link between heavy ion DCE and $0\nu\beta\beta$ nuclear matrix elements, which already performed DCE reaction experiments for ^{40}Ca(^{18}O,^{18} Ne)^{40}Ar (pilot experiment [1]) and ^{116}Sn(^{18}O,^{18} Ne)^{116}Cd heavy systems, both at $15\,AMeV$, but many other systems, invoving candidate $0\nu\beta\beta$ nuclei, are work in progress [93];

2. HIDCX at RCNP (Japan), looking for double Gamow-Teller resonance (which is related to $0\nu\beta\beta$ decay [3]) by using heavy ions [94, 95].

3. RIBF at RIKEN (Japan), exploring exotic nuclear systems (neutron drip-line nuclei) through DCE reactions with radioactive beams [82].

the first two looking for a connection with $\beta\beta$ decays, which is the focus of the present work. In particular, the formalism developed for heavy ion DCE reactions, described in terms of a sequence of two SCE processes is illustrated in chapter 4.

1.2.3 Transfer Reactions

Transfer reactions are nuclear processes characterized by the exchange, or a sequence of exchanges, of nucleons (or cluster of nucleons) between projectile and target nuclei, caused by nuclear mean field potential interactions; hence, such reactions bring on changes in the mass number and/or in the charge of both target and projectile nuclei. Multi-nucleon transfer transitions can lead to a change of the only charge of the interacting nuclei, like the "direct" single and double charge exchange reactions, described above. Transfer reactions represent the main processes competing with the direct charge exchange: already at single charge exchange

level, transfer processes are described by operators of completely different nature with respect to those describing Gamow-Teller- and Fermi-like transitions [92, 96–99], thus do not carrying any information on beta decay matrix element.

Fig. 1.11 shows the nuclei involved in multi - nucleon transfer transitions e. g. for the nucleus ^{116}Cd, which is one of the ions used as target in NUMEN experiment. The upper panel of fig. 1.11 shows the two

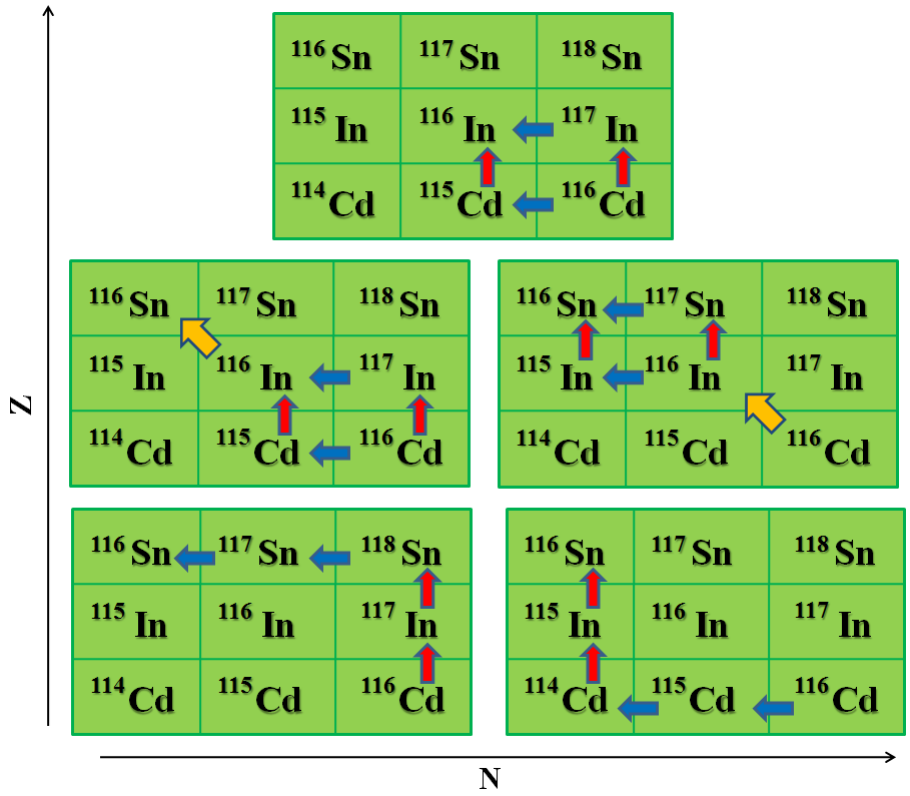

Figure 1.11: Example of the pattern, in nuclear chart, followed by nuclear transfer reactions leading from ^{116}Cd to ^{116}In (upper panel) and to ^{116}Sn (central and lower panels). The blue and the red arrows, in the figure, represent neutron and proton exchange, respectively. E. g. the single charge exchange transition ^{116}Cd $\rightarrow^{116}$ In can proceed, by means of transfer processes, via two possible patterns: ^{116}Cd $\rightarrow^{115}$ Cd $\rightarrow^{116}$ In (lower path) or ^{116}Cd $\rightarrow^{117}$ In $\rightarrow^{116}$ In (upper path). The same holds for double charge exchange processes, which can proceed via different SCE direct and transfer combinations (third order processes), shown in the intermediate panels, or by four-nucleon transfer (fourth order processes), in the two lower panels.

possible patterns, across the table of nuclides, through which the single charge exchange via two nucleon transfer can proceed:

by one neutron pick-up and one proton stripping (see chapter 2), viz.

$$\begin{aligned} &A(Z_A, N_A) + a(Z_a, N_a) \rightarrow C(Z_A, N_A - 1) + c(Z_a, N_a + 1) \\ &\rightarrow B(Z_A + 1, N_A - 1) + b(Z_a - 1, N_a + 1) \end{aligned} \tag{1.54}$$

or by one proton stripping and one neutron pick-up

$$\begin{aligned} &A(Z_A, N_A) + a(Z_a, N_a) \rightarrow C(Z_A + 1, N_A) + c(Z_a - 1, N_a) \\ &\rightarrow B(Z_A + 1, N_A - 1) + b(Z_a - 1, N_a + 1) \end{aligned} \tag{1.55}$$

both cases revealing that they are second order processes, while direct single charge exchange is of first order (see fig. 1.8).

The intermediate and lower panels of fig. 1.11 illustrate three (two - nucleon transfer plus direct single charge exchange) and four nucleon transfer processes, respectively, leading to a double charge exchange transition. The former ones are third order and the second are fourth order processes against the "direct" double charge exchange reactions, which are second or first order processes, depending on the DCE mechanism explored.

Because transfer reactions are higher order processes than the corresponding direct charge exchange transitions, they are expected to be neglegible with respect to the latter ones.

Studies performed in the early '70s show that heavy ion transfer cross section, for beam energies well above Coulomb barrier, can be large if some kinematical conditions (Brink's kinematical conditions), depending on the $Q-$value of the transfer reaction, are satisfied [100]. Conversely, by properly choosing beam energy, projectile and target nuclei, it is possible to mismatch these conditions, thus keeping transfer cross section (for heavy nuclei) lower than that for "direct" processes.

In fact, a work of the late '80s [101] proved that for heavy systems ($A \sim 12$) at energies $E \sim 100\, AMeV$ the "direct" charge exchange pro-

cesses safely dominate over the transfer ones, as illustrated in fig. 1.12.

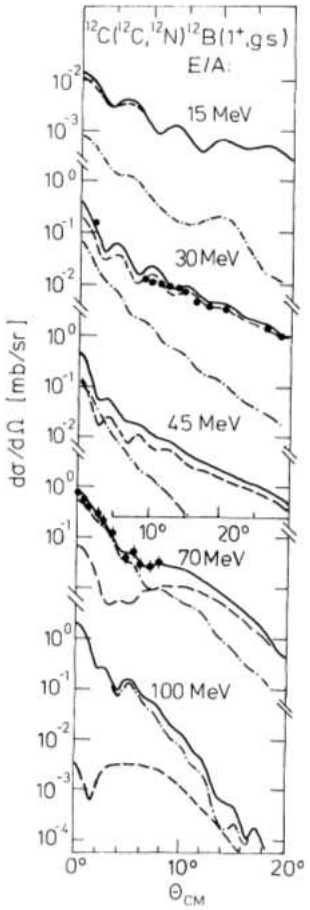

Figure 1.12: Comparison between "direct" (dotted-dashed line) and two-nucleon transfer (dashed line) single charge exchange angular distributions, for the reaction $^{12}C(^{12}C,^{12}N_{1^+_{g.s.}})^{12}B_{1^+_{g.s.}}$, for incident energies (per nucleon) in the range [10; 100] MeV [101].

Recent preliminary studies on the competition between "direct" and transfer single charge exchange processes for heavier nuclear systems at low and intermediate energies show a dominance of the "direct" process for small angular momentum transfer ($\Delta J \leqslant 1$) [102]; other preliminary results show that "direct" DCE processes dominate over all competing mechanisms [81], illustrated in the central and lower panels of fig. 1.11.

CHAPTER 2

CHARGE EXCHANGE NUCLEAR REACTIONS

2.1 Nuclear Reaction theory: some basic concepts

The main tool to get information on a nucleus is represented by the scattering of a given probe off the nucleus of interest; the probe can be a photon, a lepton, a meson, a nucleon or a complex nucleus, depending on the type of information one wants to get.

In this chapter, some basic theoretical concepts of the scattering theory are shown.

A free particle, moving with momentum $\mathbf{k}$,[1] is simply described by a plane wave, $\phi_{\mathbf{k}}(\mathbf{r}) = \langle \mathbf{r}|\phi_{\mathbf{k}}\rangle = e^{-i\mathbf{k}\cdot\mathbf{r}}$, which is eigenfunction of the kinetic hamiltonian operator (in non-relativistic regime) $\hat{H}_0 = \frac{\hat{\mathbf{k}}^2}{2m}$, with eigenvalue E, i. e. it is a solution of the time-independent Schrödinger equation

$$\hat{H}_0|\phi_{\mathbf{k}}\rangle = E|\phi_{\mathbf{k}}\rangle \tag{2.1}$$

A scattering process of a free particle (*projectile*) off the nucleus of

[1] Natural units, $\hbar = c = 1$, are used in the whole thesis, unless otherwise indicated.

interest (*target*) can be described in terms of a free particle encountering a short-ranged potential $V(\mathbf{r})$, i. e. $V(\mathbf{r}) \approx 0$ for $r \gg a$, where a is the size of the target; thus, the wave function describing the system is a solution of the following Schrödinger equation

$$(\hat{H}_0 + \hat{V})|\psi_{\mathbf{k}}\rangle = E|\psi_{\mathbf{k}}\rangle \tag{2.2}$$

One can immediately see that the latter equation reduces to the Schrödinger equation for free particles, eq. (2.1), for $r \gg a$. In order to solve eq. (2.2), i. e. to determine in which way the free hamiltonian eigenfunction is modified by the presence of the potential $V(\mathbf{r})$, it is usefull to reorder eq. (2.2) as

$$(E - \hat{H}_0)|\psi_{\mathbf{k}}\rangle = \hat{V}|\psi_{\mathbf{k}}\rangle \tag{2.3}$$

so that it can be treated as an inhomogeneous partial differentail equation (p.d.e.), with the inhomogeneity term just given by the potential; the total solution of such a p.d.e. is obtained by summing the solution of the corresponding homogeneous p.d.e., which is nothing but eq. (2.1), and a particular solution, given by $|\psi^{(\pm)}_{\mathbf{k}}\rangle = G^{(\pm)}(E)\hat{V}|\psi^{(\pm)}_{\mathbf{k}}\rangle$, where $G^{(\pm)}(E) = \frac{1}{E-H_0\pm i\epsilon}$ is the Green function; thus, the total solution is

$$|\psi^{(\pm)}_{\mathbf{k}}\rangle = |\phi_{\mathbf{k}}\rangle + \frac{1}{E - \hat{H}_0 \pm i\epsilon}\hat{V}|\psi^{(\pm)}_{\mathbf{k}}\rangle \tag{2.4}$$

or equivalentely, by introducing a transition operator, $\hat{T}$, such that $\hat{T}|\phi_{\mathbf{k}}\rangle = \hat{V}|\psi^{(+)}_{\mathbf{k}}\rangle$, and by multiplying both sides of eq. (2.4) by $\hat{V}$ on the left,

$$\begin{aligned} \hat{V}|\psi^{(+)}_{\mathbf{k}}\rangle &= \hat{V}|\phi_{\mathbf{k}}\rangle + \hat{V}\frac{1}{E - \hat{H}_0 \pm i\epsilon}\hat{V}|\psi^{(+)}_{\mathbf{k}}\rangle \\ \Rightarrow \quad \hat{T}|\phi_{\mathbf{k}}\rangle &= \hat{V}|\phi_{\mathbf{k}}\rangle + \hat{V}\frac{1}{E - \hat{H}_0 \pm i\epsilon}\hat{T}|\phi_{\mathbf{k}}\rangle \end{aligned} \tag{2.5}$$

Eq.s (2.4) and (2.5) represent the well known *Lippmann - Schwinger equation* [103, 104] for scattering states and for the transition operator $\hat{T}$, respectively; both are integral equations, as can be seen by projecting,

for example, eq. (2.4) on the coordinate space

$$\langle \mathbf{r}|\psi_{\mathbf{k}}^{(\pm)}\rangle = \langle \mathbf{r}|\phi_{\mathbf{k}}\rangle + \int d^3r' \langle \mathbf{r}|\frac{1}{E-\hat{H}_0 \pm i\epsilon}|\mathbf{r}'\rangle\langle \mathbf{r}'|\hat{V}|\psi_{\mathbf{k}}^{(\pm)}\rangle \tag{2.6}$$

It is possible to show that the kernel of eq. (2.6),

$$G^{(\pm)}(\mathbf{r},\mathbf{r}') \equiv \frac{1}{2m}\langle \mathbf{r}|\frac{1}{E-\hat{H}_0 \pm i\epsilon}|\mathbf{r}'\rangle \tag{2.7}$$

is just the solution of Helmholtz equation

$$(\nabla^2 + k^2)G^{(\pm)}(\mathbf{r},\mathbf{r}') = \delta(\mathbf{r}-\mathbf{r}') \tag{2.8}$$

i. e.

$$G^{(\pm)}(\mathbf{r},\mathbf{r}') = -\frac{1}{4\pi}\frac{e^{\pm ik|\mathbf{r}-\mathbf{r}'|}}{|\mathbf{r}-\mathbf{r}'|} \tag{2.9}$$

Hence, (2.6) becomes

$$\langle \mathbf{r}|\psi_{\mathbf{k}}^{(\pm)}\rangle = \langle \mathbf{r}|\phi_{\mathbf{k}}\rangle - 2m\int d^3r' \,\frac{1}{4\pi}\frac{e^{\pm ik|\mathbf{r}-\mathbf{r}'|}}{|\mathbf{r}-\mathbf{r}'|}\langle \mathbf{r}'|\hat{V}|\psi_{\mathbf{k}}^{(\pm)}\rangle \tag{2.10}$$

$G^{(\pm)}(\mathbf{r},\mathbf{r}')$ is also called "propagator" of the interaction. It is straightforward to note that the total wave function can be written as the sum of the incident wave, $\langle \mathbf{r}|\phi_{\mathbf{k}}\rangle$, and the "scattered" wave function. Experimentally, it is possible to gain information on the physical system through its interaction with the deterctors, which are placed at a distance r much greater than the interacton potential range, r', i. e. detectors are placed in the asymptotic region; thus, in the limit $r \gg r'$, the modulus $|\mathbf{r}-\mathbf{r}'|$ in the exponential of the propagator can be approximated to $r - \hat{\mathbf{r}}\cdot\mathbf{r}'$ and $|\mathbf{r}-\mathbf{r}'|$ at the denominator simply reduces to r, so that the propagator simplifies to

$$G^{(\pm)}(\mathbf{r},\mathbf{r}') \underset{r\to\infty}{\longrightarrow} -\frac{1}{4\pi}\frac{e^{\pm ikr}e^{\mp i\mathbf{k}'\cdot\mathbf{r}'}}{r} \tag{2.11}$$

where $\mathbf{k}' \equiv k\hat{\mathbf{r}}$ is the momentum of the (elastically) scattered nucleus. Hence, asymptotically eq. (2.10) becomes

$$\langle \mathbf{r}|\psi_{\mathbf{k}}^{(+)}\rangle \underset{r\to\infty}{\longrightarrow} \langle \mathbf{r}|\phi_{\mathbf{k}}\rangle - \frac{m}{2\pi}\frac{e^{ikr}}{r}\int d^3r' \, e^{-i\mathbf{k}'\cdot\mathbf{r}'}\langle \mathbf{r}'|V|\psi_{\mathbf{k}}^{(+)}\rangle \tag{2.12}$$

or

$$\psi_{\mathbf{k}}^{(+)}(\mathbf{r}) \underset{r\to\infty}{\longrightarrow} \frac{1}{(2\pi)^{3/2}}\left[e^{i\mathbf{k}\cdot\mathbf{r}} + \frac{e^{ikr}}{r}f(\mathbf{k},\mathbf{k}')\right] \tag{2.13}$$

i. e. the total scattered wave function can be expressed as the sum of the original *incoming* plane wave plus an *outcoming* spherical wave, which represents the effect of the scattering, with "scattering amplitude" given by

$$f(\mathbf{k},\mathbf{k}') \equiv -\frac{m}{2\pi}(2\pi)^{3/2}\langle\phi_{\mathbf{k}'}|\hat{V}|\psi_{\mathbf{k}}^{(+)}\rangle \tag{2.14}$$

or, in terms of transition operator $\hat{T}$

$$f(\mathbf{k},\mathbf{k}') \equiv -\frac{m}{2\pi}(2\pi)^{3/2}\langle\phi_{\mathbf{k}'}|\hat{T}|\phi_{\mathbf{k}}\rangle \tag{2.15}$$

The solution $\psi_{\mathbf{k}}^{(-)}(\mathbf{r})$, which corresponds to the time-reversed of $\psi_{\mathbf{k}}^{(+)}(\mathbf{r})$, has not been taken into account because it corresponds to the original plane wave plus an *incoming* spherical wave, but there is no source at $r \to +\infty$ producing the latter one. The scattering amplitude is of fundamental importance in scattering theory, because it is directly related to the differential scattering cross section, which is a physical observable, by the well known relation

$$\frac{d\sigma}{d\Omega} = |f(\mathbf{k},\mathbf{k}')|^2 \tag{2.16}$$

as can be derived from cross section definition.

It is important to note that in general the interaction potential $V(\mathbf{r},\mathbf{r}')$ can be non-local, but sometimes effective *local* potentials are used, i.e. $V(\mathbf{r},\mathbf{r}') = V(\mathbf{r})\delta(\mathbf{r}-\mathbf{r}')$, so that the matrix element $\langle\mathbf{r}'|V|\psi_{\mathbf{k}}^{(+)}\rangle$ simplifies to

$$\begin{aligned}\langle\mathbf{r}'|V|\psi_{\mathbf{k}}^{(+)}\rangle &= \int d^3\mathbf{r}''\langle\mathbf{r}'|V(\mathbf{r}',\mathbf{r}'')|\mathbf{r}''\rangle\langle\mathbf{r}''|\psi_{\mathbf{k}}^{(+)}\rangle \\ &\simeq V(\mathbf{r}')\langle\mathbf{r}'|\psi_{\mathbf{k}}^{(+)}\rangle \\ &= V(\mathbf{r}')\psi_{\mathbf{k}}^{(+)}(\mathbf{r}')\end{aligned} \tag{2.17}$$

so that eq. (2.12) becomes

$$\begin{aligned}\psi^{(+)}_{\mathbf{k}}(\mathbf{r}) &\underset{r\to\infty}{\longrightarrow} \frac{e^{i\mathbf{k}\cdot\mathbf{r}}}{(2\pi)^{3/2}} - \frac{m}{2\pi}(2\pi)^3\frac{e^{ikr}}{r}\int d^3r'\,\frac{e^{-i\mathbf{k}'\cdot\mathbf{r}'}}{(2\pi)^{3/2}}V(\mathbf{r}')\psi^{(+)}_{\mathbf{k}}(\mathbf{r}') \\ &= \phi_{\mathbf{k}}(\mathbf{r}) - \frac{m}{2\pi}\frac{e^{ikr}}{r}\int d^3r'\,\phi^*_{\mathbf{k}'}(\mathbf{r}')V(\mathbf{r}')\psi^{(+)}_{\mathbf{k}}(\mathbf{r}')\end{aligned} \tag{2.18}$$

Even if simplified with respect to (2.12), in eq. (2.18) one still has the unknown wave function, $\psi^{(+)}_{\mathbf{k}}(\mathbf{r})$, inside the integral, inhibiting a general analytical resolution of the problem.

By observing that plane waves, $|\phi_{\mathbf{k}}\rangle$, represent a basis (of the Hilbert space of free particle states), equation (2.5) can be trasformed into a relation among operators

$$T = V + V\frac{1}{E - H_0 \pm i\epsilon}T \tag{2.19}$$

The solution of this equation can be found iteratively, as

$$T = V + V\frac{1}{E - H_0 \pm i\epsilon}V + V\frac{1}{E - H_0 \pm i\epsilon}V\frac{1}{E - H_0 \pm i\epsilon}V + \cdots \tag{2.20}$$

which gives an exact expression for T. In this way, it is possible to express the scattering amplitude as a series

$$f(\mathbf{k},\mathbf{k}') = \sum_{n=1}^{\infty} f^{(n)}(\mathbf{k},\mathbf{k}') \tag{2.21}$$

2.1.1 Plane Wave Born Approximation

Hence, in order to analytically solve Lippmann Schwinger equation, it is necessary to make some approximation. The most simple approximation is represented by the (first order) Born approximation. The first order Born approximation (or Plane Wave Born Approximation, PWBA), just consists in the identity $T = V$, which means nothing but replacing $\psi^{(+)}_{\mathbf{k}}(\mathbf{r})$ inside the integral with a plane wave, so that the scattering amplitude simplifies to

$$f(\mathbf{k},\mathbf{k}') = f_{\mathbf{k},\mathbf{k}'}(\theta) = -\frac{m}{2\pi}\int d^3r'\,e^{i\mathbf{q}\cdot\mathbf{r}'}V(\mathbf{r}') \tag{2.22}$$

where θ is the angle between $\mathbf{k}$ and $\mathbf{k}'$, i. e. the scattering angle; eq. (2.22) is just the Fourier transform of the interaction potential and is a function of the momentum transfer $\mathbf{q} = \mathbf{k} - \mathbf{k}'$. It is well known that first order Born approximation violates the Optical Theorem

$$\sigma_{tot} = \frac{4\pi}{k} Im(f_{\mathbf{k},\mathbf{k}'}(\theta = 0)) \tag{2.23}$$

being k the modulus of the initial momentum of the projectile nucleus; indeed, first order Born scattering amplitude is purely real, so that one obtaines zero total cross section. This problem can be overcome by noting that the Optical Theorem gives an exact expression, so that it is necessary to stop at the correct order of the Born amplitude; thus, because at first order $f_{\mathbf{k},\mathbf{k}'}(\theta)$ has zero imaginary part, it is necessary to stop at the second order Born amplitude to calculate the first order Born scattering cross section.

The PWBA is a (non-perturbative) expansion of the transition matrix element in powers of the potential V, around $V = 0$, and works only when the following condition is satisfied:

$$C(k) = |\frac{\phi_k(0) - \psi_k(0)}{\phi_k(0)}| \ll 1 \tag{2.24}$$

Using eq. (2.10) for $\psi_k(\mathbf{r})$ at $\mathbf{r} = \mathbf{0}$, the condition (2.24) becomes

$$|2m(2\pi)^{\frac{3}{2}} \int d^3r' \, \frac{1}{4\pi} \frac{e^{ikr'}}{r'} \langle \mathbf{r}' | \hat{V} | \phi_{\mathbf{k}} \rangle| \ll 1 \tag{2.25}$$

which is verified at high energies, i. e. for $k \gg 1$, so that $e^{ikr'} \to 0$, because of its rapid oscillations, while, at low eneriges, i. e. when k is small compared with the inverse of the range of the interaction potential ($\sim 1/r'$), so that $e^{ikr'} \simeq 1$, the above condition is realized when the potential is neither too much intense nor too long ranged.

2.1.2 Distorted Wave Born Approximation

When Born approximation cannot be applied, as for the very strong potentials involved in nuclear reactions, a more sophisticated method,

called *distorted wave Born approximation* (DWBA), is often used. This approximation can be applied whenever the interaction potential can be expressed as the sum of two potentials, $V = V_I + V_{II}$, such that the Schrödinger equation for a particle subject to V_I is exactly (or at least within a good approximation) solvable and the effects of the remaining term, V_{II}, are small compared to V_I, so that its wave function can be calculated within the first order Born approximation. Thus, in DWBA the eigenfunction of the hamiltonian $\hat{H}_I = \hat{H}_0 + \hat{V}_I$, i. e. the solution of the Lippmann-Schwinger equation

$$\chi_{\mathbf{k}}(\mathbf{r}) \underset{r\to+\infty}{\longrightarrow} \phi_{\mathbf{k}}(\mathbf{r}) - \frac{m}{2\pi}\frac{e^{ikr}}{r}\int d^3r'\, e^{-i\mathbf{k}'\cdot\mathbf{r}'} V_I(\mathbf{r}')\chi_{\mathbf{k}}(\mathbf{r}') \tag{2.26}$$

can be easily calculated; $\chi_{\mathbf{k}}(\mathbf{r})$ is called *distorted wave*. Then, the total scattering wave function must solve the Schrödinger equation

$$\left(E_I - \hat{H}_I\right)\psi^{(+)}_{\mathbf{k}}(\mathbf{r}) = V_{II}\psi^{(+)}_{\mathbf{k}}(\mathbf{r}) \tag{2.27}$$

or the equivalent Lippmann-Schwinger equation

$$\psi^{(+)}_{\mathbf{k}}(\mathbf{r}) = \chi^{(+)}_{\mathbf{k}}(\mathbf{r}) + \int d^3r'\, G_I(\mathbf{r},\mathbf{r}')V_{II}(\mathbf{r}')\psi^{(+)}_{\mathbf{k}}(\mathbf{r}') \tag{2.28}$$

where now G_I describes the propagation of the wave function in presence of the distorting potential V_I, i. e. $G_I(\mathbf{r},\mathbf{r}') = \langle\mathbf{r}|\frac{1}{E_I-\hat{H}_I+i\epsilon}|\mathbf{r}'\rangle$, which asymptotically becomes $G_I(\mathbf{r},\mathbf{r}') \underset{r\to+\infty}{\longrightarrow} -\frac{1}{4\pi}\frac{e^{ikr}}{r}\chi_{\mathbf{k}'}(\mathbf{r}')^{(-)*}$, thus leading to the asymptotic scattering wave function

$$\begin{aligned}\psi^{(+)}_{\mathbf{k}}(\mathbf{r}) &\underset{r\to+\infty}{\longrightarrow} \chi^{(+)}_{\mathbf{k}}(\mathbf{r}) - \frac{m}{2\pi}\frac{e^{ikr}}{r}\int d^3r'\,\chi_{\mathbf{k}'}(\mathbf{r}')^{(-)*}V_{II}(\mathbf{r}')\psi^{(+)}_{\mathbf{k}}(\mathbf{r}') \\ &\overset{DWBA}{\simeq} \chi^{(+)}_{\mathbf{k}}(\mathbf{r}) - \frac{m}{2\pi}\frac{e^{ikr}}{r}\int d^3r'\,\chi_{\mathbf{k}'}(\mathbf{r}')^{(-)*}V_{II}(\mathbf{r}')\chi^{(+)}_{\mathbf{k}}(\mathbf{r}')\end{aligned} \tag{2.29}$$

In order to derive the DWBA expression for the scattering amplitude, let's consider the Lippmann-Schwinger equations for distorted and total scattering wave functions in terms of kets

$$|\chi^{(+)}_{\mathbf{k}}\rangle = |\phi_{\mathbf{k}}\rangle + G^{(+)}V_I|\chi^{(+)}_{\mathbf{k}}\rangle \tag{2.30}$$

and

$$|\psi_{\mathbf{k}}^{(+)}\rangle = |\phi_{\mathbf{k}}\rangle + G^{(+)}\left(V_I + V_{II}\right)|\psi_{\mathbf{k}}^{(+)}\rangle \tag{2.31}$$

The transition matrix element is defined as

$$\langle\phi_{\mathbf{k}'}|T|\phi_{\mathbf{k}}\rangle \equiv \langle\phi_{\mathbf{k}'}|\left(V_I + V_{II}\right)|\psi_{\mathbf{k}}^{(+)}\rangle \tag{2.32}$$

using eq. (2.30), the plane wave bra on the right hand side can be expressed in terms of the distorted wave $\chi_{\mathbf{k}}^{(+)}$, so that

$$\begin{aligned}
&\langle\phi_{\mathbf{k}'}|\left(V_I + V_{II}\right)|\psi_{\mathbf{k}}^{(+)}\rangle = \{\langle\chi_{\mathbf{k}'}^{(+)}| - \langle\chi_{\mathbf{k}'}^{(+)}|V_I G^{(+)}\}\left(V_I + V_{II}\right)|\psi_{\mathbf{k}}^{(+)}\rangle \\
&= \langle\chi_{\mathbf{k}'}^{(+)}|V_{II}|\psi_{\mathbf{k}}^{(+)}\rangle + \langle\chi_{\mathbf{k}'}^{(+)}|V_I|\phi_{\mathbf{k}}\rangle \\
&\overset{DWBA}{\simeq} \langle\chi_{\mathbf{k}'}^{(+)}|V_{II}|\chi_{\mathbf{k}}^{(+)}\rangle + \langle\chi_{\mathbf{k}'}^{(+)}|V_I|\phi_{\mathbf{k}}\rangle \\
&= t_I + \langle\chi_{\mathbf{k}'}^{(+)}|V_{II}|\chi_{\mathbf{k}}^{(+)}\rangle
\end{aligned} \tag{2.33}$$

where in the second step eq. (2.31) is used and t_I is the transition matrix element obtained from V_I. Thus, the second term in the DWBA transition amplitude can be interpreted as the Born approximation for scattering by V_{II} in the presence of the distorting potential V_I. From eq. (2.33) it is straightforward to derive the DWBA scattering amplitude

$$f_{DWBA}(\mathbf{k},\mathbf{k}') = f_I(\mathbf{k},\mathbf{k}') - \frac{e^{ikr}}{4\pi r}\int d^3r'\,\chi_{\mathbf{k}'}^{(-)*}(\mathbf{r}')V_{II}(\mathbf{r}')\chi_{\mathbf{k}}^{(+)}(\mathbf{r}') \tag{2.34}$$

being $f_I(\mathbf{k},\mathbf{k}')$ the scattering amplitude for a particle interacting only through $V_I(\mathbf{r})$.

Often, in nuclear reaction theory the distorted waves account for elastic scattering, while the effect of the inelastic nuclear interaction under study is described by the potential V_{II}. Hence, the validity of the DWBA depends upon elastic scattering being the most important event which occurs when two nuclei collide, so that other events can be treated as perturbations [105]. The DWBA, differentely from PWBA, allows to obtain good predictions of absolute cross sections and works pretty well for different nuclear systems in a wide energy range [106], [96].

2.1.3 Optical Potential

An improvement of the DWBA can be obtained by using a complex V_I potential,$V_I = U_I + iW_I$, in order to take into account both elastic scattering and all inelastic channels other than the reaction channel considered, constituting the so called "initial/final state interactions". Indeed, it is the analogy between optical diffraction phenomena and the diffraction pattern shown by most of the nuclear reaction angular distributions, that leads to the introduction of a complex potential, with real and imaginary parts playing the same role as that of a complex refraction index in optics: the real part describes the scattering of the projectile nucleus (the incident wave) on the target nucleus (the obstacle) while the imaginary part deals with the loss of probability flux from the elastic channel and the channel of interest (light does not pass through the obstacle, i. e. light is absorbed) into other open reaction channels. In this way, the introduction of an imaginary potential takes into account the inelastic reaction channels competing with the process of interest.

Optical potentials are often parameterized in terms of energy - dependent Woods - Saxon functions as follows

$$\begin{aligned}
&\mathfrak{Re}(U_{opt}(r)) = V(r) = -V_0 f(r, R, a) \\
&\mathfrak{Im}(U_{opt}(r)) = W(r) = W_V(r) + W_S(r) = \\
&- W_{0_V}(E) f(r, R_{I_V}, a_{I_V}) + 4a_{I_S} W_{I_S} \frac{df(r, R_{I_S}, a_{I_S})}{dr} \\
&\mathfrak{Re}(U^{LS}_{opt}(r)) = V^{LS}(r) = V^{LS}_0(E) \frac{1}{r} \frac{df(r, R_{LS}, a_{LS})}{dr} \\
&\mathfrak{Im}(U^{LS}_{opt}(r)) = W^{LS}(r) = W^{LS}_0(E) \frac{1}{r} \frac{df(r, R_W, a_W)}{dr}
\end{aligned} \tag{2.35}$$

where E is the beam energy and $f(r, R_i, a_i) = \left[1 + e^{\frac{r-R_i}{a_i}}\right]^{-1}$, with parameters determined by fitting elastic scattering cross section data. The subscripts V, S and LS indicate volume, surface and spin-orbit components of the interaction potentials, respectively, the latter term, in turn including a volume and a surface component, too.

In case of lack of experimental elastic cross section data, both real and imaginary parts of the optical potential can be derived through single or double folding of a phenomenological nucleon-nucleon potential with projectile and target nuclear density profiles; such phenomenological potential depends on parameters that are optimized to fit nucleon - nucleon available elastic cross sections.

For treating inelastic scattering processes in which initial and final channels can be related by more than one step, the *coupled channel* method [107][108] is often used, instead of higher order expansion of PWBA and DWBA. Indeed, the coupled channel method accounts also for the couplings among all the possible reaction channels leading to the final channel of interest (e. g. all those channels of the direct reaction model space) [108], while the coupling with the inelastic processes, involving channels other than the one of interest, is taken into account by means of complex optical potentials.

2.1.4 Partial wave expansion

DWBA scattering amplitude, eq. (2.34), cannot be simply expressed as the Fourier transform of the interaction potential, like in PWBA case, and in general distorted waves cannot be combined easily as for plane waves; hence, in order to simplify calculations, it is convenient to work in terms of *partial wave componets* of the system wave function.

It is well known that for spherically symmetric potentials, the wave function of the system can be factorized into the product of radial ($R(r)$) and angular ($F(\hat{r})$) functions and the 3D Schrödinger equation

$$\left(\nabla^2 + k^2\right) \psi_{\mathbf{k}}(\mathbf{r}) = U(\mathbf{r})\psi_{\mathbf{k}}(\mathbf{r}) \tag{2.36}$$

reduces to 1D radial equation plus a centrifugal barrier[2],

$$\left[\frac{d^2}{d\rho^2} + \frac{2}{\rho}\frac{d}{d\rho} + 1 - \frac{l(l+1)}{\rho^2}\right] R_l(\rho) = \mathcal{U}(\rho) R_l(\rho) \tag{2.37}$$

being the angular dependence described by the spherical harmonics, $F(\hat{r}) = Y_{lm}(\hat{r})$. The solution for the easiest scenario, a free system, is given by the plane wave,

$$\psi_{\mathbf{k}}(\mathbf{r}) = \frac{e^{i\mathbf{k}\cdot\mathbf{r}}}{(2\pi)^{3/2}} =< \mathbf{r}|\mathbf{k} > \tag{2.38}$$

on the one side; on the other side, eq. (2.37) in the free case reduces to the well known Ricatti - Bessel equation, whose solutions are given by the spherical Bessel functions, $j_l(\rho)$, thus leading to a total wave function of the form

$$\psi_{\mathbf{k}}(\mathbf{r}) = C_l j_l(kr) Y_{lm}(\hat{r}) =< \mathbf{r}|Elm > \tag{2.39}$$

being C_l a normalization constant. Due to the unicity of the solution of a partial derivative differential equation with fixed boundary conditions, the two solutions of the Schrödinger equation must coincide; in fact, it is possible to link the two solutions, simply by writing

$$< \mathbf{r}|\mathbf{k} >= \sum_{l,m} \int dE \ < \mathbf{r}|Elm >< Elm|\mathbf{k} > \tag{2.40}$$

where $< Elm|\mathbf{k} >$ is nothing but the complex conjugated of the Fourier transform of (2.39),

$$\psi(\mathbf{k}) = B_l \delta\left(\frac{\hbar^2 k^2}{2\mu} - E\right) Y_{lm}(\hat{k}) \tag{2.41}$$

where B_l is a normalization constant. After some simplifications, the relation (2.40) leads to the well known partial wave expansion of the plane wave

$$\varphi_{\mathbf{k}}(\mathbf{r}) = 4\pi \sum_l i^l j_l(kr) \sum_m Y_{lm}(\hat{r}) Y^*_{lm}(\hat{k}) \tag{2.42}$$

[2]After some standard passages, like posing $\rho = kr$ and $\mathcal{U}(\rho) = U/E$, being E the total energy of the system.

that can be easily generalized to the case of a spherical symmetric potential

$$\chi_{\mathbf{k}}(\mathbf{r}) = 4\pi \sum_l i^l \frac{\chi_{l,k}(r)}{kr} \sum_m Y_{lm}(\hat{r}) Y^*_{lm}(\hat{k}) \tag{2.43}$$

Thus, the 3-dimensional Schrödinger equation for the distorted wave can be simplified into a sum of 1-dimensional radial Schrödinger equations, by making the partial wave decomposition of the distorted wave, i. e. making an expansion of the angular dependence of the wave function in terms of spherical harmonics. Moreover, working with partial waves allows to have a deeper insight into the angular components contributing to the total wave function of the system and hence to the cross section.

In terms of partial waves, the scattering amplitude can be expressed as the sum of partial wave scattering amplitudes, $f_l(E)$

$$\begin{aligned}
&f_{\mathbf{k}\mathbf{k}'}(\theta) = -\mu(2\pi)^2 < \mathbf{k}'|\hat{T}|\mathbf{k} > \\
&= -\mu(2\pi)^2 \sum_{l,m} \sum_{l',m'} \int dE \int dE' \ < \mathbf{k}'|E'l'm' >< E'l'm'|\hat{T}|Elm >< Elm|\mathbf{k} > \\
&= -\frac{\pi}{k} \sum_l (2l+1) T_l(E) P_l(\cos\theta) \\
&= \sum_l (2l+1) f_l(E) P_l(\cos\theta)
\end{aligned} \tag{2.44}$$

where μ is the reduced mass of the system; now the information on the scattering process is decomposed into its angular momentum components, with the radial part stored into the partial wave scattering amplitude, through the partial wave transition matrix $T_l(E)$,

$$f_l(E) \equiv -\frac{\pi}{k} T_l(E) \tag{2.45}$$

In the absence of inelastic processes (loss of probability flux out of the elastic channel), the partial wave scattering matrix $S_l \equiv 1 - 2\pi i T_l$ is a unitary operator and so it can be expressed as a phase shift term, $S_l = e^{2i\delta_l}$, so that partial wave scattering amplitude becomes

$$f_l(E) = \frac{S_l - 1}{2ik} = \frac{1}{k} e^{i\delta_l} \sin\delta_l = \frac{1}{k\,(cgt\delta_l - i)} \tag{2.46}$$

Hence, the total cross section can be expressed as

$$\sigma_{tot}(E) = \frac{4\pi}{k} Im\left[f_{\mathbf{kk'}}(\theta = 0)\right] = \sum_l \sigma_l(E) = \frac{2\pi}{k^2}\sum_l (2l+1)\left(1 - Re\left[S_l\right]\right) \tag{2.47}$$

being the elastic and inelastic cross sections components

$$\begin{aligned} \sigma_{elast}(E) &= \int d\Omega \left| f_{\mathbf{kk'}}(\theta)\right|^2 \\ &= \frac{4\pi}{k^2}\sum_l (2l+1)\sin^2\delta_l \\ &= \frac{\pi}{k^2}\sum_l (2l+1)|S_l - 1|^2 \end{aligned} \tag{2.48}$$

and

$$\sigma_{react}(E) = \sigma_{tot}(E) - \sigma_{elast}(E) = \frac{\pi}{k^2}\sum_l (2l+1)\left(1 - |S_l|^2\right) \tag{2.49}$$

respectively. Thus, in the absence of scattering, all cross sections are zero, which implies $S_l = 1$; in case of pure elastic scattering, $|S_l| = 1$, e. g. $S_l = e^{2i\delta_l}$, and the elastic scattering cross section maxiumum value is obtained for $S_l = -1$, that is also the value maximizing the total cross section, which in turn implies that the total cross section can reach its maximum only in the case of pure elastic scattering process. The cross section for inelastic processes reaches its maximum value for $S_l = 0$; moreover, for this value, elastic and inelastic cross sections are equal.

2.1.5 Nuclear interaction potential

The nucleus is clearly a many body system. In order to simplify the description of many - body interactions, it is often useful to start with an effective two body interaction, thus assuming that only two - body interaction among nucleons dominates [109]. In general, a two - body interaction potential is a non - local operator, depending on the following quantities

$$V(1,2) = V(\mathbf{r}_1, \mathbf{p}_1, \boldsymbol{\sigma}_1, \boldsymbol{\tau}_1, \mathbf{r}_2, \mathbf{p}_2, \boldsymbol{\sigma}_2, \boldsymbol{\tau}_2) \tag{2.50}$$

where the indices $(1, 2)$ identify the two interacting nucleons, $\boldsymbol{\sigma}_i$ and $\boldsymbol{\tau}_i$ are the spin and isospin Pauli matrices, respectively, and the momentum dependence follows from the non - locality of the operator. The form of this general function can be restricted through symmetry considerations [109]:

- In order to preserve the antisymmetric nature of the total wave function of the system of two fermions, the potential must be symmetic under exchange of all coordinates of the two interacting nucleons.

- Imposing translational invariance implies that the interaction potential depends only on the relative coordinate $\mathbf{r}_{\alpha,\beta} = \mathbf{r}_1 - \mathbf{r}_2$.

- The potential must be the same in every inertial rest frame (Galileian invariance), i. e. it depends only on the relative momentum $\mathbf{k} = \frac{\mathbf{k}_1 - \mathbf{k}_2}{2}$.

- Because strong interactions do not violate parity, then the interaction potential must be symmetric under space reflection.

- Because strong nuclear interactions preserves isospin symmetry (as widely confirmed by nuclear scattering experiments), the corresponding potential must be symmetric under isospin transformation.

- Nuclear interaction potential must preserve time - reversal symmetry, this implying that transition matrix element must be invariant under time - reversal.

- Moreover, one can impose rotational invariance in coordinate space.

- Finally, in order to simplify the description, a local effective nuclear potential is often used; the locality implies the momentum independence of such potential.

All these symmetries lead to the following expression of the effective nucleon - nucleon interaction potential

$$\begin{aligned} V(1,2) &= V_C(1,2) + V_t(1,2) + V_{LS}(1,2) + V_{LL}(1,2) \\ &= \sum_T \{ \sum_S V_{ST}^C(r)(\boldsymbol{\sigma}_1 \cdot \boldsymbol{\sigma}_2)^S + V_{1T}^t(r) S_{12} + V_T^{LS}(r) \mathbf{L} \cdot \mathbf{S} \\ &+ V_T^{LL}(r) \left[(\boldsymbol{\sigma}_1 \boldsymbol{\sigma}_2)\mathbf{L}^2 - \frac{1}{2} \left((\boldsymbol{\sigma}_1 \mathbf{L})(\boldsymbol{\sigma}_2 \mathbf{L}) + (\boldsymbol{\sigma}_2 \mathbf{L})(\boldsymbol{\sigma}_1 \mathbf{L}) \right) \right] \} (\boldsymbol{\tau}_1 \cdot \boldsymbol{\tau}_2)^T \end{aligned} \tag{2.51}$$

where $V_C(1,2)$ accounts for the central interaction, depending only on the modulus of the relative coordinate $\mathbf{r}_{\alpha,\beta}$; unfortunately, pure central force cannot explain some experimental data, like the quadrupole moment of the deuteron; for this reason tensor interactions have been included, through the term $V_t(1,2)$, in which the well known rank -2 tensor operator, $S_{12} = \frac{3}{r_{\alpha,\beta}^2} (\boldsymbol{\sigma}_1 \cdot \mathbf{r}_{\alpha,\beta}) (\boldsymbol{\sigma}_2 \cdot \mathbf{r}_{\alpha,\beta}) - \boldsymbol{\sigma}_1 \cdot \boldsymbol{\sigma}_2$, appears. The spin - orbit term, $V_{LS}(1,2)$, is considered, because it allows to explain nuclear magic numbers; one can also take into account the second - order spin - orbit term, $V_{LL}(1,2)$, in order to improve calculations, together with other correction terms (relativistic and higher order corrections), not shown here. In eq. (2.51), $\mathbf{L}$, is the relative orbital angular momentum operator of the two interacting nucleons, $\mathbf{L} = (\mathbf{r}_1 - \mathbf{r}_2) \times (\mathbf{k}_1 - \mathbf{k}_2)/2$, while $\mathbf{S} = \frac{1}{2}(\boldsymbol{\sigma}_1 + \boldsymbol{\sigma}_2)$ is the total two - nucleon spin operator [9].

In the calculations discussed in chapters 3 and 4, we focus on the analogy with beta decay processes and thus on small momentum transfer region, so that only central and tensor interaction terms are considered, while spin - orbit terms can be neglected.

2.1.6 Direct reactions

Nuclear reactions can be classified into two big groups [105, 110]:

- **compound nucleus reactions** are processes characterized by the formation of a compound system, obtained from projectile and target thermalization, living within a time interval $\Delta t_c \sim 10^{-19}$ –

$10^{-14}\,s$, which is longer than the characteristic time of the nuclear strong interactions, ($\Delta t_s \sim 10^{-21}\,s$); actually, Δt_c is sufficiently long to ensure thermalization of projectile and target nucleons; the thermalization implies that the probability to obtain certain nuclei from compound nucleus decay is independent of the initial channel system, i. e. there is a loss of memory about the initial channel (*Bohr's hypothesis of independence*); this characteristic has been verified experimentally by S. N. Ghoshal [111] in 1950, through the study of the two reactions $p + {}^{63}$Cu and $\alpha + {}^{60}$Ni, both leading to the same compound nucleus, ^{64}Zn*, which in both cases decays into one of the three channels ${}^{63}\mathrm{Zn} + n$, ${}^{62}\mathrm{Cu} + n + p$ and ${}^{62}\mathrm{Zn} + 2n$, with nearly the same branching ratios. Hence, the decay mode of the compound nucleus depends only on its mass, atomic number, excitation energy and angular momentum. Due to the thermalization of all projectile and target nucleons, forming the compound nucleus, these kind of reactions are characterized by an energy distribution à la Boltzmann; moreover, because of the equilibration, the information on the beam direction is lost and, consequently, angular distributions are symmetric with respect to the direction of the total angular momentum of the compound system. The extreme limit of compound nucleus reactions is represented by nuclear *fusion* processes.

- **direct reactions**, differently from the former, are processes which happen in one step, i. e. processes where there are not two time scales and so where no compound nucleus can be formed. Hence, no thermalization occurs, this meaning that such reactions strongly depend on the nuclei involved in the entrance channel. This makes direct reactions an important source of information about nuclear structure [96]. These kind of processes are mainly surface reactions, that is they involve only projectile and target surface nucleons, thus

involving less degrees of freedom with respect to compound nucleus reactions; this in turn implies that such reactions are only weakly coupled to the bulk of nuclear reactions and, hence, are characterized by small momentum transfer, thus allowing the use of DWBA and of the optical potentials in the description of the nuclear reaction, both for light and heavy ion systems. Moreover, they dominate in a narrow range around the partial wave angular momentum corresponding to the grazing angle of the process, because of their surface nature.

The separation between these two extreme cases is not at all sharp. Indeed, nuclear reactions experiments reveal the existence of intermediate processes, referred to by the expression of *pre-equilibrium* nuclear reactions, where the projectile undergoes more than one scattering inside the target nucleus, in a time interval not sufficient to reach thermalization, so that no compound nucleus can be formed; finally, the projectile can escape from the target nucleus, leaving the latter in an excited state (*multi - step direct* reactions) or can stay bound with the target nucleus, emitting particles before forming a compound state (*multi - step compound* reactions).

Of course, in a nuclear reaction all these kinds of processes can occur, each one with a certain probability; the relative weight of the two processes depends on the excitation energy of the system (and so on the beam energy) and on the scattering angle: direct reactions dominate at forward scattering angles and for low excitation energies, which means high energies of the projectile - like ejectile, as shown in fig. 2.1.

In order to extract the nuclear matrix element, which contains the whole nuclear structure information on the system, it is mandatory to study reactions of the second type.

The term “direct reaction” indicates a broad class of nuclear reactions:

- **transfer** reactions, that are processes characterized by the ex-

change of one or more nucleons between target and projectile nuclei. Transfer reactions can be further classified into

  - **stripping** reactions, where a particle from the projectile is absorbed (stripped) by the target, e. g. A(d,n) $[B = \mathrm{p} + A]$;
  - **pick up** reactions, where a particle from the taget nucleus is absorbed (picked up) by the projectile, which is nothing but the time - reversed of stripping processes;
  - **knock out** reactions, where due to the interaction between projectile and target nuclei, a nucleon or light cluster is ejected ("knocked out") from the target by the projectile.
  - **break up** reactions, in which a loosely bound projectile (like the deuteron) dissociates ("breaks up") in the field of the target nucleus.

- **charge exchange** reactions, where in a single step the two interacting nuclei change their charge, but leaving each of their mass number unchanged; this process is due to the (off - shell) exchange of charged mesons among projectile and target nucleons and is fully treated in the next chapters.

- **collective excitations** describing the excitation of collective (vibrational and/or rotational) nuclear states.

The use of DWBA to describe direct reactions allows one to write the differential cross section[3] as

$$\frac{d^2\sigma}{dEd\Omega} = \frac{E_\alpha E_\beta}{4\pi^2(\hbar c)^4}\frac{k_\beta}{k_\alpha}\frac{1}{(2J_A+1)}\frac{1}{(2J_a+1)}$$
$$\sum_{\substack{m_a,m_A\\ m_b,m_B}} \mid \sum_{\substack{\tau=C,T\\ SO}}\sum_{ij}\int d^3s_\alpha \int d^3s_\beta\, \chi^{(-)*}_{k_\beta}(\mathbf{r}_\beta) < \psi_B\phi_b|\hat{\mathbb{V}}^{(\tau)}_{\alpha\beta}(\boldsymbol{\xi}_\alpha,\boldsymbol{\xi}_\beta)|\psi_A\phi_a > \chi^{(+)}_{k_\alpha}(\mathbf{r}_\alpha)|^2 \tag{2.52}$$

[3]Cross section in the center of mass rest frame is used, in order to simplify calculations.

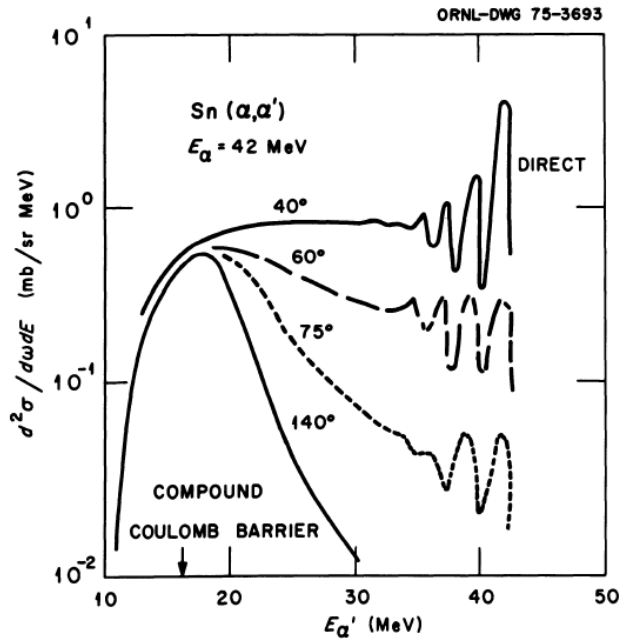

Figure 2.1: Example of double differential cross section as a function of the energy of the projectile - like ejectile and of the scattering angle, for the inelastic $\mathrm{Sn}(\alpha, \alpha')$ reaction [105].

where α (β) represents the entrance (exit) reaction channels and $\mathbf{r}_\alpha$ ($\mathbf{r}_\beta$) and $\mathbf{k}_\alpha$ ($\mathbf{k}_\beta$) are the relative projectile - target space and momentum coordinates in the initial (final) channel, respectively, $\mathbf{s}_\alpha = \mathbf{r}_1^{'} - \mathbf{r}_2^{'} = \mathbf{r}_\alpha + \mathbf{r}_j - \mathbf{r}_i$ ($\mathbf{s}_\beta = \mathbf{r}_\beta + \mathbf{r}_j - \mathbf{r}_i$) and $\mathbf{r}_\alpha = \mathbf{r}_2 - \mathbf{r}_1$ ($\mathbf{r}_\beta = \mathbf{r}_{2f} - \mathbf{r}_{1f}$) are the relative nucleon - nucleon and nucleus - nucleus spatial coordinate in the entrance (exit) channel, respectively; the sums over i and j are over projectile and target nucleons and are embedded in $\mathbf{r}_{\alpha,\beta}$ definition and $\boldsymbol{\xi}_{\alpha,\beta} \equiv (\mathbf{s}_{\alpha,\beta}, \boldsymbol{\sigma}_{\alpha,\beta}, \boldsymbol{\tau}_{\alpha,\beta})$. The coordinate system used is that illustrated in fig.2.2. According to such reference system and resembling the experimental situation, it follows that $r_i\,, r_j \ll r_{1,2}, r_{1,2}^{'}$, being r_i and r_j both of the order of projectile and target nuclear radii and $r_{1,2}$ and $r_{1,2}^{'}$ representing the distance between the scattering point and the detectors, so that one can approximate $r_{1,2} \approx r_{1,2}^{'}$ and then $\mathbf{s}_{\alpha,\beta} \approx \mathbf{r}_{\alpha,\beta}$.

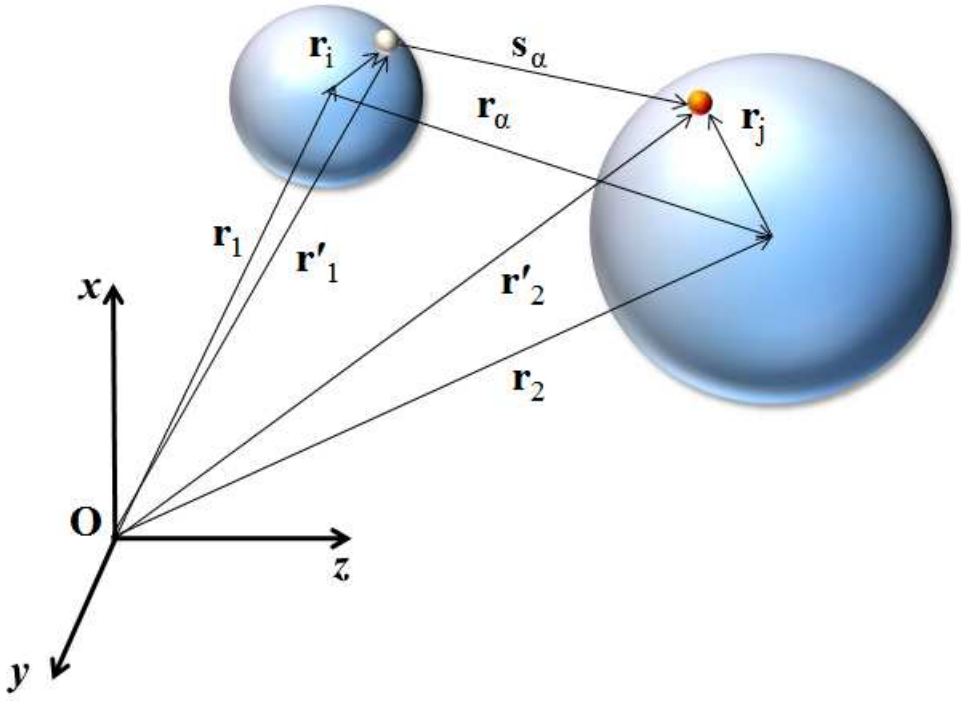

Figure 2.2: Reference frame used to describe nucleus - nucleus scattering. For nucleon - nucleus ($p-A$) scattering, projectile coordinate $\mathbf{r}_i = \mathbf{0}$ and $\mathbf{r}_1' \equiv \mathbf{r}_1$, so that $\mathbf{s}_\alpha = \mathbf{r}_\alpha + \mathbf{r}_j$ (the same for the exit channel, β).

2.1.7 Useful approximations

Hence, the main ingredient of the Cross Section is represented by the transition matrix element

$$\mathcal{M}^{(\tau)}_{\alpha\beta}(\mathbf{k}_\alpha, \mathbf{k}_\beta) = \int d^3r_\alpha \int d^3r_\beta \, \chi^{(-)*}_{k_\beta}(\mathbf{r}_\beta) < \psi_B\phi_b|\hat{\mathbb{V}}^{(\tau)}_{\alpha\beta}(\boldsymbol{\xi}_\alpha, \boldsymbol{\xi}_\beta)|\psi_A\phi_a > \chi^{(+)}_{k_\alpha}(\mathbf{r}_\alpha) \tag{2.53}$$

carrying the whole information on the nuclear reaction process, through the nuclear interaction potential $\hat{\mathbb{V}}^{(\tau)}_{\alpha\beta}(\boldsymbol{\xi}_\alpha, \boldsymbol{\xi}_\beta)$, which is non - local, in general.

2.1.7.1 Zero-range approximation

In order to simplify calculations, very often the realistic non - local potential is replaced by an effective local one [112], because of the short

range nature of the nuclear interaction between target and projectile nuclei; this in turn implies that the main contribution in the integrals, appearing within the transition matrix element, is obtained for $\mathbf{r}_\alpha \simeq \mathbf{r}_\beta \equiv \mathbf{r}$, thus justifying the use of the following approximation

$$\hat{\mathbb{V}}(\boldsymbol{\xi}_\alpha, \boldsymbol{\xi}_\beta) \simeq \hat{\mathbb{V}}(\mathbf{s}_\alpha, \boldsymbol{\sigma}_\alpha, \boldsymbol{\tau}_\alpha, \mathbf{s}_\beta, \boldsymbol{\sigma}_\beta, \boldsymbol{\tau}_\beta)\delta(\mathbf{r}_i - \mathbf{r}_j) \tag{2.54}$$

and then

$$\hat{\mathbb{V}}(\mathbf{r}_\alpha, \boldsymbol{\sigma}_\alpha, \boldsymbol{\tau}_\alpha, \mathbf{r}_\beta, \boldsymbol{\sigma}_\beta, \boldsymbol{\tau}_\beta) \simeq \hat{V}(\mathbf{r}_\alpha, \boldsymbol{\sigma}_\alpha, \boldsymbol{\tau}_\alpha, \boldsymbol{\sigma}_\beta, \boldsymbol{\tau}_\beta)\delta(\mathbf{r}_\alpha - \mathbf{r}_\beta) \tag{2.55}$$

called *zero range approximation*, where $\hat{V}$ is an effective local nuclear interaction potential, generally depending on internal coordinates of the sistem.

2.1.7.2 Effective local Potential

Because the interaction involves nucleons, it is necessary to take care of their fermionic nature through the Pauli principle, which is often implemented by multiplying the effective nuclear potential by the exchange operator [9, 96, 97, 113]

$$P_x = 1 - P_\sigma P_\tau P_l \tag{2.56}$$

which exchanges spin, isospin and space coordinates of one nucleon in the projectile with that of another nucleon in the target [9]; in this way, the interaction potential can be replaced by the following effective expression

$$\hat{\mathbb{V}}(\boldsymbol{\xi}_\alpha, \boldsymbol{\xi}_\beta) \to \hat{\mathbb{V}}(\boldsymbol{\xi}_\alpha, \boldsymbol{\xi}_\beta)P_x \tag{2.57}$$

By using the *zero range approximation* and the effective local potential in (2.57), eq. (2.53) simplifies to

$$\begin{aligned} &\mathcal{M}^{(\tau)}_{\alpha\beta}(\mathbf{k}_\alpha, \mathbf{k}_\beta) = \\ &\int d^3r\, \chi^{(-)*}_{k_\beta}(\mathbf{r}) < \psi_B\phi_b|\hat{V}^{(\tau)}_{\alpha\beta}(\mathbf{r}, \boldsymbol{\sigma}_\alpha, \boldsymbol{\tau}_\alpha, \boldsymbol{\sigma}_\beta, \boldsymbol{\tau}_\beta)P_x|\psi_A\phi_a > \chi^{(+)}_{k_\alpha}(\mathbf{r}) \end{aligned} \tag{2.58}$$

2.1.7.3 Impulse Approximation

Another important feature to be taken into account, both for light $(p-A)$ and heavy ion $(A-A)$ reactions, is that the nuclear interaction potential deals with nucleon - nucleon $(N-N)$ interaction within the nuclear medium. It is widely used to describe nucleus - nucleus $(A-A)$ reactions in terms of $N-N$ bare interactions, by means of the *single - scattering approximation*, where it is assumed that each projectile nucleon interacts only with one nucleon, inside the target; the latter approximation relies upon the fact that typical nuclear reaction cross sections are of the order of $\sim 10\, mb$, which implies a mean free path of the order of some fm, that is the typical dimension of nuclei. The single scattering approximation allows to express $A-A$ scattering amplitude as a sum, over all target and projectile nucleons, of single scattering amplitudes. Each of these single scattering amplitudes contains information on the nuclear medium effects on $N-N$ interaction and this effects are quite difficult to calculate. For this reason another important hypothesis is often used to further simplify calculations: the *impulse approximation*, which consists in neglecting the interaction between each projectile nucleon with every target nucleon; hence, this approximation allows the substitution of the in - medium single scattering amplitudes with the bare (free - nucleons) ones, i. e. the effective interaction potential $\hat{V}$ can be replaced by the bare one, $\hat{V}_{NN}$.

The validity range of the *impulse approximation* is expressed by the following relation

$$\tau_{coll} \ll \tau_{nucl} \quad \Leftrightarrow \quad \frac{\tau_{coll}}{\tau_{nucl}} \ll 1 \tag{2.59}$$

which depends on two time - scales:

- the *reaction* time, $\tau_{nucl} \simeq \frac{2\pi}{\omega_{nucl}} \simeq \frac{2\pi\hbar}{B}$, that is the time characteristic of nuclear response and is, thus, related to the typical nuclear

frequency, ω_{nucl}, and so to the binding energy[4], $B \sim \omega_{nucl}\hbar$, which is characteristic of the given nuclear system;

- the *collision* time, $\tau_{coll} \simeq \frac{R_{int}}{v}$, which is the time taken by the projectile to cross the region of nuclear interaction, having dimension R_{int}; hence, it is related to the velocity v of the projectile.

The relation (2.59) means that the impulse approximation works well when the nuclear response time is greater than the collision time.

Thus, the impulse approximation is valid for beam energies greater than $E = 5\,AMeV$, starting from which the ratio $\frac{\tau_{coll}}{\tau_{nucl}} \simeq 0.1$ is already sufficientely small.

2.1.7.4 Eikonal Approximation

If beam energy corresponds to a De Broglie wavelenght, $\lambda = \frac{1}{k}$, much smaller than the characteristic lenght - scale of the interaction potential, that is

$$V(r + \Delta r) - V(r) \sim const \quad \Delta r \simeq \lambda \tag{2.60}$$

then, it is possible to express the wave function of the scattered particle as the product of a plane wave, propagating along z axis[5], times a function, $\phi(z, \mathbf{b})$, which varies slowly with z and the impact parameter b

$$\psi(\mathbf{r}) \simeq e^{ikz}\phi(z, \mathbf{b}) \tag{2.61}$$

being

$$|\nabla^2\phi| \ll k|\nabla\phi| \tag{2.62}$$

Such approximation is called *eikonal approximation*.

The condition (2.62) implies that, making Taylor expansion of ϕ with respect to the reaction point (generally coinciding with $z = 0$), the second and higher order terms can be neglected, so that $\phi \simeq \phi_0 + \nabla\phi \cdot \delta\mathbf{z} \sim$

[4]Typical nuclear binding energy values are about $6 - 8\,MeV$.

[5]Genarally, z axis coincides with the beam direction.

$\phi_0 + \nabla\phi \cdot \mathbf{k}$, just meaning that ϕ varies slowly with z and b. Hence, the latter assumption implies that the function ϕ, containing all information about the interaction, can be simply expressed as a phase.

Thus, the eikonal approximation means that at sufficientely high energies the projectile is mainly forward scattered, so that one should expect an angular distribution strongly peaked at small scattering angles. It is important to note that the validity condition of the eikonal approximation is different from that for the Born approximation; indeed, while the latter one requires that the interaction potential does not modify the scattered wave function too much with respect to the plane wave, the condition (2.60) for sufficientely high beam energies, and so high momenta, k, is always valid, no matter what the shape and the magnitude of the interaction potential is.

From the expression of the scattered wave in eq. (2.61) it is straightforward to note that in the eikonal approximation, considering the simplest case of spherically symmetric potential, the physical system "looses one degree of freedom", in the sense that the spherical symmetry reduces to a cilindrical one, i. e. the system does no more depend on the orientation of $\mathbf{b}$. Thus, an explicit expression of ψ as function of the interaction potential can be obtained by solving the time - independent Schrödinger equation in cilindrical coordinates

$$-\frac{\hbar^2}{2\mu}e^{ikz}\{\nabla^2\phi + 2ik\frac{\partial\phi}{\partial z} - k^2\phi - \frac{2\mu}{\hbar^2}V(\mathbf{r})\phi + \frac{2\mu}{\hbar^2}E\phi\} = 0 \tag{2.63}$$

thus obtaining

$$\phi(\mathbf{b}, z) = e^{-\frac{i}{\hbar v}\int_{-\infty}^{z} dz'\, V(\mathbf{b},z')} = e^{i\chi(\mathbf{b},z)} \tag{2.64}$$

where $v = \frac{\hbar k}{\mu}$ is the velocity of the system with mass equal to the reduced mass, μ, of projectile - target nuclei and momentum given by the relative momentum $\mathbf{k}$ (relative system) and the coordinate space vector is splitted into its transversal and longitudinal components, $\mathbf{r} = (\mathbf{b}, z)$. $\chi(\mathbf{b}, z)$ is called *eikonal phase*.

In this way, the scattered wave function can be expressed as a plane wave, moving along z axis times a phase shift, representing the effect of the interaction, as stated above

$$\psi(\mathbf{r}) = e^{ikz+i\chi(\mathbf{b},z)} \tag{2.65}$$

In order to relate the eikonal phase to the scattering amplitude, let's consider, for the sake of simplicity, the elastic scattering case, hence the case in which $|\mathbf{k}'| = |\mathbf{k}|$). The scattering amplitude is

$$\begin{aligned} f_{kk'}(\theta) &= -\frac{2\mu}{4\pi\hbar^2}\int d^3r\, e^{-i\mathbf{k}'\cdot\mathbf{r}}V(\mathbf{r})\psi_k(\mathbf{r}) \\ &= -\frac{2\mu}{4\pi\hbar^2}\int d^2b \int_{-\infty}^{+\infty} dz\, e^{-i(\mathbf{k}'\cdot\mathbf{b}+\mathbf{k}'\cdot\hat{k}z)}V(\mathbf{b},z)e^{ikz}e^{-\frac{i}{\hbar v}\int_{-\infty}^{z}dz'\,V(\mathbf{b},z')} \\ &= -\frac{2\mu}{4\pi\hbar^2}\int d^2b\, e^{i(\mathbf{k}-\mathbf{k}')\cdot\mathbf{b}}\int_{-\infty}^{+\infty} dz\, e^{i(\mathbf{k}-\mathbf{k}')\cdot\hat{k}z}V(\mathbf{b},z)\exp\{-\frac{i}{\hbar v}\int_{-\infty}^{z}dz'\,V(\mathbf{b},z')\} \end{aligned} \tag{2.66}$$

where in the last line the hypothesis $\mathbf{k}//\vec{z}$ is used, so that $1 = e^{i\mathbf{k}\cdot\mathbf{b}}$.

The eikonal approximation implies $\theta \ll 1$, so that $(\mathbf{k}-\mathbf{k}')\cdot\hat{\mathbf{k}} = k^2(1-\cos\theta) \simeq 0$; thus, the integral in dz becomes

$$\begin{aligned} &\int_{-\infty}^{+\infty} dz\, V(\mathbf{b},z)\exp\{-\frac{i}{\hbar v}\int_{-\infty}^{z}dz'\,V(\mathbf{b},z')\} \\ &= i\hbar v\exp\{-\frac{i}{\hbar v}\int_{-\infty}^{z}dz'\,V(\mathbf{b},z')\}|_{-\infty}^{+\infty} = i\hbar v\left[e^{i\chi(\mathbf{b})}-1\right] \end{aligned} \tag{2.67}$$

defining $\chi(\mathbf{b}) = \chi(\mathbf{b}, z = +\infty)$. The difference between initial and final channel relative momenta, $\mathbf{q} = \mathbf{k}-\mathbf{k}'$, represents the momentum transfer of the system.

For spherically symmetric potentials, $V(\mathbf{b},z) = V(b,z)$, the eikonal phase becomes indipendent from the orientation of the trasversal vector $\mathbf{b}$, $\chi(\mathbf{b},z) = \chi(b,z)$, so that the scattering amplitude becomes

$$\begin{aligned} f_{kk'}(\theta) &= \int db\, b \underbrace{\int d\varphi e^{iqbcos\varphi}}_{2\pi j_0(qb)}(i\hbar v)\left[e^{i\chi(b)}-1\right] \\ &= -ik\int db\, b\, j_0(qb)\left[e^{i\chi(b)}-1\right] \end{aligned} \tag{2.68}$$

and can be determined just by solving two one dimensional integrals: the integral within the eikonal phase and that in the transverse coordinate, *db*.

2.1.7.5 Black Disk Approximation

Another important approximation, very useful for treating heavy ion reactions, is the *black sphere* or *black disk approximation* (BDA). This approximation is based on the assumption that distorted waves are totally absorbed inside the nucleus, i.e. the imaginary part of the optical potential dominates on the real optical and Coulomb potentials. An estimate of black disk radius, R_{BD}, can be obtained from the evaluation of the total absorption cross section, that for a totally absorbing sphere is roughly given by

$$\sigma_{abs} = \frac{2\mu_\alpha}{k_\alpha} \int d^3r \, |\chi^{(+)}_{\mathbf{k}_\alpha}(\mathbf{r})|^2 W(\mathbf{r}) \simeq \pi R^2_{BD} \tag{2.69}$$

where $W(\mathbf{r})$ represents the imaginary part of the optical potential, μ_α is the reduced mass of the nuclear system in the entrance channel and $\chi^{(+)}_{\mathbf{k}_\alpha}(\mathbf{r})$ is the incoming distorted wave describing initial state interactions. For heavy ion reactions at intermediate energies, $E_p \sim 10\, AMeV$, typical Cross Section values are $\sigma_{abs} \sim 1 - 3\ b$, that imply $R_{BD} \sim 5 - 10\, fm$. Of course, the higher beam energy is, the worst is the BDA. Eq. (2.69) shows that black disk radius is related to the imaginary part of the optical potential, so that a very preliminary estimation of R_{BD} can be obtained by taking the coordinate space value at which $W(r) = 0.01W(0)$.

2.2 Nuclear Structure Theory for direct reactions

Nuclei are very complex many - body systems. The simplest way to treat them is to consider nucleons inside the nucleus as independent particles, each one feeling the presence of the other nucleons by means of a

mean field (Hartree - Fock) potential. Most of the nuclear structure theories, used for the description of spin - isospin excitations in nuclei, have an independent particle picture as starting point. In this first approximation, energy spectrum of the nucleus shows a "shell" structure and its ground state is described by a Slater determinant of single - particle orbitals, where all the lowest energy single - particle states are occupied up to Fermi energy [9]; the single - particle wave functions are eigenfunctions of the single - particle Hamiltonian

$$H_{sp} = T + U(r) \tag{2.70}$$

where T is the sum of single - particle kinetic energy operators and $U(r) = V_{loc}(r) + V_{SL}(r)\mathbf{L}\cdot\mathbf{S} + V_C(r) + V_{sym}(r)$ is the full two - body interaction potential, being $V_{loc}(r)$ a local two - body potential, $V_{SL}(r)$ the spin - orbit, $V_C(r)$ the Coulomb and, finally, $V_{sym}(r)$ the symmetry potential[6]. An analytical expression for the single - particle potential is quite difficult to be determined, so that Hartree and Fock suggested that $U(r)$ can be written as the sum of a mean field potential, $U_{MF}(r)$, plus a residual potential, $V_{res}(r) = U(r) - U_{MF}(r)$, the latter being neglegible within the independent - particle framework. The mean field potential is expressed in terms of single - particle wavefunctions, according to the following relation

$$\begin{aligned} U_{MF}(\mathbf{r})\phi_k(\mathbf{r}) = &\left(\int d^3r'\, V(\mathbf{r}-\mathbf{r}') \sum_{i=1}^{A} |\phi_i(\mathbf{r}')|^2\right)\phi_k(\mathbf{r}) \\ &- \sum_{i=1}^{A}\phi_i(\mathbf{r}) \int d^3r'\, V(\mathbf{r}-\mathbf{r}')\phi_i^*(\mathbf{r}')\phi_k(\mathbf{r}') \end{aligned} \tag{2.71}$$

where the first term, inside round parenthesis, has the simple interpretation of the potential generated by the density distribution of the nucleons

[6]The symmetry potential is proportional to the symmetry parameter $\frac{(N-Z)}{A}$, enhancing the ground state energy of the system and thus favoring a nuclear configuration with an equal number of protons and neutrons

inside the nucleus [114], while the last term properly accounts for the antisymmetrization of the total wavefunction of the system; in this way, the Hartree - Fock mean field potential can be calculated by means of a self - consistent - field iterative method: once a set of trial single - particle wave functions are chosen and used to build a "trial" mean field, the variational principle is used to minimize the eigenvalues (single - particle ground state energies) of the corresponding hamiltonian, thus allowing to determine its "new" eigenfunctions, which in turn will be iteratively used to build the "new" mean field potential, until convergence in the ground state energy value is reached. The many - body ground state thus obtained is called Hartree - Fock ground state and is characterized by a Fermi - Dirac density distribution at zero temperature: all energy levels below Fermi energy (ϵ_F) are occupied, while all states above ϵ_F are empty.

By promoting one particle from a state ϕ_i below the Fermi sea ($\epsilon_i < \epsilon_F$) to a state ϕ_m with eigenenergy $\epsilon_m > \epsilon_F$, a "1-particle - 1-hole" ($1p-1h$) excited state is obtained [9]. By considering different combinations of independent $1p-1h$ states, one can in principle obtain all the excited states. Up to this level, where only independent $1p-1h$ configurations are considered, it is possible to describe well the ground state and low-lying excited states of doubly - closed - shell nuclei. In order to describe (spherically and not spherically[7] symmetric nuclei) higher excited states, such as the giant resonances, which are identified as collective states, it is necessary to take into account correlations between nucleons. This can be achieved by considering the residual interaction, previously neglected. Hence, one can start from the Hartree - Fock ground state and then construct all the excited states though a *coherent* superposition of $1p-1h$ states (Tam - Dankoff Approximation, TDA) or take into account

[7]Restricting the attention to nuclei with a small number of valence nucleons outside a filled shell.

correlations among nucleons already in the ground state (Random Phase Approximation, RPA). In the latter case a better explaination of the experimental energy spectra is obtained, as long as the ground state correlations are not too strong with respect to that of excited states.

For describing weakly - bounded open-shell nuclei, pairing correlations between nucleons have to be explicitely taken into account, by considering pairing interaction already in the ground state. This can be achieved by the Hartree - Fock - Bogoliubov (HFB) theory, based on the Bogoliubov - Valatin transformations (shown in the next section), through which the quasi - particle formalism is introduced. In this way, the ground state of a weakly bounded nucleus is no more characterized by a zero temperature Fermi - Dirac distribution of nucleons, but it resembles a Fermi - Dirac distribution for non - zero temperature system, i. e. the Fermi surface of weakly bounded nuclei has a significant diffuseness, which in turn means that the ground state occupation numbers are no more 1 below and 0 above Fermi surface, but in both regions the occupation probability becomes a number between 0 and 1.

2.2.1 QRPA formalism

As stated above, for nuclei away from closed shells the pairing correlations play a fundamental role. Bohr, Mottelson, and Pines (1958) and Belyaev (1959) introduced pairing interactions in nuclei in analogy to the BCS theory (Bardeen, Cooper and Schrieffer, 1957) of superconductors. The self - consistent version of BCS theory is represented by the HFB theory, where one determines the most general wave function of independently moving *quasiparticles* by minimizing the ground - state energy simultaneously with respect to the long - ranged Hartree - Fock field and the short - ranged, attractive, pairing field [9][109]. Similarly to HF theory, the BCS ground state can be determined from a variational

principle, leading to the following expression

$$|0\rangle = \prod_{k>0} \left(u_k + v_k \hat{a}_k^\dagger \hat{a}_{\overline{k}}^\dagger \right) |\rangle \tag{2.72}$$

where the product runs over half the configuration space ($k > 0$) to avoid double counting, $|\rangle$ represents the bare vacuum, $\hat{a}_k^\dagger$ ($\hat{a}_k$) is the single particle creation, or hole annihilation, operator (hole creation, or particle annihilation operator) and u_k and v_k are the variational parameters. The index k represents the set of quantum numbers describing the system (particle), e. g. it can coincide with the ones giving the spherical basis, $k = (nlm_l sm_s)$ or equivalentely $k = (njm)$; in the latter case, the index $\overline{k} = (nj - m)$, which identifies the conjugate state (hole), such that the set $(k, \overline{k})$ identifies the whole particle - hole space [109].

It is possible to describe the system of pairwise *interacting* particles in terms of *non - interacting* Bogoliubov's *quasiparticles*, by introducing the so called *Bogoliubov - Valatin transformations* [109]

$$\begin{aligned} \hat{\alpha}_k^\dagger &= u_k \hat{a}_k^\dagger - (-1)^{j+m} v_k \hat{a}_{\overline{k}} \\ \hat{\alpha}_k &= u_k \hat{a}_k - (-1)^{j+m} v_k \hat{a}_{\overline{k}}^\dagger \end{aligned} \tag{2.73}$$

which allow to convert particle - hole into quasiparticle states, being $\hat{\alpha}_k^\dagger$ and $\hat{\alpha}_k$ the 1 - quasiparticle (1QP) creation and annihilation operators, respectively; u_k and v_k represent the *emptiness* and *occupation* amplitudes, respectively, for the nuclear state with quantum numbers k, satisfying the following condition

$$u_k^2 + v_k^2 = 1 \tag{2.74}$$

The relation (2.74) implies that quasiparticle operators, defined by eq.s (2.73), satisfy fermionic anticommutation relations

$$\{\alpha_k, \alpha_{k'}\} = \left\{ \alpha_k^\dagger, \alpha_{k'}^\dagger \right\} = 0 \qquad \left\{ \alpha_k, \alpha_{k'}^\dagger \right\} = \delta_{kk'} \tag{2.75}$$

Thus, Bogoliubov's quasiparticles are fermions represented by a linear combination of particle and hole states; in the limit of vanishing pairing

correlations such quasiparticles reduce to a particle or a hole, depending on whether their kinetic energy ϵ_k is higher or lower than Fermi energy, ϵ_F, respectively. By introducing $\alpha_k^\dagger$ and α_k, BCS ground state, $|0\rangle$, can be defined as

$$\hat{\alpha}_k|0\rangle = 0 \qquad \forall k \tag{2.76}$$

In order to determine the emptiness and occupation amplitudes, one can start from the single - particle hamiltonian (containing the kinetic and the two - body interaction operators) in the particle - hole second quantization formalism

$$\hat{H}_{sp} = \sum_{k_1,k_2} T_{k_1,k_2}\hat{a}^\dagger_{k_1}\hat{a}_{k_2} + \frac{1}{2}\sum_{\substack{k_1,k_2\\k_3,k_4}} V_{k_1,k_2,k_3,k_4}\hat{a}^\dagger_{k_1}\hat{a}^\dagger_{k_2}\hat{a}_{k_3}\hat{a}_{k_4} \tag{2.77}$$

where the index k_i identifies the different nuclear states, T_{k_1,k_2} and V_{k_1,k_2,k_3,k_4} are the kinetic and the antisymmetrized two - body potential matrix elements, respectively; then, intorducing quasiparticle operators, by inverting the relations (2.73), one obtaines a quasiparticle hamiltonian containing a term which violates particle number conservation; by imposing that the latter term is zero, the expressions (2.78) for v_k and u_k are obtained,

$$u_k^2 = \frac{1}{2}\left(1 + \frac{\epsilon_k}{\sqrt{\epsilon_k^2 + \Delta_k^2}}\right) \qquad v_k^2 = \frac{1}{2}\left(1 - \frac{\epsilon_k}{\sqrt{\epsilon_k^2 + \Delta_k^2}}\right) \tag{2.78}$$

as a function of the single particle energy ϵ_k and of the state - dependent pairing potential $\Delta_{k\,k'}$, called *gap parameter*. The simplest case of diagonal potential, $\Delta_{k\,k'} = \Delta_k\delta_{k\,k'}$ is often used, with Δ_k defined as

$$\Delta_k = -\sum_{k'>0} V_{k,\overline{k},k',\overline{k'}}u_{k'}v_{k'} \tag{2.79}$$

In eq.s (2.78), $\sqrt{\epsilon_k^2 + \Delta_k^2}$ is the quasiparticle energy [114]. By inserting eq. (2.78) into eq. (2.79) the *gap equation*

$$\Delta_k = -\frac{1}{2}\sum_{k'} V_{k,\overline{k},k',\overline{k'}}\frac{\Delta_{k'}}{\sqrt{\epsilon_{k'}^2 + \Delta_{k'}^2}} \tag{2.80}$$

is obtained. The gap equation can be solved analytically only in few very simplified cases, but is very useful for the numerical determination of Δ_k.

A nuclear excited state can be obtained from BCS ground state by applying the 2 - quasiparticle (2QP) creation operator

$$\hat{Q}^{\dagger}_{K} = \sum_{m,\,m'} \langle jmj'm'|JM\rangle \hat{\alpha}^{\dagger}_{k}\hat{\alpha}^{\dagger}_{k'} \tag{2.81}$$

creating a quasiparticle in the excited state with total angular momentum j and magnetic quantum number m and another quasiparticle in the state characterized by quantum numbers j' and m', so that the excited state created is characterized by quantum numbers J and M, embedded into the index K. In the case of single charge exchange reactions, which represents the starting point of the present work, the 2QP operator $Q^{\dagger}_{K}$ creates e. g. a quasiproton with quantum numbers (j, m) and a quasineutron in the state (j', m'). The complete operator for charge exchange excitation is

$$\hat{\omega}^{\dagger}_{K} = \sum_{j,j'} \Big[x_K(j,j')\hat{Q}^{\dagger}_{K}(j,j') - (-1)^{J-M} y_K(j,j')\hat{Q}_{\overline{K}}(j,j') \Big] \tag{2.82}$$

where x_K and y_K represent the QRPA amplitudes for a charge exchange process, or in general for the exchange of a quasiparticle, and its time reversed, respectively.

In order to describe some nuclear energy states, it is necessary to take into account higher order quasiparticle (e. g. 4QP and higher) configurations, so that the true nuclear eigenstates are given by the excitation operator

$$\hat{\Omega}^{\dagger}_{K} = \sum_{i} z^{J}_{i}\hat{\omega}^{\dagger}_{K}(i) + \hat{\eta}^{\dagger}_{K} \tag{2.83}$$

where the sum is over all 2QP configurations, z^{J}_{i} is the *spectroscopic amplitude* representing the probability amplitude to find the model state, obtained by using the operator $\hat{\omega}^{\dagger}_{K}(i)$, distributed over the states obtained from $\hat{\Omega}^{\dagger}_{K}$, generally characterized by an energy different from the one

obtained by simply considering 2QP configurations only; finally, $\hat{\eta}_K^\dagger$ is the excitation operator, orthogonal to $\hat{\omega}_K^\dagger(i)$, accounting for all higher order configurations. Both $\hat{\omega}_K^\dagger$ and $\hat{\Omega}_K^\dagger$ operators describe a transition and its time reversed, e. g. for a single charge exchange process they account for $p \to n$ ($n \to p$) and $n \to p$ ($p \to n$) transitions, respectively; of course in a charge exchange transition, one nucleus can only undergo one of the two transformations and this is accounted for by means of the lowering (τ^-) or raising (τ^+) isospin operators.

HFB theory represent an extention of the BCS one, being based on more general quasiparticles, generated (annihilated) by creation (annihilation) operators which are linear combinations of $\hat{\alpha}_k^\dagger$ ($\hat{\alpha}_k$)

$$\hat{\beta}_k^\dagger = \sum_{k'} C_{kk'} \hat{\alpha}_{k'}^\dagger \tag{2.84}$$

where $C_{kk'}$ are the elements of the unitary matrix, allowing to express the HFB Hamiltonian of the many - body system in the *canonical* basis where the (*normal*) density matrix becomes diagonal. The indices k and k' now allow to distinguish between *paired* states ($0 < u_p < 1$, $0 < v_p < 1$, like in BCS case) and *blocked* levels, which in turn can be *occupied* ($v_i = 1, u_i = 0$) or *empty* ($v_m = 0, u_m = 1$).

HFB Hamiltonian mixes all possible long - range *ph*-interactions (accounted for by the self - consistent HF mean field potential) and the short - range pairing one (described by the BCS pairing field, $\Delta_{kk'}$), thus allowing to describe both closed shell and open shell nuclei, together with possible ground state deformations, in terms of mean field potentials [109].

The description of nuclear structure properties by means of nuclear wavefunctions is not very satisfactory when closely - spaced - high excited and continuum states are taken into account and becomes impracticable in the limit of a large number of particles, implying the use of a huge configuration space.

A more powerfull method to obtain nuclear structure information, overcoming these limitations, is represented by the Green's function formulation of the QRPA [109, 114], consisting in the determination of the nuclear *response function*, rather than solving Schrödinger equation.

The response function, R, is a measure of the change of nuclear properties, and thus of nuclear observables [115], in the presence of an external field, P_λ, where the index λ specifies the nature of the external field used to probe the nuclear system, e. g. $\lambda = 1, \sigma, \tau, \sigma\tau$, ... Indeed, the response function is defined in terms of the transition probability from the QRPA ground state, $|0\rangle$, to the excited state, $|n\rangle$, with energy ω_n, determined by the action of the external field, P_λ,

$$R(\omega, P_\lambda) = \sum_{n\neq 0} |\langle n|P_\lambda|0\rangle|^2 \delta(\omega - \omega_n) \tag{2.85}$$

By introducing the interacting Green function, $G(\omega)$, of the total Hamiltonian H of the nuclear system

$$G(\omega) = \frac{1}{H - \omega - i\epsilon} + \frac{1}{H + \omega - i\epsilon} \tag{2.86}$$

the response function can be equivalentely expressed as

$$\begin{aligned} R(\omega, P_\lambda) &= \frac{1}{\pi} Im \sum_{n\neq 0} |\langle n|P_\lambda|0\rangle|^2 \left[\frac{1}{\omega_n - \omega - i\epsilon} + \frac{1}{\omega_n + \omega - i\epsilon}\right] \\ &= \frac{1}{\pi} Im \langle 0|P_\lambda^\dagger G(\omega) P_\lambda|0\rangle \end{aligned} \tag{2.87}$$

i. e. as the imaginary part of the *polarization propagator* [116], Π_λ, defined as the QRPA vacuum expectation value of the external field P_λ combined with the interacting Green function $G(\omega)$,

$$\Pi_\lambda = \langle 0|P_\lambda^\dagger G(\omega) P_\lambda|0\rangle \tag{2.88}$$

The response function integral

$$S_N(P_\lambda) = \int d\omega\, \omega^N R(\omega, P_\lambda) \tag{2.89}$$

gives the energy - weighted ($N = 1$) or non - energy weighted ($N = 0$) sum rules, which have the peculiarity to be model - independent quantities. In particular, for Fermi ($\lambda = \tau$) and Gamow - Teller ($\lambda = \sigma\tau$) transitions, the difference between the non - energy weighted sum rule (NEWSR) for a transition and that for its time reversed is simply related to the number of nucleons of the given nucleus

$$\begin{aligned} S_0(\tau^-) - S_0(\tau^+) &= \sum_{n\neq 0} |\langle n|\tau^-|0\rangle|^2 - \sum_{n\neq 0} |\langle n|\tau^+|0\rangle|^2 = N - Z \\ S_0(\sigma\tau^-) - S_0(\sigma\tau^+) &= \sum_{n\neq 0} |\langle n|\sigma\tau^-|0\rangle|^2 - \sum_{n\neq 0} |\langle n|\sigma\tau^+|0\rangle|^2 = 3(N - Z) \end{aligned} \tag{2.90}$$

These relations are known as Ikeda's sum rules [117], which represent a powerfull way to check the consistency of numerical calculations and constitute a guideline for analyzing total Fermi and Gamow - Teller strenghts.

CHAPTER 3

SINGLE CHARGE EXCHANGE NUCLEAR REACTIONS

Single charge exchange nuclear reactions are well established tools for nuclear spectroscopic studies [80].

"Direct" single charge exchange (SCE) nuclear reactions are mainly due to the long range tail of the strong nuclear interaction, scilicet the main contribution is represented by pion exchange. For momentum transfer sensibly smaller than the pion mass, an "effective" description of SCE processes is possible, where the corresponding mesonic form factors can be safely replaced by smoothly energy dependent coupling factors, on the same line of Fermi's coupling constant in the homonymous effective theory of beta decay. In this way, the analogy between Fermi and Gamow-Teller modes in the beta decay and in SCE nuclear reactions becomes closer [80]. Both light and heavy ion charge exchange nuclear reactions are characterized by high linear and angular momentum transfer, differently from weak processes which strongly select $\Delta L = 0$ modes; thus, beta decay - forbidden nuclear matrix elements become also available with such nuclear reactions, allowing the study of spin- and spin-isospin flipping collective excitations, like the spin dipole resonance and

Gamow-Teller giant resonance, together with non-spin flipping and high multipolarity collective modes of nuclei.

3.1 First single charge exchange attempts

A proportionality relation between β^- decay strenght, extracted from β decay measurements, and the zero degree (p,n) cross section, has been found in 1980 by Goodman and coworkers, at IUCF SWINGER facility [7], by using a $120\,MeV$ proton beam on ^{7}Li, ^{12,13}C, ^{25,26}Mg, ^{27}Al, ^{28}Si and ^{90}Zr target nuclei; some year later, the corresponding theoretical framework has been provided by Taddeucci [2], on the basis of previous formulations of the charge exchange part of the effective two-body interaction potential [118–120], and tested with (p,n) data for the following reactions: $^{7}\mathrm{Li}(p,n)^{7}\mathrm{Be}$, $^{12,14}\mathrm{C}(p,n)^{12,14}\mathrm{N}$, $^{28}\mathrm{Si}(p,n)^{28}\mathrm{P}$, $^{42}\mathrm{Ca}(p,n)^{42}\mathrm{Sc}$, $^{54}\mathrm{Fe}(p,n)^{54}\mathrm{Cn}$, $^{90}\mathrm{Zr}(p,n)^{90}\mathrm{Nb}$ and $^{208}\mathrm{Pb}(p,n)^{208}\mathrm{Bi}$ at intermediate beam energies $(120-200\,MeV)$.

Theoretical formulations of light ion "direct" single charge exchange reactions were then summarized by Osterfeld [9], while experiments performed up to the late '90s were reviewed by Alford [13].

Heavy ion nuclear reactions can involve linear and angular momentum transfer higher than light ion ones, so that it is possible to gain information on higher multipolarity collective modes and to get simultaneously information both on target and projectile SCE (and also DCE) nuclear matrix elements and so on the corresponding beta decay strengths.

Heavy ion charge exchange reactions represent the core of the NUMEN experiment, currentely performed at INFN/LNS (Italy). As stated in chapter 1, NUMEN experiment is ambitiously lookig for a determination of $0\nu\beta\beta$ nuclear matrix element from heavy ion DCE cross section measurements at forward scattering angles, possible thanks to MAGNEX spectrometer, which allows to performe high mass, angle and energy resolution measurements at zero degree, also for very low yields, even if an

increase of beam intensity (to increase statistics) and a consequent upgrade of the materials constituting the detectors (so as to improve their radiation hardness) are needed in order to get results with an accuracy significant for neutrino physics community [80]. This goal presupposes the existence of a proportionality relation between heavy ion DCE forward angular distribution and $0\nu\beta\beta$ nuclear matrix element, which is still a matter of study [5] and is providing a very tricky task, so that at the actual state-of-art the analogy between the nuclear matrix elements involved in these two (weak and strong) processes is still not guaranteed. To further increase statistics, beam energy, projectile and target nuclei have been properly chosen in order to set the kinematical condition disfavouring multi-nucleon transfer processes and enhancing the magnitude of DCE (and SCE) cross sections [1, 80], which is expected to be small in heavy ions, because they are strongly absorbing systems. Thus, in order to increase the magnitude of such charge exchange cross sections, it should be desirable to use nuclei belonging to the same $SU(4)$ spin-isospin multiplet and characterized by a Gamow-Teller strength not much fragmented.

For this reasons, e. g. ^{18}O projectile has been chosen, because ^{18}O and ^{18}Ne (DCE) belong to the same isospin multiplet ($T = 1$) and the former nucleus represents the lightest non-radioactive isotope belonging to this multiplet, so that it can be produced easily and with high beam intensity [121]; moreover, both (^{18}O,^{18} F) and (^{18}F,^{18} Ne) transitions are characterized by large values of GT strengths, which are mainly concentrated in the ground state of ^{18}F (1^+).

(^{18}O,^{18} Ne) reactions probe $\beta^+\beta^+$ transitions in target nuclei, while most of the research on $0\nu\beta\beta$ decay is focusing on $\beta^-\beta^-$ transitions. For this reason, also (^{20}Ne,^{20} O), or alternatively (^{12}C,^{12} Be), probing $\beta^-\beta^-$ transitions in target nuclei, are being taken into account, even if they are characterized by a strength smaller than the one of (^{18}O,^{18} Ne)

reactions. In 2013, NUMEN first experiment has been performed for the reaction ^{40}Ca(^{18}O,^{18} Ne)^{40}Ar, used as "pilot" process to test the feasibility of the experiment, indicating that suitable information from DCE reactions can be extracted [80]. In view of the study of reactions involving nuclei which are $0\nu\beta\beta$ decay candidates[1] both (^{18}O,^{18} Ne) and (^{20}Ne,^{20} O) reactions with target nuclei heavier than the pilot ones are being studied, such as ^{116}Sn(^{18}O,^{18} Ne)^{116}Cd, ^{116}Cd(^{20}Ne,^{20} O)^{116}Sn, ^{76}Se(^{18}O,^{18} Ne)^{76}Ge, ^{76}Ge(^{20}Ne,^{20} O)^{76}Se and ^{130}Te(^{20}Ne,^{20} O)^{130}Xe, all with beam energy of $15\,AMeV$ and it is planned to study the reaction ^{106}Cd(^{18}O,^{18} Ne)^{106}Pd, at $15\,AMeV$ beam energy, too. Within the NUMEN collaboration, a study of heavy ion SCE processes, involved in the DCE reactions described above, is also performed to further constraining models regarding both nuclear structure and nuclear reaction dynamics and is also useful for DCE calculations (see chapter 4).

In the following sections the formalism by Taddeucci for (p, n) reactions at high energies and then its extention to heavy ion reactions at low energies, above the Coulomb barrier, developed during the present work, are illustrated.

3.2 Light ion single charge exchange reactions

The simplest strong interaction-mediated charge changing nuclear reaction is represented by single charge exchange via (p, n) or (n, p) re-

[1]The nuclei candidate to decay $0\nu\beta\beta$

^{48}Ca,^{76} Ge,^{82} Se,^{96} Zr,^{100} Mo,^{110} Pd,^{116} Cd,^{124} Sn,
$^{128,\,130}$Te,^{136} Xe,$^{148,\,150}$ Nd,^{154} Sm,^{160} Gd,^{198} Pt

for $\beta^-\beta^-$ decay and

^{78}Kr,^{92} Mo,^{96} Ru,^{106} Cd,^{124} Xe,^{130} Ba,^{136} Ce

as $\beta^+\beta^+$, β^+EC or $ECEC$ candidates [80].

	SCE	β decay
$(S=1)$	$\sum_{ij} V_{\sigma\tau}(\mathbf{r}_{ij})\boldsymbol{\sigma}_i \cdot \boldsymbol{\sigma}_j \boldsymbol{\tau}_i \cdot \boldsymbol{\tau}_j$	$g_A \sum_i \boldsymbol{\sigma}_i \boldsymbol{\tau}_i$
$(S=0)$	$\sum_{ij} V_{\tau}(\mathbf{r}_{ij})\boldsymbol{\tau}_i \cdot \boldsymbol{\tau}_j$	$g_V \sum_i \boldsymbol{\tau}_i$

Table 3.1: Comparison between the spin - isospin operators describing the central part of the nuclear strong interaction involved in direct SCE nuclear reaction and the weak interaction in single beta decay process, both in the two cases of spin - flip ($S = 1$), i. e. Gamow - Teller (GT), and non spin - flip ($S = 0$), i. e. Fermi (F), transitions.

actions. As stated in chapter 1, these kind of processes can be due to two-nucleon transfer or "direct" one - step reactions, i. e. a simultaneous exchange of two nucleons between target and projectile; the latter type of processes, from now on simply referred to as single charge exchange (SCE) nuclear reactions, are due to meson exchange (hard process) and are described by the same spin - isospin structure of single beta decay [2, 96, 122, 123], as shown in Tab. 3.1, while the former processes are caused by nuclear mean field interaction (soft processes) and are characterized by spin - isospin operators different from the one involved in Gamow-Teller and Fermi beta decays [105].

Guided by the analogies in tab. 3.1, it is immediate to look at the SCE nuclear reactions as a tool to gain information on beta decay nuclear matrix element for a candidate nucleus. This peculiarity, together with the plethora of nuclear structure information provided by such nuclear reactions (from single particle to collective modes), led to pay special attention to the development of a formalism of SCE reactions, starting from the simplest case of (p, n) processes.

Taddeucci (1987) starts from (p, n) double differential cross section,

in the center of mass frame,

$$\frac{d^2\sigma}{dEd\Omega} = \frac{E_\alpha E_\beta}{4\pi^2(\hbar c)^4}\frac{k_\beta}{k_\alpha}\frac{1}{(2J_A+1)}\frac{1}{2}\sum_{\substack{m_A,m_B\\ m_a,m_b}}|\sum_\tau \mathcal{M}^\tau_{\alpha\beta}(\mathbf{k}_\alpha,\mathbf{k}_\beta)|^2 \qquad (3.1)$$

by using DWBA together with impulse[2] and zero-range approximations, so that the transition matrix element reduces to that of eq. (2.58), referred to nucleon - nucleon interaction, and for (p,n) processes further simplifies to

$$\begin{aligned}
&\mathcal{M}^{(\tau)}_{\alpha\beta}(\mathbf{k}_\alpha,\mathbf{k}_\beta) = \\
&\sum_{S,T}\int d^3r\,\chi^{(-)*}_{\mathbf{k}_\beta}(\mathbf{r}) < \psi_B,n|\hat{\mathbb{V}}^{\tau,(ST)}_{\alpha\beta}(\mathbf{r},\boldsymbol{\sigma}_\alpha,\boldsymbol{\tau}_\alpha,\boldsymbol{\sigma}_\beta,\boldsymbol{\tau}_\beta)P_x|p,\psi_A > \chi^{(+)}_{\mathbf{k}_\alpha}(\mathbf{r}) \\
&= \sum_{S,T}\int d^3r\,\chi^{(-)*}_{\mathbf{k}_\beta}(\mathbf{r}) < \psi_B,n|\sum_j \hat{V}^{(\tau)}_{ST}(\mathbf{r})\mathcal{O}_j\mathcal{O}_pP_x|p,\psi_A > \chi^{(+)}_{\mathbf{k}_\alpha}(\mathbf{r})
\end{aligned} \qquad (3.2)$$

where $|p\rangle$ and $|n\rangle$ represent proton and neutron wave functions in spin-isospin space, respectively[3]; the sum $\sum_j$ in the last line of eq. (3.2) runs over all nucleons in the target and the spin - isospin dependence of nucleon-nucleon effective potential has been made explicit through the introduction of the spin - isospin operators $\mathcal{O}_j$ and $\mathcal{O}_p$ accounting for the transition in target and projectile nuclei, respectively. By writing the transition matrix element in momentum space, so that projectile and target coordinates are separated, and considering only central effective nucleon-nucleon interaction ($\tau = C$), eq. (3.2) becomes

$$\mathcal{M}^{(\tau)}_{\alpha\beta}(\mathbf{k}_\alpha,\mathbf{k}_\beta) = \int d^3q\, t^{\tau,(ST)}(q)\rho_{ST}(\mathbf{q})d(\mathbf{q},\mathbf{k}_\alpha,\mathbf{k}_\beta) \qquad (3.3)$$

where

$$t^{C,(ST)}(q) = 4\pi\int_0^\infty dr\, r^2 V^{(C)}_{ST}(r)\left[j_0(qr) + (-1)^l j_0(k_\alpha r)\right] \qquad (3.4)$$

[2]DWBA plus impulse approximation will be refered with the acronym DWIA.

[3]The coordinate space wave functions for proton and neutron do not appear, because for energies less than $1\,GeV$, nucleons can be treated as point-like particles.

is nothing but the Fourier transform of the direct (first term inside square parenthesis) and exchange (second term inside square parenthesis) components of $V_{ST}^{(C)}$ (the factor $(-1)^l$ in the exchange term, i. e. the term obtained through the action of the antisymmetrizing operator P_x introduced in chapter 2, accounting for a properly antisymmetrized conversion between S, T and singlet-triplet even-odd representation of the effective potential),

$$\rho_{ST}(\mathbf{q}) = \langle \psi_B | \sum_j \mathcal{O}_j e^{-i\mathbf{q}\cdot\mathbf{r}_j} | \psi_A \rangle \langle n | \mathcal{O}_p | p \rangle \tag{3.5}$$

represents the Fourier transform of the transition density, which contains all information on the nuclear structure of the target nucleus, thus playing a major role in nuclear spectroscopic studies, and

$$d(\mathbf{q}, \mathbf{k}_\alpha, \mathbf{k}_\beta) = \frac{1}{(2\pi)^3} \int d^3r \, \chi^{(-)*}_{\mathbf{k}_\beta}(\mathbf{r}) \chi^{(+)}_{\mathbf{k}_\alpha}(\mathbf{r}) e^{-i\mathbf{q}\cdot\mathbf{r}} \tag{3.6}$$

is the *distortion coefficient*, which contains all the information on initial and final state interactions, encoded into the distorted waves, and is crucial in the determination of a proportionalty relation between forward (p, n) angular distribution and beta decay strength.

3.2.1 Light ion single charge exchange cross section factorization

Considering the small linear momentum transfer range and assuming that only $\Delta L = 0$ transition is important for small scattering angles (so as to reproduce the kinematical conditions characterizing beta decays), after few passages exploiting Wigner $3-j$ symbol properties, the Fourier transform of the transition density reduces to

$$\begin{aligned} &\rho_{ST}(\mathbf{q}) = \sqrt{2J_A+1}\sqrt{2\Delta S+1}\sqrt{8} e^{-\frac{1}{6}q^2\langle r^2\rangle_\rho} M_{ST}(X) \\ &\sum_{M_s} \begin{pmatrix} J_A & J_B & \Delta S \\ m_A & -m_B & M_S \end{pmatrix} (-1)^{J_B - m_A - M_s} \begin{pmatrix} \frac{1}{2} & \frac{1}{2} & \Delta S \\ m_p & -m_n & M_S \end{pmatrix} \end{aligned} \tag{3.7}$$

where ΔS is the spin transferred in the reaction, $\langle r^2 \rangle_\rho$ is the mean square radius of the transition density, $m_i \, (i = A, B, p, n)$ are the eigenval-

ues associated to the third component of total angular momentum and $M_{ST}(X)$ is the reduced nuclear matrix element of the target nucleus, with $X = GT$, F identifying Gamow-Teller or Fermi transitions. The square modulus of nuclear matrix element is just equal to beta decay strength of the same nucleus, as illustrated by the following well - established relations (first line for Gamow-Teller transitions and second line for Fermi transitions) [118]

$$\begin{aligned} B(GT) &= \frac{1}{2J_A+1}|\langle J_B||\boldsymbol{\sigma}\tau^-||J_A\rangle|^2 \equiv |M_{ST}(GT)|^2 \\ B(F) &= \frac{1}{2J_A+1}|\langle J_B||\tau^-||J_A\rangle|^2 \equiv |M_{ST}(F)|^2 \end{aligned} \tag{3.8}$$

with both Fermi and Gamow-Teller strengths normalized to the corresponding nucleon strengths.

In the small momentum transfer limit, $t^{C,(ST)}(q)$ simplifies to

$$t^{C,(ST)}(q) \simeq J_0^{C,(ST)} e^{-\frac{1}{6}q^2\langle r^2\rangle_t} \tag{3.9}$$

being $J_0^{C,(ST)}$ the volume integral of both direct and exchange terms of the central effective nuclear interaction potential $V_{ST}^{(C)}(r)$ and $\langle r^2\rangle_t$ is the mean square radius of the effective interaction.

Moreover, treating distorted waves by means of the eikonal approximation, making the naive assumption of a three-dimensional square-well optical potential, choosing zero impact parameter and properly fitting the dependence on the target mass number A, the distortion coefficient reduces to

$$d(\mathbf{q}, \mathbf{k}_\alpha, \mathbf{k}_\beta) = e^{\frac{1}{2}\left[-xA^{1/3}+p(\omega)\right]}\delta(\mathbf{q}-\mathbf{q}_{\alpha\beta})e^{i\phi} \tag{3.10}$$

where $\mathbf{q}_{\alpha\beta} = \mathbf{k}_\alpha - \mathbf{k}_\beta$ is the relative momentum transfer, ϕ is a real eikonal phase due to the real part of the optical potential, $x = 4r_0 W_\alpha/\hbar c\beta_\alpha$, being W_α the maximum value of the imaginary part of the optical potential, $r_0 = 1.2\,fm$, β_α the projectile velocity and $p(\omega) = a_0 + a_1\omega + a_2\omega^2$ is a second order polynomial of the "energy loss" $\omega = E_x - Q_{reac}$, with

E_x the target excitation energy and Q_{reac} the $Q-$value of the reaction, according to the formailsm in [2].

Through the distortion coefficient of eq. (3.10), Taddeucci provided a proportionality relation between (p,n) cross section at small momentum transfer and beta decay strength of the given target nucleus, as shown by the following (factorized) expression

$$\begin{aligned}\frac{d^2\sigma}{dEd\Omega} &= \frac{E_\alpha E_\beta}{\pi^2(\hbar c)^4}\frac{k_\beta}{k_\alpha}|J_0^{C,(ST)}|^2 e^{-\frac{1}{3}q^2_{\alpha\beta}\langle r^2\rangle}e^{-xA^{1/3}+p(\omega)}B(X)\\ &= K(E_b,\omega)|J_0^{C,(ST)}|^2 N^D B(X)\\ &\equiv \hat{\sigma}_X(E_b,A)F_X(q,\omega)B(X)\end{aligned} \tag{3.11}$$

where $E_\alpha = \sqrt{\mu_\alpha^2+k_\alpha^2}$ ($E_\beta = \sqrt{\mu_\beta^2+k_\beta^2}$) is the reduced energy of the initial (final) channel that in non relativistic limit reduces to μ_α (μ_β); in the second line of eq. (3.11), the kinetic factor

$$K(E_b,\omega) = \frac{E_\alpha E_\beta}{\pi^2(\hbar c)^4}\frac{k_\beta}{k_\alpha} \tag{3.12}$$

is introduced, which depends on ω and on beam energy E_b, and

$$N^D = e^{-\frac{1}{3}q^2_{\alpha\beta}\langle r^2\rangle}e^{-xA^{1/3}+p(\omega)} \tag{3.13}$$

which in the limit of zero momentum transfer and zero energy loss reduces to the *distortion factor* definition, given by Goodman [7][133]

$$N^D = \frac{(d^2\sigma/dEd\Omega)^{(DWBA)}_{0^o}}{(d^2\sigma/dEd\Omega)^{(PWBA)}_{0^o}} \tag{3.14}$$

In the last line of eq. (3.11), the so called "unit cross section" has been introduced, defined as

$$\hat{\sigma}_X(E_b,A) \equiv K(E_b,0)|J_0^{(ST)}|^2 e^{-xA^{1/3}+a_0} \tag{3.15}$$

and

$$F_X(q,\omega) = \frac{K(E_b,\omega)}{K(E_b,0)}e^{-\frac{1}{3}q^2_{\alpha\beta}\langle r^2\rangle}e^{p(\omega)-a_0} \tag{3.16}$$

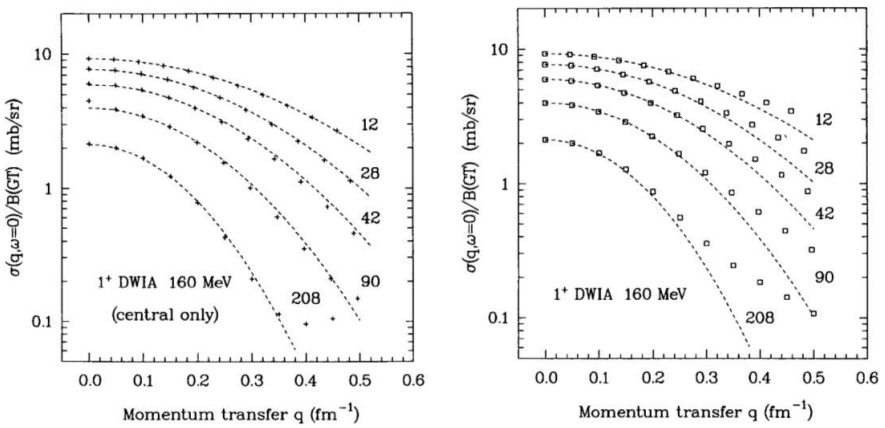

Figure 3.1: Cross section from eq. (3.11) (dashed line) versus momentum transfer, normalized to full DWIA calculations for 1^+ transitions (squares) obtained by using only central (left panel) and central plus tensor effective nuclear interaction (right panel) [2].

is the factor accounting for the shape of the cross section and goes to unity for $(q, \omega) \rightarrow (0, 0)$ [2], thus stressing the importance of the unit cross section, which represents the proportionality factor between the zero degree cross section and the beta decay strength.

The gaussian momentum dependence of light ion SCE cross section at intermediate energies, thus found by Taddeucci, represents a quite realistic approximation, in that the agreement with full DWIA calculations (i. e. relaxing small momentum, $\Delta L = 0$ only, eikonal and square well optical potential approximations) is good for a large range of momentum transfer values, while reduces to $q_{\alpha\beta} \leqslant 0.25\, fm^{-1}$ if compared with full calculations including tensor effective nuclear interaction, as shown in the two plots in fig. 3.1, and, above all, because it fits pretty well the shape of the data for 1^+ transitions, even if the fit becomes worst for 0^+ transitions to isobaric analog state, as shown in fig. 3.2, the latter discrepancy probabily due to transition density shapes differing from a gaussian one.

An analogous factorized expression has been deduced for heavy ion single charge exchange reactions, within the present PhD work, following

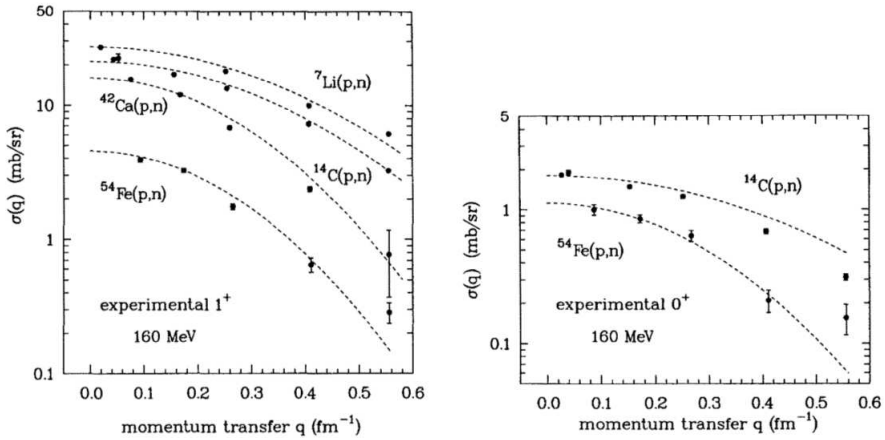

Figure 3.2: Cross section from eq. (3.11), normalized to the data for 1^+ (left panel) and 0^+ (right panel) transitions, as a function of momentum transfer [2].

the same validation procedure, as shown in the section below and in the last chapter, where the results are illustrated.

The most recent high energy resolution (^{3}He, t) experiment performed at RCNP, Osaka University [8][126] shows a good correlation between SCE and $\beta-$decay Gamow - Teller strengths for same nuclear states, as shown in fig. 3.3.

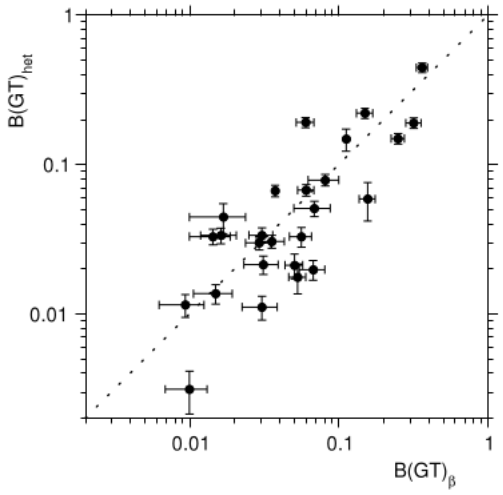

Figure 3.3: Gamow - Teller strength from ^{41}K(^{3}He, t)^{41}Ca reaction cross section measurements, $B(GT)_{het}$, versus the corresponding beta decay strength, obtained from ^{41}Ti(β^+)^{41}Sc $\beta-$decay measurements at RCNP [8].

Similar results have been found also for β^+ transitions, through $(d,^2\mathrm{He})$ reactions at KVI (Netherlands) [127–130] and RIKEN (Japan) [131, 132] laboratories.

3.3 Heavy ion single charge exchange reactions

Within the present PhD work, the formalism developed by Taddeucci for (p,n) reactions at intermediate energies, has been extended to heavy ion SCE processes at low energies. Of course, heavy ion SCE reaction cross section calculation is more involved than that for (p,n) reactions, because for heavy ions the internal degrees of freedom of projectile nucleus have to be also taken into account, as dealt with in the following.

The direct nature of charge exchange reactions and the short range nature of the strong nuclear interactions allow to use DWBA and zero range approximation, so that the transition matrix element becomes

$$\begin{aligned}&\mathcal{M}^{(\tau)}_{\alpha\beta}(\mathbf{k}_\alpha,\mathbf{k}_\beta) = \\ &\int d^3r\, \chi^{(-)*}_{\mathbf{k}_\beta}(\mathbf{r}) < \psi_B\phi_b|\hat{V}^{(\tau)}_{\alpha\beta}(\mathbf{r},\boldsymbol{\sigma}_\alpha,\boldsymbol{\tau}_\alpha,\boldsymbol{\sigma}_\beta,\boldsymbol{\tau}_\beta)P_x|\psi_A\phi_a > \chi^{(+)}_{\mathbf{k}_\alpha}(\mathbf{r})\end{aligned} \tag{3.17}$$

which is just eq. (2.58).

Generally, calculations are performed in momentum space, where projectile and target coordinates are separated, due to Fourier transform properties, so that transition matrix element becomes

$$\mathcal{M}^{(\tau)}_{\alpha\beta}(\mathbf{k}_\alpha,\mathbf{k}_\beta) = \sum_{ST}\int d^3p\, K^{(ST)}_{\alpha\beta}(\mathbf{p})N^D(\mathbf{p}) \tag{3.18}$$

where

$$N^D(\mathbf{p}) = \int \frac{d^3r}{(2\pi)^3}\,\chi^*_{\mathbf{k}_\beta}(\mathbf{r})\chi_{\mathbf{k}_\alpha}(\mathbf{r})e^{-i\mathbf{r}\cdot\mathbf{p}} \tag{3.19}$$

is just the *distortion coefficient* introduced by Taddeucci, which is nothing but the Fourier transform of the product of the distorted waves in

the initial ($\chi_{\mathbf{k}_\alpha}(\mathbf{r})$) and final ($\chi_{\mathbf{k}_\beta}(\mathbf{r})$) channels, thus accounting for the reaction dynamics of the process, and

$$\begin{aligned} K^{(ST)}_{\alpha\beta}(\mathbf{p}) &= V^{(C)}_{ST}(p) F^{(ST)\dagger}_{ab}(\mathbf{p}) \cdot F^{(ST)}_{AB}(\mathbf{p}) \\ &+ \delta_{S1}\sqrt{\frac{24\pi}{5}} V^{(T)}_{ST}(p) Y^*_2(\hat{p}) \cdot \left[F^{(ST)\dagger}_{ab}(\mathbf{p}) \otimes F^{(ST)}_{AB}(\mathbf{p}) \right]_2 \end{aligned} \tag{3.20}$$

called "reaction kernel", accounts for the whole nuclear structure information of the process, being a combination of the Fourier transform of the radial coordinate component of the effective local nuclear interaction potential, $V^{(\tau)}_{ST}(p)$, with projectile (lowercase letter subscripts) and target (capital letter subscripts) form factors. The latter terms are just the equivalent of Taddeucci's transition density in momentum space; indeed, they are given by the matrix element of the operators $\mathcal{O}^{(ST)}_{AB}$ and $\mathcal{O}^{(ST)}_{ab}$, accounting for spin-isospin transition in target and projectile nuclei, respectively, as shown by the following expression e. g. for projectile nucleus

$$\begin{aligned} F^{(ST)}_{ab}(\mathbf{p}) &= < J_b m_b | \frac{1}{4\pi} e^{i\mathbf{p}\cdot\mathbf{r}_a} \mathcal{O}^{(ST)}_{ab} | J_a m_a > \\ &= \sum_{\substack{L, M_L \\ J_1, M_1}} (J_a, m_a, J_b, m_b | J_1, M_1) \, (L, M_L, S, M_S | J_1, M_1) \, \rho^{(L,S,J_1)}_{ab}(p) i^L Y_{L,M_L}(\hat{p}) \end{aligned} \tag{3.21}$$

(same expression holds for target). The scalar product in the first term (central potential) of eq. (3.20) implies the contraction of spin and isospin z-projection indices, while the rank - 2 tensorial term couples the spin degrees of freedom only, as follows

$$Y^*_2(\hat{p}) \cdot \left[F^{(ST)\dagger}_{ab}(\mathbf{p}) \otimes F^{(ST)}_{AB}(\mathbf{p}) \right]_2 = \sum_M Y^*_{2M}(\hat{p}) \left[F^{(ST)\dagger}_{ab}(\mathbf{p}) \otimes F^{(ST)}_{AB}(\mathbf{p}) \right]_{2M} \tag{3.22}$$

being

$$\left[F^{(ST)\dagger}_{ab}(\mathbf{p}) \otimes F^{(ST)}_{AB}(\mathbf{p}) \right]_{2M} = \sum_{m_1, m_2} (1, m_1, 1, m_2 | 2, M) \, F^{(ST)m_1\dagger}_{ab}(\mathbf{p}) F^{(ST)m_2}_{AB}(\mathbf{p}) \tag{3.23}$$

The radial term

$$\rho_{ab}^{(L,S,J_1)}(p) = 4\pi \int_0^\infty dr\, r^2 \rho_{ab}(r) j_L(pr) \tag{3.24}$$

is the Fourier transform of the radial transition density, which at low momentum transfer reduces to

$$\rho_{ab}^{(L,S,J_1)}(p \to 0) = 4\pi \frac{p^L}{(2L+1)!!} \int_0^\infty dr\, r^{2+L} \rho_{ab}(r) + \mathcal{O}(p^2) \tag{3.25}$$

The integral in the first order term, i. e.

$$b_{ab}^{(L,S,J_1)} = \int_0^\infty dr\, r^{2+L} \rho_{ab}(r) \tag{3.26}$$

is directly related to the Fermi/Gamow - Teller multipole operator

$$\mathcal{B}_{ab}^{(L,S,T)J_1,M_1}(\mathbf{r}) = r^L \left[Y_L \otimes (\boldsymbol{\sigma})^S \right]_{J_1 M_1} (\boldsymbol{\tau})^T \tag{3.27}$$

by the following proportionality relation [6]

$$|b_{ab}^{(L,S,J_1)}|^2 = \frac{1}{2J_1+1} |\langle J_b || \mathcal{B}_{ab}^{(L,S,T)J_1,M_1}(\mathbf{r}) || J_a \rangle|^2 \tag{3.28}$$

being J_1 the total angular momentum transfer.

3.3.1 Heavy ion single charge exchange cross section factorization

An euristic extention to heavy ions, at low and intermediate energies, of Taddeucci's factorized expression of the cross section, can be given by noting that, due to the direct nature of charge exchange reactions, it is possible to identify two momentum scales:

- the one describing the range in which the distortion factor is not negligible, that depends on the optical potential momentum scale, given by $\Delta k_{reac} \simeq \frac{1}{R_{opt}} \leqslant 50\, MeV$, where R_{opt} is the optical potential radius.

- the one describing the reaction kernel momentum dependence, which is governed by nuclear form factors, characterized by a momentum range of the order of Fermi momentum of protons and neutrons, $\Delta k_{nucl} \simeq k_F \simeq 300\, MeV$.

From these observations, it follows that the distortion factor can be treated as a Dirac delta distribution, peaked at the "on - shell" momentum transfer, $\mathbf{q}_{\alpha\beta}$; hence, the reaction kernel, which varies over a wider momentum range, can be expressed as the product of a term calculated at $\mathbf{q}_{\alpha\beta}$ and the residual function depending on the "off - shell" (i. e. the integrated) momentum, $\mathbf{q}$.

On a quantitative level, in order to obtain a proportionality relation between Fermi/Gamow - Teller β decay strength and SCE cross section, it is necessary to take out of momentum integral in eq. (3.18) at least one of the two factors shown above, in particular the reaction kernel, which contains the wanted projectile and target strengths.

Observing that direct reactions are surface processes, one expects that the corresponding radial transition densities can be described through gaussian distributions, peaked at the nuclear surface; this has been nicely verified by performing simulations through the HIDEX code [106], as shown in fig. 3.4, for SCE nuclear reactions ^{40}Ca(^{18}O,^{18} F)^{40}K$_{1^+_{2.3\,\mathrm{MeV}}}$, ^{40}K$_{1^+_{2.3\,\mathrm{MeV}}}$(^{18}F,^{18} Ne)^{40}Ar, ^{116}Sn(^{18}O,^{18} F)^{116}In, ^{116}In(^{18}F,^{18} O)^{116}Cd, leading to pn (np) transitions in target (projectile) nuclei, ^{116}Cd(^{20}Ne,^{20} F$_{1^+_{1.056\,MeV}}$) ^{116}In and ^{116}In(^{20}F$_{1^+_{1.056\,\mathrm{MeV}}}$,^{20} O)^{116}Sn, inducing np (pn) transitions in target (projectile) nuclei, studied within the NUMEN collaboration. These radial transition densities are calculated for zero angular momentum transfer[4], $L = 0$, for example, for the SCE transitions with $J^\pi = 1^+$. The slightly different position of the peaks for ^{40}Ca$_{\mathrm{g.s.}} \rightarrow^{40}$ K$_{1^+_{2.3\,\mathrm{MeV}}}$ and ^{40}Ar$_{\mathrm{g.s.}} \rightarrow^{40}$ K$_{1^+_{2.3\,\mathrm{MeV}}}$ transition densities shows shell effects, because ^{40}Ca is a doubly magic nucleus, while ^{40}Ar is not; this is the same reason of the

[4]This may allow the non - zero value of $\rho(r = 0)$.

peak shift for the heavier nuclei transition densities $^{116}\mathrm{Sn}_{\mathrm{g.s.}} \rightarrow ^{116}\mathrm{In}_{\mathrm{g.s.}}$ and $^{116}\mathrm{Cd}_{\mathrm{g.s.}} \rightarrow ^{116}\mathrm{In}_{\mathrm{g.s.}}$, because ^{116}Sn is a magic nucleus (the proton shell is closed, while neutron shell is not), while for ^{116}Cd both proton and neutron shells are not closed.

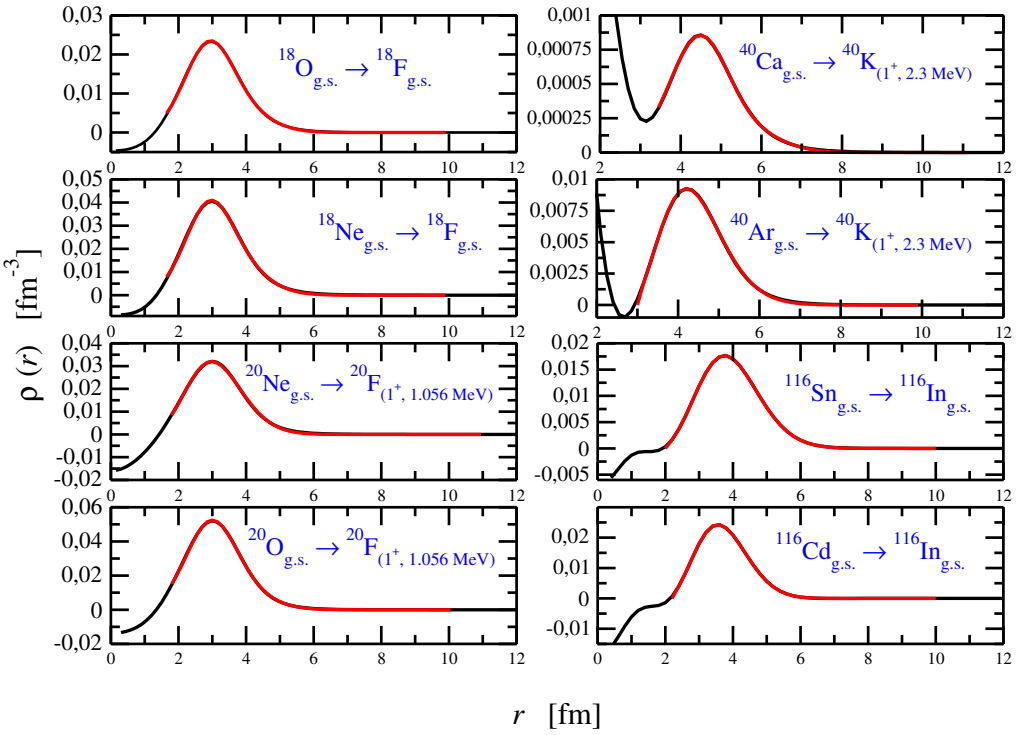

Figure 3.4: Radial transition densities for different projectiles (left panels), and targets (right panels), for zero angular momentum transfer, $L = 0$.

The gaussian shape of both projectile and target radial transition densities, shown in fig. 3.4 in coordinate space, allows to write each of the two transition form factors in terms of properly normalized gaussians, peaked at the nuclear surface and with standard deviation proportional to the surface thickness of the corresponding nucleus, which in coordinate space means

$$F_{XY}^{(ST)}(\mathbf{r}) = U_{0X} e^{-\frac{(\mathbf{r}-\mathbf{R}_X)^2}{2\sigma_X^2}} \tag{3.29}$$

being $XY = AB$ for target and ab for projectile transitions and R_a (R_A) and $\sqrt{2}\sigma_a$ ($\sqrt{2}\sigma_A$) are projectile (target) nuclear radius, $R = 1.2A^{\frac{1}{3}}$, and

projectile (target) nuclear surface thickness, respectively.

For the increasingly deformed nuclei ^{116}Sn, ^{116}Cd and ^{40}Ar, the transition densities can be fit through gaussians with peak position parameter smaller than the nuclear radius, because spherically symmetric transition densities are considered, but just the same results are obtained by using gaussians with parameter R_A corresponding to the nuclear radius and by slightly increasing the value of the other parameter, σ_A.

Switching from spatial to momentum coordinates, the form factor in eq. (3.29) of course remains a gaussian, according to the properties of gaussian distributions, as shown in eq. (3.30)

$$F_{XY}^{(ST)}(\mathbf{p}) = U'_{0X} e^{-\frac{1}{2}\sigma_X^2 p^2} e^{i\mathbf{p}\cdot\mathbf{R}_X} \tag{3.30}$$

From eq. (3.20), one can note that the reaction kernel is given by a combination of projectile and target transition form factors and in particular the central term contains their product; thus, after performing an investigation on the interplay between central and tensor components of the effective nuclear interaction potential (by means of HIDEX simulations [106]), which confirm that central components dominate over tensor ones at small scattering angles (for details, see chapter 6), one can safely consider only the central part of the reaction kernel, i. e. the reaction kernel simply given by the product of the effective nuclear interaction potential with projectile and target transition form factors.

The gaussian trend of the transition form factors, together with the smooth momentum dependence of effective NN interaction potential Fourier transform, shown in fig. 3.5, allows in turn to describe the whole reaction kernel in terms of a gaussian

$$\begin{aligned} K_{\alpha\beta}^{(ST)}(\mathbf{p},\mathbf{R}) &= V_{ST}^{(C)}(p = q_{\alpha\beta}) U_{0a} U_{0A} e^{-\frac{1}{2}\sigma_a^2 p^2} e^{i\mathbf{p}\cdot\mathbf{R}_a} e^{-\frac{1}{2}\sigma_A^2 p^2} e^{i\mathbf{p}\cdot\mathbf{R}_A} \\ &= V_{ST}^{(C)}(p = q_{\alpha\beta}) U_{0a} U_{0A} e^{-\frac{1}{2}\left(\sigma_a^2+\sigma_A^2\right)p^2} e^{i\mathbf{p}\cdot(\mathbf{R}_a+\mathbf{R}_A)} \\ &= U'_0 e^{-\frac{1}{2}\sigma^2 p^2} e^{i\mathbf{p}\cdot\mathbf{R}} \end{aligned} \tag{3.31}$$

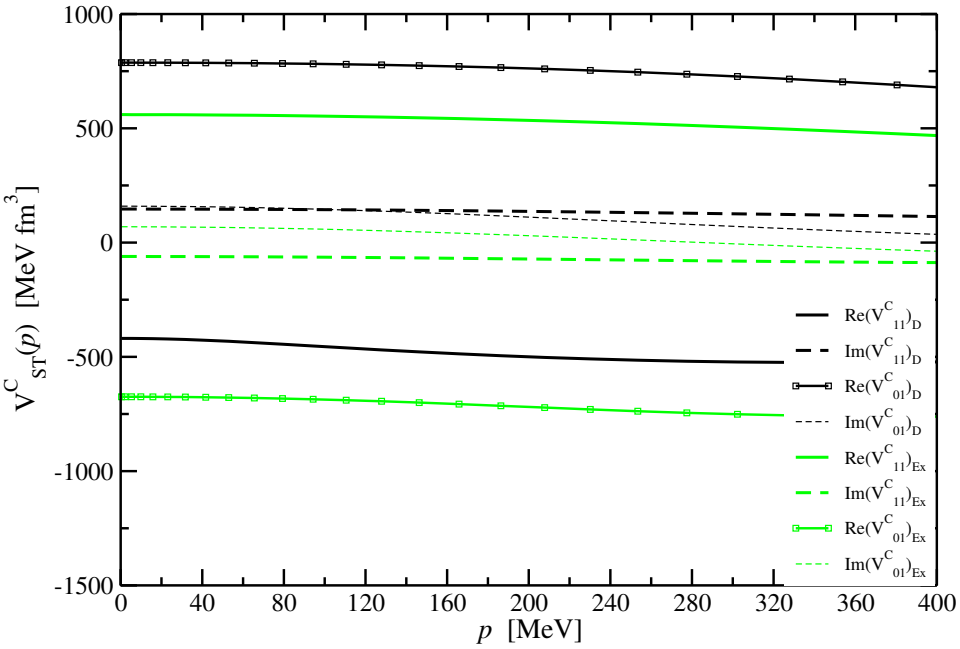

Figure 3.5: Direct (black lines) and exchange (green lines) components of central effective local NN interaction potential, both for Fermi and Gamow - Teller channels $(S,T) = (0,1)$ and $(1,1)$, respectively. The curves are obtained, through HIDEX code, by using $M3Y$ potential.

depending on the two parameters $R = \sqrt{R_a^2 + R_A^2}$ and $\sqrt{2}\sigma = \sqrt{2\sigma_a^2 + 2\sigma_A^2}$, which are nothing but the sum in quadrature of projectile and target nuclear radii and surface thicknesses, respectively, while the square of the parameter $U_0' = V_{ST}^{(C)}(p = q_{\alpha\beta})U_{0a}U_{0A}$ gives the magnitude of the reaction cross section corresponding to a scattering angle and an excitation energy fixed by the value of the momentum transfer modulus, $q_{\alpha\beta}$.

The dependence on the "on - shell" momentum transfer, $\mathbf{q}_{\alpha\beta}$, is made explicit through the change of integration variable, $\mathbf{p} = \mathbf{q}_{\alpha\beta} - \mathbf{q}$, so that the reaction kernel becomes

$$\begin{aligned} K_{\alpha\beta}^{(ST)}(\mathbf{q}, \mathbf{q}_{\alpha\beta}, \mathbf{R}) &= U_0' e^{-\frac{1}{2}\sigma^2 q_{\alpha\beta}^2} e^{i\mathbf{q}_{\alpha\beta}\cdot\mathbf{R}} e^{-\frac{1}{2}\sigma^2 q^2} e^{-i\mathbf{q}\cdot\mathbf{R}} e^{\sigma^2 \mathbf{q}\cdot\mathbf{q}_{\alpha\beta}} \\ &= K_{\alpha\beta}^{(ST)}(\mathbf{q}_{\alpha\beta}, \mathbf{R}) h_{\alpha\beta}^{(ST)}(\mathbf{q}, \boldsymbol{\rho}) \end{aligned} \tag{3.32}$$

where

$$h_{\alpha\beta}^{(ST)}(\mathbf{q}, \boldsymbol{\rho}) = e^{-\frac{1}{2}\sigma^2 q^2} e^{-i\mathbf{q}\cdot\mathbf{R}} e^{\sigma^2 \mathbf{q}\cdot\mathbf{q}_{\alpha\beta}} \tag{3.33}$$

called "separation function", still depends on momentum transfer, $\mathbf{q}_{\alpha\beta}$, through the complex vector (pseudo - radius) $\boldsymbol{\rho} = \mathbf{R} + 2i\sigma^2\mathbf{q}_{\alpha\beta}$.

Eq. (3.32) shows that reaction kernel factorizes into the product of two terms: $K^{(ST)}_{\alpha\beta}(\mathbf{q}_{\alpha\beta}, \mathbf{R})$, which can be taken out of the momentum integral in eq. (3.18), and the separation function, $h^{(ST)}_{\alpha\beta}(\mathbf{q}, \boldsymbol{\rho})$, still depending on the integration variable $\mathbf{q}$. Inserting expression (3.32) into eq. (3.18), the desired transition matrix element (and thus cross section) factorization is obtained

$$\mathcal{M}^{(\tau)}_{\alpha\beta}(\mathbf{k}_\alpha, \mathbf{k}_\beta) = \sum_{ST} K^{(ST)}_{\alpha\beta}(\mathbf{q}_{\alpha\beta}) \int d^3q\, h^{(ST)}_{\alpha\beta}(\mathbf{q}, \boldsymbol{\rho}) N^D(\mathbf{q}) \tag{3.34}$$

even if the factorization is exact only for $\mathbf{q}_{\alpha\beta} = \mathbf{0}$, because the integrand still depends on $\mathbf{q}_{\alpha\beta}$, through the separation function.

3.3.1.1 Analytical expression for Distortion factor: Black Disk Approximation

Within BDA, the distortion coefficient can be expressed as the difference between a Dirac delta, peaked at the momentum transfer, i. e. $\mathbf{q} = \mathbf{0}$, and a term accounting for the absorption effects, $N^D_{BD}(\mathbf{q})$,

$$N^D(\mathbf{q}) = \delta(\mathbf{q}) - N^D_{BD}(\mathbf{q}) \tag{3.35}$$

being $\delta(\mathbf{q})$ nothing but the distortion coefficient in PWBA case and

$$N^D_{BD}(\mathbf{q}) = \frac{1}{2\pi^2}\frac{R_{BD}}{q}\left(-\frac{\partial}{\partial q}\right) j_0(qR_{BD}) \tag{3.36}$$

By using eq. (3.35), the transition matrix element can be expressed as

$$\begin{aligned}\mathcal{M}^{(\tau)}_{\alpha\beta}(\mathbf{k}_\alpha, \mathbf{k}_\beta) &\simeq \sum_{ST} K^{(ST)}_{\alpha\beta}(\mathbf{q}_{\alpha\beta}) \left(1 - \int d^3q\, h^{(ST)}_{\alpha\beta}(\mathbf{q}, \boldsymbol{\rho}) N^D_{BD}(\mathbf{q})\right) \\ &= \sum_{ST} K^{(ST)}_{\alpha\beta}(\mathbf{q}_{\alpha\beta})\,(1 - n_{BD})\end{aligned} \tag{3.37}$$

where

$$n_{BD} = \int d^3q\, h^{(ST)}_{\alpha\beta}(\mathbf{q}, \boldsymbol{\rho}) N^D_{BD}(\mathbf{q}) \tag{3.38}$$

so that the cross section, for a specific (S,T) channel, becomes

$$\frac{d^2\sigma^{(ST)}}{dE_x d\Omega} = \frac{E_\alpha E_\beta}{4\pi^2(\hbar c)^4}\frac{k_\beta}{k_\alpha}\frac{1}{(2J_A+1)}\frac{1}{(2J_a+1)} \sum_{\substack{m_a,m_A \\ m_b,m_B}} |K^{(ST)}_{\alpha\beta}(\mathbf{q}_{\alpha\beta})|^2 |1-n_{BD}|^2 \tag{3.39}$$

The spherical symmetry implied by black disk approximation allows to assume a spherically symmetric distortion coefficient and thus angular integration can be easily performed, obtaining the following expression for transition matrix element

$$\mathcal{M}^{(\tau)}_{\alpha\beta}(\mathbf{k}_\alpha,\mathbf{k}_\beta) \simeq \sum_{ST} K^{(ST)}_{\alpha\beta}(\mathbf{q}_{\alpha\beta}) \left(1 - \int dq\, q^2 h^{(ST)}_{\alpha\beta}(q,\rho) N^D(q)\right) \tag{3.40}$$

with $h^{(ST)}_{\alpha\beta}(q,\rho) = 4\pi e^{-\frac{1}{2}\sigma^2 q^2} j_0(q\rho)$, where $\rho = \sqrt{R^2 - \sigma^4 q^2_{\alpha\beta} + 2i\sigma^2 \mathbf{q}_{\alpha\beta}\cdot\mathbf{R}}$ is still complex. By using this angular averaged expression for $h^{(ST)}_{\alpha\beta}(q,\rho)$, the integral in n_{BD} can be analytically solved, obtaining the following expression

$$n_{BD} = \frac{1}{2}\left[erf\left(\frac{1}{\sqrt{2}\sigma}(R_{BD}-\rho)\right) + erf\left(\frac{1}{\sqrt{2}\sigma}(R_{BD}+\rho)\right)\right] - \frac{1}{\sqrt{2\pi}}\frac{\sigma}{\rho}\left[e^{-\frac{1}{2\sigma^2}(R_{BD}-\rho)^2} - e^{-\frac{1}{2\sigma^2}(R_{BD}+\rho)^2}\right] \tag{3.41}$$

Eq. (3.41) shows that the distortion coefficient is a complex function for $q_{\alpha\beta} \neq 0$, because of the dependence on the pseudo - radius ρ, and gives a *distortion factor*, $|1-n_{BD}|^2$, i. e. the reaction term appearing in the cross section as given by eq. (3.39), with a dependence on the absorption radius shown in fig. 3.6, where one can note that the greater the absorption radius is, the stronger the absorption is, i. e. the smaller is the distortion factor, as expected.

The distortion coefficient takes into account all multipolarities involved in the nuclear transition, which are encoded in the non - zero value of the linear momentum transfer $\mathbf{q}_{\alpha\beta}$, contained in the argument

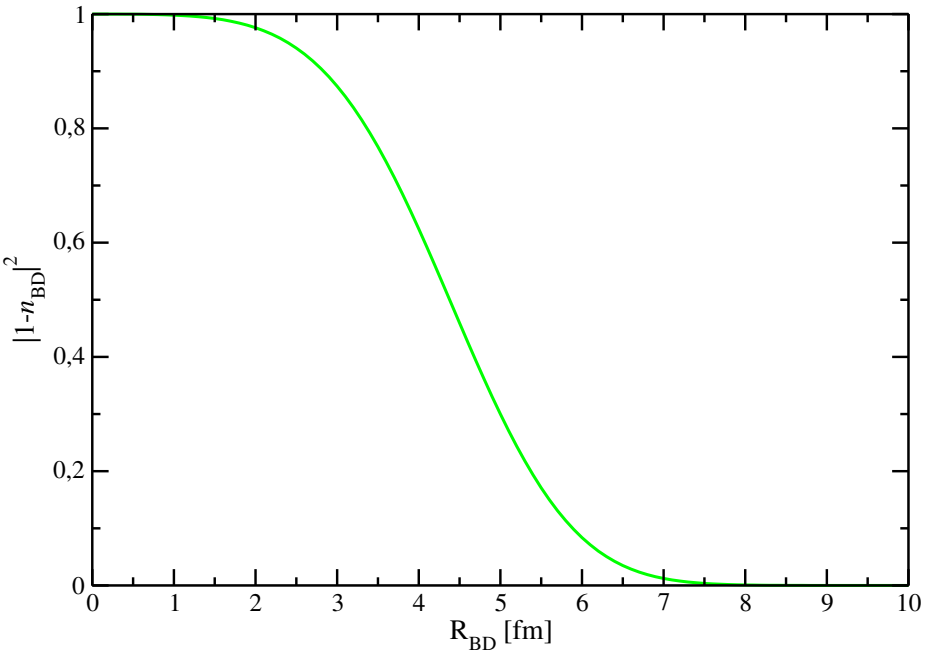

Figure 3.6: Distortion factor as a function of the black disk radius, i. e. the absorption radius, R_{BD}, for example, for the reaction ^{40}Ca(^{18}O,^{18} F)^{40}K at 15 $AMeV$ [6].

of the zeroth - order spherical Bessel function of the first kind, in the expression of the separation function $h^{(ST)}_{\alpha\beta}$.

Thus to get deeper insight into the multipole structure, it is useful to consider the multipole expansion of $j_0(q\rho)$

$$j_0(q\rho) = \sum_{lm} i^l Y_{lm}(\hat{\mathbf{q}}_{\alpha\beta}) Y^*_{lm}(\hat{\mathbf{R}}) j_l(qR) i_l(\sigma^2 q_{\alpha\beta} q) \tag{3.42}$$

where $i_l(x) = i^l j_l(ix)$ is the modified spherical Bessel function of the first kind.

In the limit of small momentum transfer ($q_{\alpha\beta} \ll 1/\sigma \simeq 200\, MeV$), the monopole component dominates in this multipole expansion, so that the separation function becomes

$$h^{(ST)}_{\alpha\beta}(q,\rho) = e^{-\frac{1}{2}\sigma^2 q^2} j_0(qR) i_0(\sigma^2 q_{\alpha\beta} q) \tag{3.43}$$

It is important to underline that due to the residual dependence on $\mathbf{q}_{\alpha\beta}$ inside momentum integral, the factorization procedure shown above

is not exact, but for $q_{\alpha\beta} = 0$; thus, an important check is to establish the range of momentum transfer values within which this factorization works. Thus, on the same vein of Taddeucci's work, SCE transition matrix elements have been calculated in PWBA, in full DWBA (i. e. without using any factorized expression) and by using the separation function at three different levels of approximation, which represent nothing but different approximations for the reaction kernel: the full, angular averaged, expression, its monopole component and the simplified expression for $q_{\alpha\beta} = 0$. The results of this check are shown in the next chapter, together with the ones for heavy ion "direct" double charge exchange cross section at low beam energy.

In order to derive an explicit analytical expression for energy and mass dependence of the distortion factor the following procedure has been used [6], based on the eikonal approximation:

a spherically symmetric optical potential of Gaussian shape

$$W(r) = -W_0 e^{-r^2/R_W^2} \tag{3.44}$$

has been assumed, where the radius parameter R_W is fixed by fitting the full DWBA results, obtained by using HIDEX code [106] (see chapter 5), turning out to be $R_W = 0.783\sqrt{(A_P^{2/3} + A_T^{2/3})}$, and the maximum value parameterized in terms of projectile and target mass numbers as $W_0 = w_0 \left(A_P^{2/3} + A_T^{2/3}\right)^{-\frac{3}{4}}$, according to the so called $UR^{\alpha}-$law found by Hodgson [124, 125], with the fit parameter $w_0 = 5902.743\, MeV$ [6].

Looking at the reactions performed within the NUMEN collaboration, in particular at the SCE processes ^{40}Ca(^{18}O,^{18}F)^{40}K and ^{116}Sn(^{18}O,^{18}F)^{116}In at $15\, AMeV$, one can note that the product of the relative momentum in the initial channel, $k_\alpha \simeq 11\, fm^{-1}$, and the radius characterizing the optical potential describing such transitions (see chapter 5 on simulations), $R_{opt} \simeq 4\, fm$, is $k_\alpha R_{opt} \sim 40 \gg 1$, thus satisfying the eikonal condition (2.60). Hence, by using eikonal approximation to treat distorted waves

in eq. (2.69) and by using a gaussian imaginary optical potential $W(r)$, like in eq. (3.44), it is possible to calculate analytically the integral in the definition of eikonal phase and that in the absorption cross section, eq. (2.69), obtaining the following relation for the absorption radius R_{BD}, in eq. (3.41),

$$R_{BD} = f^{\frac{1}{2}}(\xi(W_\alpha, k_\alpha))R_W \tag{3.45}$$

where the variable ξ depends on initial channel imaginary optical potential parameters, relative momentum and on kinetic energy in the center of mass frame (T_{CM}) through the following expression

$$\xi(W_\alpha, k_\alpha) = \sqrt{\pi} k_\alpha R_W \frac{W_{0,\alpha}}{T_{CM}} \tag{3.46}$$

and

$$f(\xi) = \gamma + \log(\xi) + Ei(1, \xi) \tag{3.47}$$

being $\gamma = 0.5772...$ the Eulero-Mascheroni's constant and $Ei(1, \xi)$ an exponential integral. Fig. 3.7 and the upper panel of fig. 3.8 show mass and energy dependence, respectively, of the distortion factor calculated within BDA, with R_{BD} obtained through the above (eikonal) procedure, for different projectile mass numbers. Compairing such energy dependence of the distortion factor with the one obtained by using the distortion factor definition in eq. (3.14), illustrated in the lower panel of fig. 3.8, one can note that the energy trend is similar in the two cases, thus giving a first confirmation of the validity of the above approximations.

3.3.1.2 Heavy ion single charge exchange unit cross section

Let's consider the kinematical conditions in the "beta decay" limit, i. e. zero angular momentum transfer $\Delta L = 0$ and $q_{\alpha\beta} \to 0$, and only the central part of the effective nuclear interaction potential; thus, by using the Taylor expansion of Bessel function in eq. (3.24) up to the second order ($j_0(x) \simeq 1 - \frac{1}{6}x^2 \simeq \exp(-\frac{1}{6}q^2_{\alpha\beta}\langle r^2\rangle_{a,A})$, with $\langle r^2\rangle_{a,A}$ indicating the

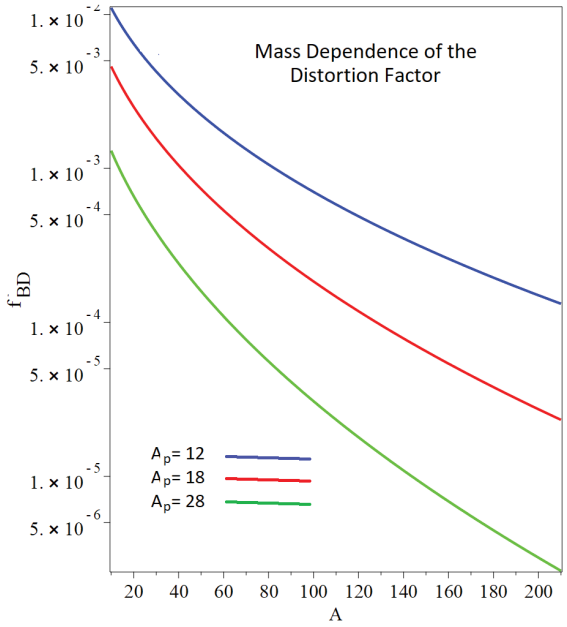

Figure 3.7: Distortion factor as a function of the target mass, fixing projectile nucleus as ^{18}O with a beam energy of 15 $AMeV$, with R_{BD} from eq. (3.45) [6].

mean square radius of projectile/target transition density), heavy ion SCE cross section in eq. (3.39) can be recast in the form

$$\begin{aligned}
&\frac{d^2\sigma}{dEd\Omega} = \frac{E_\alpha E_\beta}{4\pi^2(\hbar c)^4}\frac{k_\beta}{k_\alpha}(2S+1)|V_{ST}^{(C)}(q_{\alpha\beta}=0)|^2 \\
&|b_{ab}^{(0,S,S)}|^2|b_{AB}^{(0,S,S)}|^2 e^{-\frac{1}{3}q_{\alpha\beta}\left(\langle r^2\rangle_a+\langle r^2\rangle_A\right)}|1-n_{BD}|^2 \\
&= K_f(T_{lab},\omega)(2S+1)|V_{ST}^{(C)}(q_{\alpha\beta}=0)|^2 \\
&|b_{ab}^{(0,S,S)}|^2|b_{AB}^{(0,S,S)}|^2 e^{-\frac{1}{3}q_{\alpha\beta}^2\left(\langle r^2\rangle_a+\langle r^2\rangle_A\right)}|1-n_{BD}|^2 \\
&= \hat{\sigma}(T_{lab},A,a)F(q_{\alpha\beta},\omega)|b_{ab}^{(0,S,S)}|^2|b_{AB}^{(0,S,S)}|^2
\end{aligned} \tag{3.48}$$

where the spin multiplicity factor $(2S+1)$ originates from the sum over target and projectile total angular momentum z-projections in the cross section expression in eq. (3.39).

In the second line of eq. (3.48), the kinematical factor $K_f(T_{lab},\omega)$, defined as in light ion case, has been introduced, essentially depending on beam energy, T_{lab}, and on the energy loss $\omega = E_x - Q_{reac}$, introduced just in analogy to Taddeucci's formalism, with $E_x = E_x^{(b)} + E_x^{(B)}$ now

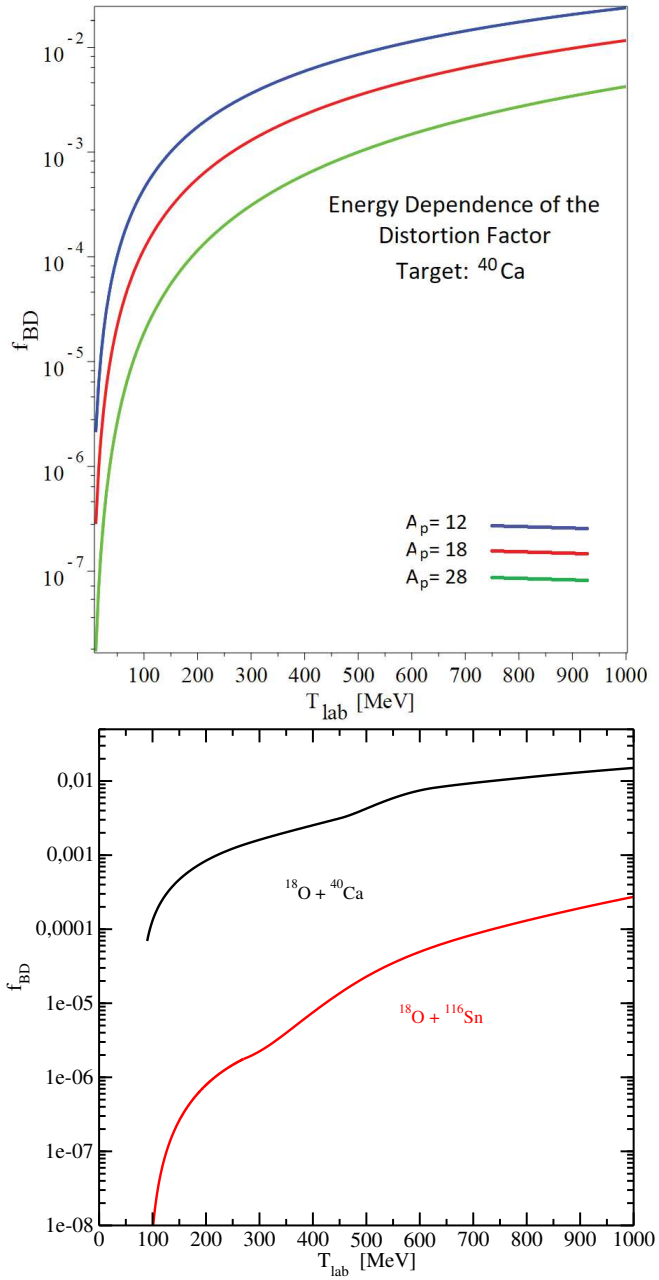

Figure 3.8: Distortion factor ,$f_{BD} \equiv |1 - n_{BD}|^2$, as a function of the beam energy, [6], by using BDA approximation with R_{BD} from the eikonal procedure, shown in this section, for different projectiles and by fixing ^{40}Ca as target nucleus (upper panel). Lower panel shows distortion factor dependence on beam energy, obtained by making the ratio of PWBA to DWBA cross sections, at zero degree, for the SCE reactions ^{40}Ca(^{18}O,^{18} F)^{40}K and ^{116}Sn(^{18}O,^{18} F)^{116}In and for total excitation energy fixed at projectile ground state and the first 1^+ target excited state. The latter cross sections have been obtained by means of HIDEX simulations [106].

representing the sum of the total excitation energy of ejectile and target-like nuclei.

In the last line of eq. (3.48), the "unit cross section"

$$\hat{\sigma}(T_{lab}, A, a) = K_f(T_{lab}, 0)|V_{ST}^{(C)}(0)|^2|1 - n_{BD}|^2 \tag{3.49}$$

whose dependence on projectile and target mass numbers is encoded in the distortion factor, has been introduced together with the factor

$$F(q_{\alpha\beta}, \omega) = \frac{K_f(T_{lab}, \omega)}{K_f(T_{lab}, 0)} e^{-\frac{1}{3}q_{\alpha\beta}^2\left(\langle r^2\rangle_a + \langle r^2\rangle_A\right)} \tag{3.50}$$

accounting for the shape of cross section and reducing to unity for $(q_{\alpha\beta}, \omega) \rightarrow (0, 0)$.

Thus the cross section expression reached in the last line of eq. (3.48) strongly resambles the one obtained by Taddeucci for (p, n) reactions, given by the last line of eq. (3.11).

In plane wave limit, the unit cross section reduces to

$$\hat{\sigma}(T_{lab}, A, a) = K_f(T_{lab}, 0)|V_{ST}^{(C)}(0)|^2 \tag{3.51}$$

so that it is characterized by a weak mass dependence. On the other hand, the distortion factor $|1 - n_{BD}|^2$ may vary significantly with the system mass, as shown by figs. 3.7 and 3.8 [6].

CHAPTER 4

DOUBLE CHARGE EXCHANGE NUCLEAR REACTIONS

In analogy to single charge exchange, double charge exchange nuclear reactions can be classified among surface processes (direct reactions), which can proceed via (charged) isovector mesons exchange, this leading to a simultaneous exchange of two nucleons between projectile and target nuclei (collisional DCE reactions), or via mean field forces, this giving a sequential transfer of nucleons between the interacting nuclei (multi-nucleon transfer reactions). As a general feature, inelastic two - step processes represent the basic mechanism of multi - step direct reaction (MSDR) theory [135–137]; moreover, as stated in chapter 1, both collisional and sequential charge exchange processes are very important tools for nuclear spectroscopy and for studying pairing interaction features [134]. In particular, the collisional mechanism (DCE) could carry precious information on new nuclear matter phenomena, like the excitation of the double Gamow-Teller giant resonance [127–132], and on double beta decay nuclear matrix elements. Heavy ion DCE reactions at low energies, but above the Coulomb barrier, turn out to be particularly useful systems for investigating the latter topic and are exploited by the

NUMEN experiment, with a special interest on the possibility to determine a relation with $0\nu\beta\beta$ decay nuclear matrix elements, as stated in the previous chapters.

4.1 Brief review on double charge exchange experiments

First attempts on heavy ion double charge exchange reactions have been performed at LBNL (California, USA) by employing the reactions ^{24,26}Mg(^{18}O,^{18} Ne)^{24,26}Ne, at beam energy of $124\,MeV$ [138], for determining mass and spectroscopic features of exotic light nuclei, but these reactions were characterized by low yelds and high background, thus not allowing a significant comparison among the various nuclear structure theoretical approaches. Few years later, studies on exotic nuclei were performed through an experiment on ^{40}Ca(^{14}C,^{14} O)^{40}Ar reaction at $51\,MeV$ [91], i. e. close to the Coulomb barrier, exploiting projectile and ejectile ground states belonging to the same isospin triplet ($T = 1$), like for the previous experiment, to enhance double charge exchange cross section, thus finding a "surpraisingly large" cross section ($\frac{d\sigma}{d\Omega} \sim 10\,\mu b/sr$); but the kinematical conditions of this experiment were such to make the multi - nucleon transfer mechanism (two neutron stripping and two proton pick up) dominant over other possible double charge exchange reaction mechanisms [92], as confirmed by the large values of cross sections for other multi - nucleon transfer processes performed by the same experiment, like ^{40}Ca(^{14}C,^{16} O)^{38}Ar ($\frac{d\sigma}{d\Omega} \sim 1\,mb/sr$). In 1982 the first heavy ion double charge exchange experiment involving projectile and ejectile nuclei not belonging to the same isospin triplet, was performed by Naulin and coworkers [89], by means of the reaction ^{48}Ca(^{18}O,^{18} C)^{48}Ti at $100\,MeV$, for studying the properties of neutron - drip line nuclei, but with poor results, due to the very low reaction cross section of that

process ($\frac{d\sigma}{d\Omega} \sim 40\, nb/sr$).

The hypothesis of a connection between heavy ion induced - double charge exchange reactions and double beta decays was first moved by Blomgren et al. [90], resuming the reaction ^{24}Mg(^{18}O,^{18} Ne)^{24}Ne previously performed at LBNL, but at energies of $100\, AMeV$ (at NSCL-MSU) and $76\, AMeV$ (at GANIL), in order to look for double Gamow-Teller excitations. Unfortunately they observed that the cross section for double Gamow-Teller transitions induced by heavy ion reactions are strongly suppressed with respect to the pion - induced ones, probabily due to a destructive interference between direct and sequential mechanisms. For this reason such reactions were abandoned until recent high resolution experiments, performed on the reactions ^{12}C(^{18}O,^{18} Ne)^{12}Be and ^{9}Be(^{18}O,^{18} Ne)^{9}He at RCNP facilities [94, 139, 140], provided that heavy ion -induced double charge exchange reactions represent a powerful tool for the study of nuclear systems far from stability.

In the wake of this renewed interest, the NUMEN experiment fits [1, 80, 93, 142, 143]. As stated before (see chapters 1 and 3), this experiment focuses on the connection between heavy ion - induced DCE reactions, at low energies ($15 - 20\, AMeV$), and double beta decays, waiting for a theoretical framework able to establish such a connection, in the hope to make future experimental results, on $0\nu\beta\beta$ decaying candidate nuclei, useful for extracting significant information on the wanted $0\nu\beta\beta$ nuclear matrix element. Of course, from the theoretical point of view, the road is still long and winding.

The state - of - art of the theoretical formalism for heavy ion DCE processes described in terms of two uncorrelated SCE ones, is shown in the next sections.

4.2 Heavy ion double charge exchange reactions

As stated in chapter 1, double charge exchange nuclear reactions can proceed via "direct" (DCE) or sequential (multi - nucleon transfer) mechanisms. The latter kind of nuclear reaction is at least of fourth order. On the basis of the DWBA approach to collisional single charge exchange (SCE) processes, it is straightforward to interpret "direct" double charge exchange nuclear reactions as second order DWBA processes. Thus, double charge exchange nuclear reactions via transfer mechanism can be safely neglected, because they are higher order processes with respect to the ones proceeding via "direct" mechanism, in particular when kinematical conditions are set to further suppress multi - nucleon transfer cross section.

The formalism developed during the present PhD work, and shown in the following, applies only to heavy ion double charge exchange reactions dominated by the "direct" mechanism.

Within the collisional description, two further DCE mechanisms can be distinguished, as illustrated in chapter 1. The formalism developed in the following refers to heavy ion DCE reactions described as second order DWBA processes, i. e. like a sequence of two independent SCE reactions where, after the first event, the system propagates before a second charge exchange occurs [80], as first proposed by Satchler in '80s [141]. In this way, the theoretical framework used to describe heavy ion DCE cross section takes up very closely the one for SCE ones [6]. Indeed, each one of the two SCE processes is described by a one - body transition operator, in perfect agreement to second order perturbation theory approach, thus leading to the following DWBA transition matrix element

$$\begin{aligned} &\mathcal{M}_{\alpha\beta}^{(\tau,DCE)}(\mathbf{k}_\alpha,\mathbf{k}_\beta) = \langle\beta|\hat{\mathbb{V}}_{ST}^{(\tau,DCE)}|\alpha\rangle \\ &\equiv \langle\beta|\hat{\mathbb{V}}_{ST}^{(\tau,SCE)}\hat{\mathcal{G}}\hat{\mathbb{V}}_{ST}^{(\tau,SCE)}|\alpha\rangle \end{aligned} \tag{4.1}$$

where $|\alpha>=|\chi_{\mathbf{k}_\alpha},\phi_a,\phi_A>$ and $|\beta>=|\chi_{\mathbf{k}_\beta},\phi_b,\phi_B>$ represent entrance and exit channels, respectively, $\mathbb{V}_{ST}^{(\tau,SCE)}$ is given by the first two terms of eq. (2.51) in chapter 2, $\chi_{\mathbf{k}_\alpha}$ and $\chi_{\mathbf{k}_\beta}$ denote the distorted waves obeying incoming and outgoing spherical wave boundary conditions, respectively [80]; $\hat{\mathcal{G}}$ is the full Green function operator, called "propagator", in that it accounts for the propagation of the (off - shell) nuclear system obtained from the first SCE process. To simplify the description of this intermediate channel, it is convenient to expand the propagator in terms of its eigenvalues and eigenfunctions

$$\hat{\mathcal{G}} = \sum_\gamma |\gamma\rangle G(\omega_\gamma,\omega_\alpha)\langle\tilde{\gamma}| \tag{4.2}$$

where the eigenvectors represent a complete set of DWBA nuclear eigenstates, $|\gamma\rangle = |\chi_{\mathbf{k}_\gamma},\phi_c,\phi_C\rangle$, reached through the first SCE process, while each (for a given channel γ) eigenvalue, $G(\omega_\gamma,\omega_\alpha)$, is the reduced Green function, which embeds only the energy - dependence, while the angular dependence remains encoded into the nuclear intermediate states $|\gamma\rangle$. At the lowest order (tree - level) of perturbation theory, the reduced Green function coincides with the one describing a non - interacting projectile - target nuclear system, i. e.

$$G(\omega_\gamma,\omega_\alpha) = \frac{1}{\omega_\alpha - \omega_\gamma + i\eta} \tag{4.3}$$

depending only on the total energy of the system (projectile and target) propagating in the intermediate channel,

$$\omega_\gamma = M_c + M_C + \frac{k_\gamma^2}{2\mu_\gamma} \tag{4.4}$$

and on total center - of - mass energy,

$$\omega_\alpha = M_a + M_A + \frac{k_\alpha^2}{2\mu_\alpha} \tag{4.5}$$

being M_a and M_c (M_A and M_C) initial and intermediate channel projectile (target) mass plus its excitation energy, respectively, μ_γ (μ_α) the

reduced mass of projectile - target nuclei in the intermediate (initial) channel and $\mathbf{k}_\gamma$ the (off - shell) relative momentum of the system after the first SCE process, while $\mathbf{k}_\alpha$ denotes the relative momentum in the entrance channel.

It is important to underline the different notation adopted for indicating the intermediate nuclear eigenstates ($|\gamma\rangle$) and their counterparts in dual Hilbert space ($\langle\tilde{\gamma}|$), in the context of a DWBA formulation involving complex optical potentials, instead of real ones. Indeed, the complex nature of the optical potentials breaks the hermiticity of the hamiltonian describing initial and final state interactions of the nuclear system, so that a given nuclear state, $|\gamma\rangle$, and its dual counterpart, $\langle\tilde{\gamma}| = \langle\tilde{\chi}_{\mathbf{k}_\gamma}, \phi_c, \phi_C|$, contain distorted waves which are no more solutions of the same Schrödinger equation. This is not the case for the wave functions describing internal structure of the two nuclei (involved in the intermediate channel), if real effective nucleon - nucleon interaction potential is used. Hence, the intermediate channel distorted waves must satisfy the bi - orthogonality condition

$$\mathbb{I}_\gamma = \int \frac{d^3k}{(2\pi)^3} |\tilde{\chi}^{(\pm)}_{\mathbf{k}_\gamma}\rangle\langle\chi^{(\pm)}_{\mathbf{k}_\gamma}| \tag{4.6}$$

instead of the orthogonality one, characterizing eigenstates of hermitian hamiltonians, being $\mathbb{I}_\gamma$ the identity operator for the channel γ.

In particular, one can note that the dual distorted wave function $\tilde{\chi}_{\mathbf{k}_\gamma}$ is eigenstate of the hamiltonian containing an optical potential with a positive imaginary part, $+iW(r)$, that acts as a probability current source term, instead of an absorption one, which in turn implies the use of boundary conditions more sophisticated with respect to the ones linking up with a spherical wave.

Inserting eq. (4.2) into eq. (4.1), DCE transition matrix element

becomes

$$\mathcal{M}^{(\tau,DCE)}_{\alpha\beta}(\mathbf{k}_\alpha,\mathbf{k}_\beta) = \sum_\gamma \langle \chi^{(-)}_{\mathbf{k}_\beta}, \phi_b, \phi_B | \hat{\mathbb{V}}^{(\tau,SCE)}_{ST} | \chi^{(+)}_{\mathbf{k}_\gamma}, \phi_c, \phi_C \rangle G(\omega_\gamma,\omega_\alpha)$$
$$\langle \tilde{\chi}^{(+)}_{\mathbf{k}_\gamma}, \phi_c, \phi_C | \hat{\mathbb{V}}^{(\tau,SCE)}_{ST} | \chi^{(+)}_{\mathbf{k}_\alpha}, \phi_a, \phi_A \rangle \tag{4.7}$$

which, projected in momentum space, translates into the following expression

$$\mathcal{M}^{(\tau,DCE)}_{\alpha\beta}(\mathbf{k}_\alpha,\mathbf{k}_\beta) = \sum_{\gamma=c,C} \int \frac{d^3k_\gamma}{(2\pi)^3}\, \mathcal{M}^{(\tau,SCE)}_{\beta\gamma}(\mathbf{k}_\gamma,\mathbf{k}_\beta) G(\omega_\gamma,\omega_\alpha) \tilde{\mathcal{M}}^{(\tau,SCE)}_{\gamma\alpha}(\mathbf{k}_\alpha,\mathbf{k}_\gamma) \tag{4.8}$$

showing that DCE transition amplitude can be expressed as superposition of SCE transition amplitudes

$$\mathcal{M}^{(\tau,SCE)}_{\beta\gamma}(\mathbf{k}_\gamma,\mathbf{k}_\beta) = \sum_{S,T} \int d^3q_2\, K^{(SCE)}_{\beta\gamma}(\mathbf{q}_2,\mathbf{q}_{\beta\gamma}) N^D_{\beta\gamma}(\mathbf{q}_2) \tag{4.9}$$

and

$$\tilde{\mathcal{M}}^{(\tau,SCE)}_{\gamma\alpha}(\mathbf{k}_\alpha,\mathbf{k}_\gamma) = \sum_{S,T} \int d^3q_1\, K^{(SCE)}_{\gamma\alpha}(\mathbf{q}_1,\mathbf{q}_{\gamma\alpha}) \tilde{N}^D_{\gamma\alpha}(\mathbf{q}_1) \tag{4.10}$$

The SCE reaction kernels are just the ones introduced within SCE formalism, eq. (3.20), by simply replacing the subscripts $\beta \to \gamma$, $B, b \to C, c$ in the first SCE transition and $\alpha \to \gamma$, $A, a \to C, c$ in the second SCE transition, with the dependence on the half - off - shell relative momentum transfer, $\mathbf{q}_{\beta\gamma} = \mathbf{k}_\gamma - \mathbf{k}_\beta$ and $\mathbf{q}_{\gamma\alpha} = \mathbf{k}_\alpha - \mathbf{k}_\gamma$, respectively, embedded in the integration variable $\mathbf{q}_{1,2}$; likewise SCE distortion coefficients are given by

$$\tilde{N}^D_{\gamma\alpha}(\mathbf{q}_1) = \int \frac{d^3r}{(2\pi)^3}\, \tilde{\chi}^{*(+)}_{\mathbf{k}_\gamma}(\mathbf{r}) \chi^{(+)}_{\mathbf{k}_\alpha}(\mathbf{r}) e^{-i\mathbf{q}_1\cdot\mathbf{r}} \tag{4.11}$$

which accounts for initial and final state interactions of the first SCE step and by

$$N^D_{\beta\gamma}(\mathbf{q}_2) = \int \frac{d^3r}{(2\pi)^3}\, \chi^{*(-)}_{\mathbf{k}_\beta}(\mathbf{r}) \chi^{(+)}_{\mathbf{k}_\gamma}(\mathbf{r}) e^{-i\mathbf{q}_2\cdot\mathbf{r}} \tag{4.12}$$

for the second SCE transition. The same conventions adopted for SCE formalism have been used.

Of course, SCE reactions select $T_{1,2} = 1$ isospin channel in both steps, while the spin degrees of freedom can vary, within the constraints due to the angular dependence encoded in the reaction kernels, through the transition form factors, defined in eq. (3.21) of chapter 3; the further constraint over the spin transfer during the whole DCE process (e. g. $S = 0$ for double Fermi or $S = 2$ for double Gamow-Teller transitions) follows directly from the "matching" of the angular terms involved in the two SCE transition form factors.

4.3 Approximations used

To simplify the calculation of heavy ion DCE transition matrix element illustrated above, eq. (4.8), some approximation is needed. In close analogy to double beta decay nuclear matrix elements calculations, two main approximations have been used to calculate heavy ion DCE cross sections: closure approximation and single state dominance. The present PhD thesis focuses on the development of the formalism and the numerical simulations regarding the latter case.

4.3.0.3 Closure approximation

By properly choosing the total energies of the intermediate states (closure energies), appearing in the propagator of eq. (4.8), one can exploit the completeness of the intermediate nuclear states in order to add them all, getting unity, thus realizing the closure approximation [144]. In this way, the intermediate propagator reduces to

$$G(\omega_\gamma, \omega_\alpha) = \frac{1}{M_A + M_a - \overline{M}_C - \overline{M}_c + \frac{k_\alpha^2}{2\mu_\alpha} + \frac{k_\gamma^2}{2\overline{\mu}_\gamma} + i\eta} \tag{4.13}$$

where the overlined characters indicate the use of properly chosen target and projectile masses in the intermediate channel. In this way, after a

proper rearrangement of the spin degrees of freedom involved within the two SCE reactions, the DCE transition form factor becomes [144]

$$F_{\alpha\beta}^{(DCE)}(\mathbf{k}_\alpha,\mathbf{k}_\beta) = (-1)^{2(S_1+S_2-2)}$$
$$\frac{\langle\phi_B|e^{i(\mathbf{q}_1+\mathbf{q}_2)\cdot\mathbf{r}}\left[\boldsymbol{\sigma}\right]_1^{S_1}\left[\boldsymbol{\sigma}\right]_2^{S_2}\tau_1^{\pm}\tau_2^{\pm}|\phi_A\rangle\langle\phi_b|e^{i(\mathbf{q}_1+\mathbf{q}_2)\cdot\mathbf{r}}\left[\boldsymbol{\sigma}\right]_1^{S_1}\left[\boldsymbol{\sigma}\right]_2^{S_2}\tau_1^{\mp}\tau_2^{\mp}|\phi_a\rangle}{M_A+M_a-\overline{M}_C-\overline{M}_c+\frac{k_\alpha^2}{2\mu_\alpha}+\frac{k_\gamma^2}{2\overline{\mu}_\gamma}+i\eta}$$
$$=\sum_{m_1,m_2}\frac{\langle\phi_B|\left(S_1,m_1,S_2,m_2|SM\right)e^{i(\mathbf{q}_1+\mathbf{q}_2)\cdot\mathbf{r}}\left[\sigma_{m_1}\right]^{S_1}\left[\sigma_{m_2}\right]^{S_2}\tau_1^{\pm}\tau_2^{\pm}|\phi_A\rangle}{M_A+M_a-\overline{M}_C-\overline{M}_c+\frac{k_\alpha^2}{2\mu_\alpha}+\frac{k_\gamma^2}{2\overline{\mu}_\gamma}+i\eta}$$
$$\langle\phi_b|\left(S_1,m_1,S_2,m_2|SM\right)e^{i(\mathbf{q}_1+\mathbf{q}_2)\cdot\mathbf{r}}\left[\sigma_{m_1}\right]^{S_1}\left[\sigma_{m_2}\right]^{S_2}\tau_1^{\mp}\tau_2^{\mp}|\phi_a\rangle \tag{4.14}$$

where in the last line the spin spherical tensors are introduced. This DCE transition form factor is weighted by the second order product of the effective nuclear interaction potentials, each one proportional to the square of (charged) meson[1] - nucleon - nucleon coupling constant, thus playing the role of the effective low - energy Fermi's coupling constant squared, times the axial/vector coupling constants to the fourth power in weak double beta decays. Moreover, the outgoing leptonic wave functions, contributing to the normalization of $\beta\beta$ nuclear matrix element, are replaced, in heavy ion DCE transition matrix element, by the second order product of the distortion coefficients, which reduces to a simple scaling factor in the limit of zero momentum transfer and considering only $\Delta L = 0$ transitions, as will be illustrated in fig. 6.22, in chapter 6.

Hence, on the one side, closure approximation leads to an interpretation of DCE reactions as one - step processes, described by two - body transition operators, thus making such processes diagrammatically closer to $0\nu\beta\beta$ decay; on the other side, closure approximation does not allow to eliminate the off - shell momentum integral, still involved in the two - body effective local nuclear potential and in the two distortion coefficients, together with the bi - orthogonality problems carried by the latter ones, as one can see from eq. (4.8).

[1]The main contributions come from π, ρ, ω, σ and δ mesons.

Thus, other approximations have been checked in order to disentangle as much as possible the relation between heavy ion DCE cross section and the corresponding nuclear matrix elements.

4.3.0.4 Pole approximation

For simplifying the integral over the off - shell relative momentum, $\mathbf{k}_\gamma$, in eq. (4.8), one can note that the main contribution to this integral comes from the pole of the Green function, so that by exploiting Plemelij - Sokhotskij formula

$$\lim_{\eta\to 0}\frac{1}{x\pm i\eta}=\mathcal{P}\left(\frac{1}{x}\right)\mp i\pi\delta(x) \tag{4.15}$$

and neglecting the principal value of Green function, the propagator can be replaced by

$$G(\omega_\gamma,\omega_\alpha)=-i\pi\delta(\omega_\gamma-\omega_\alpha)=-i\pi\frac{dk_\gamma}{d\omega_\gamma}\delta(k_\gamma-k_\delta) \tag{4.16}$$

being k_δ the relative momentum value at the pole, which can be expressed as $k_\delta=\sqrt{2(\mu_\gamma\omega_\alpha-M_Cm_c)}$, in non - relativistic energy regime, or $k_\delta=\sqrt{(\omega_\alpha+\mu_\delta-M_C-m_c)^2-\mu_\delta^2}$, relativistically.

Thus, the two -step DCE transition matrix element becomes

$$\begin{aligned}
&\mathcal{M}^{(\tau,DCE)}_{\alpha\beta}(\mathbf{k}_\alpha,\mathbf{k}_\beta)=-i\pi\sum_{\gamma=c,C}\int_0^{2\pi}d\varphi_\gamma\int_0^{\pi}d\theta_\gamma\sin\theta_\gamma\\
&\int dk_\gamma k_\gamma^2\,\mathcal{M}^{(\tau,SCE)}_{\beta\gamma}(\mathbf{k}_\gamma,\mathbf{k}_\beta)\delta(k_\gamma-k_\delta)\frac{dk_\gamma}{d\omega_\gamma}\tilde{\mathcal{M}}^{(\tau,SCE)}_{\gamma\alpha}(\mathbf{k}_\alpha,\mathbf{k}_\gamma)\\
&=-i\pi\sum_{\gamma=c,C}\int_0^{2\pi}d\varphi_\gamma\int_0^{\pi}d\theta_\gamma\sin\theta_\gamma\\
&k_\delta^2\mathcal{M}^{(\tau,SCE)}_{\beta\delta}(\mathbf{k}_\delta,\mathbf{k}_\beta)\frac{dk_\delta}{d\omega_\alpha}\tilde{\mathcal{M}}^{(\tau,SCE)}_{\delta\alpha}(\mathbf{k}_\alpha,\mathbf{k}_\delta)
\end{aligned} \tag{4.17}$$

Hence, pole approximation allows to eliminate the integral over the modulus of the intermediate - channel relative momentum, but still the integration over all its possible orientations remains to be performed.

4.3.0.5 Single State Dominance approximation

By assuming that exists an intermediate projectile - target nuclear state giving the main contribution in the sum $\sum_{\gamma=cC}$, in eq. (4.17), then single state dominance (SSD) approximation can be used, so that only one term remains in this sum. Thus, heavy ion DCE cross section becomes

$$\frac{d^2\sigma}{dEd\Omega} = \frac{E_\alpha E_\beta}{4(\hbar c)^4}\frac{k_\beta}{k_\alpha}\frac{1}{(2J_A+1)}\frac{1}{(2J_a+1)}\frac{\mu_\delta^2 k_\delta^2}{(2\pi)^6}$$
$$\sum_{\substack{m_a,m_A\\ m_b,m_B}} |\sum_\tau \int_0^{2\pi} d\varphi_\delta \int_0^\pi d\theta_\delta \, \sin\theta_\delta \mathcal{M}_{\delta\beta}^{(\tau,SCE)}\left(k_\delta,k_\beta,\theta_{\delta\beta}\right)\tilde{\mathcal{M}}_{\alpha\delta}^{(\tau,SCE)}\left(k_\alpha,k_\delta,\theta_{\alpha\delta}\right)|^2 \tag{4.18}$$

where

$$\theta_{\delta\beta} = \arccos\left(\sin\theta_{\alpha\beta}\sin\theta_\delta\cos\varphi_\delta + \cos\theta_{\alpha\beta}\cos\theta_\delta\right) \tag{4.19}$$

so that only the intermediate state angular integration must be performed. The presence of such angular integrals do not allow to separate DCE transition matrix element into the product of two SCE ones.

Moreover, the absorption term $(-iW(r))$ speeds up strongly the convergence of numerical calculations, while the opposite situation is verified in the presence of the source term $+iW(r)$, whose effects are described within $\tilde{\mathcal{M}}_{\delta\beta}^{(SCE)}\left(\theta_{\delta\beta}\right)$; in order to skip this problem, one can introduce the normalization matrix element

$$\tilde{S}_\delta \equiv \frac{1}{(2\pi)^3}\langle\tilde{\chi}_\delta^{(-)}|\tilde{\chi}_\delta^{(+)}\rangle = \int\frac{d^3r}{(2\pi)^3}\left(\tilde{\chi}_\delta^{(+)}(\mathbf{r})\right)^2 \tag{4.20}$$

so that eq. (4.18) becomes, e. g. in non - relativistic energy regime,

$$\frac{d^2\sigma}{dEd\Omega} = \frac{E_\alpha E_\beta}{4(\hbar c)^4}\frac{k_\beta}{k_\alpha}\frac{1}{(2J_A+1)}\frac{1}{(2J_a+1)}\frac{\mu_\delta^2 k_\delta^2}{(2\pi)^6}$$
$$\sum_{\substack{m_a,m_A\\ m_b,m_B}} |\sum_\tau \int_0^{2\pi} d\varphi_\delta \int_0^\pi d\theta_\delta \, \sin\theta_\delta \tilde{S}_\delta^\dagger \mathcal{M}_{\alpha\delta}^{(\tau,SCE)}\left(k_\alpha,k_\delta,\theta_{\alpha\delta}\equiv\theta_\delta\right)\mathcal{M}_{\delta\beta}^{(\tau,SCE)}\left(k_\delta,k_\beta,\theta_{\delta\beta}\right)|^2 \tag{4.21}$$

where in the last line the choice of identifying the initial relative momentum $\mathbf{k}_\alpha$ with the z-axis is revealed by setting the polar scattering angle related to the first SCE process, $\theta_{\alpha\delta}$, equal to the polar integration variable, $\theta_{\alpha\delta} \equiv \theta_\delta$. Moreover, both SCE transition matrix elements depend only on the polar angle, because azimuthal symmetry is assumed, justified by a possible comparison with data from reactions with unpolarized beams.

Furthermore, from the bi - orthogonality relation (4.6), it follows that the normalization matrix element for $\tilde{\chi}_\delta$ is related to the one for χ_δ by the simple relation

$$\tilde{S}_\delta^\dagger S_\delta = \mathbb{I}_\delta \tag{4.22}$$

so that $\tilde{S}_\delta^\dagger$ can be replaced with $\mathbb{I}_\delta / S_\delta$ in eq. (4.21). In this way, one can note that the DCE transition matrix element reduces to the product of two SCE transition matrix elements both dealing with absorptive effects, normalized to the distorted waves in the intermediate channel, so that the proper magnitude of the cross section is recovered; this normalization makes complete DWBA two - step DCE cross section calculation equivalent to normalize the cross section obtained through eq. (4.21), without considering $\tilde{S}_\delta^\dagger$, to the cross section obtained by considering plane waves in the intermediate channel, as shown in chapter 6.

4.4 Heavy ion double charge exchange cross section factorization

In chapter 3, heavy ion SCE reaction cross section is factorized, starting from the gaussian shape of SCE radial transition densities and thus transition form factors. This feature, together with the nearly constant trend of the central effective local nuclear interaction potential, as a function of momentum, led to the use of a gaussian reaction kernel. By considering only central effective nuclear interaction potentials in both SCE

processes involved in the two - step heavy ion DCE reaction, one can use gaussian approximation for both SCE reaction kernels; their product still returns a gaussian trend, so that DCE transition matrix element in eq. (4.8) becomes

$$\mathcal{M}^{(C,DCE)}_{\alpha\beta}(\mathbf{k}_\alpha,\mathbf{k}_\beta) = \sum_{\gamma=c,C}\sum_{\substack{S_1,S_2\\T_1=T_2=1}}\int\frac{d^3k_\gamma}{(2\pi)^3}\,K^{(C,SCE)}_{\beta\gamma}(\mathbf{q}_{\gamma\beta})G(\omega_\gamma,\omega_\alpha)K^{(C,SCE)}_{\gamma\alpha}(\mathbf{q}_{\alpha\gamma})$$
$$\int d^3q_1\int d^3q_2\,h^{(S_1,T_1)}_{\beta\gamma}(\mathbf{q}_1,\boldsymbol{\rho}_1)h^{(S_2,T_2)}_{\gamma\alpha}(\mathbf{q}_2,\boldsymbol{\rho}_2)\tilde{N}^D_{\alpha\gamma}(\mathbf{q}_2)N^D_{\gamma\beta}(\mathbf{q}_1)$$
$$\simeq \sum_{\gamma=c,C}\sum_{\substack{S_1,S_2\\T_1=T_2=1}}\int\frac{d^3k_\gamma}{(2\pi)^3}\,U_1e^{-\frac{1}{2}\sigma_1^2q^2_{\gamma\beta}}e^{i\mathbf{q}_{\gamma\beta}\cdot\mathbf{R}_1}U_2e^{-\frac{1}{2}\sigma_2^2q^2_{\alpha\gamma}}e^{i\mathbf{q}_{\alpha\gamma}\cdot\mathbf{R}_2}G(\omega_\gamma,\omega_\alpha)$$
$$\int d^3q_1\int d^3q_2\,h^{(S_1,T_1)}_{\beta\gamma}(\mathbf{q}_1,\boldsymbol{\rho}_1)h^{(S_2,T_2)}_{\gamma\alpha}(\mathbf{q}_2,\boldsymbol{\rho}_2)\tilde{N}^D_{\alpha\gamma}(\mathbf{q}_2)N^D_{\gamma\beta}(\mathbf{q}_1) \tag{4.23}$$

In this way, the integrand of the off - shell relative momentum integral factorizes into the second order product of reaction factors, dealing with distortion effects in initial, intermediate and final channels, times a DCE nuclear structure term (which can be related to $2\nu\beta\beta$ decay nuclear matrix element), in turn given by the product of two SCE reaction kernels and an intermediate propagator. Thus, because of sum over all possible intermediate states and the off - shell relative momentum integral, the "exact" factorization of DCE transition matrix element, and consequentely of DCE cross section, cannot be reached. Hence, one can assume SSD, so that the sum $\sum_{\gamma=c,C}$ reduces to only one term, but the dependence on $\mathbf{k}_\gamma$ remains; by using pole approximation, the Green function reduces to a Dirac delta projecting the intermediate relative momentum on - shell, thus allowing to eliminate the radial part of the integral on the relative intermediate - channel momentum, but not the corresponding angular part.

To further simplify calculations, $\sigma_1 \simeq \sigma_2 \equiv \sigma$ and $\mathbf{R}_1 \simeq \mathbf{R}_2 \equiv \mathbf{R}$ can be assumed, as justified by the shapes of the radial transition densities

for each SCE reaction (see fig. 3.4), and one can focus to the range of small scattering angles, $\theta_{\alpha\beta} \approx 0$, so that eq. (4.19) reduces to

$$\cos\theta_{\delta\beta} \approx \cos\theta_{\delta} \tag{4.24}$$

To get deeper insight on the effects of optical potentials in the intermediate channel, simulations have been performed first by naively assuming the DCE reaction kernel as simply given by the product of two SCE reaction kernels, fixing the intermediate channel - angular dependence encoded in both, compairing the results obtained by adopting different approximations for the expression of each SCE separation function, and then by using eq. (4.21), implemented (not only in SSD) in a Fortran code (DCEx), developed during the present PhD work. Such results are shown and discussed in chapter 6, together with the other results obtained in the course of this thesis.

CHAPTER 5

NUMERICAL SIMULATIONS

Relying on the formalism developed in chapters 3 and 4 for heavy ion SCE and DCE reactions, respectively, the corresponding cross sections, at low beam energy, have been calculated through simulations performed by means of three main codes: HIDEX, FRESCO and DCEx. All these codes need nuclear structure inputs, i. e. projectile and target form factors, in order to calculate the transition matrix element and thus the reaction cross section. To produce such inputs, a sequence of Fortran codes has been used, developed by H. Lenske [101, 106, 145], customized for SCE nuclear reactions, both for light and heavy nuclei and for a wide energy range, working within QRPA nuclear transition densities and by employing the Michigan-3-Yukawa (M3Y) effective local nucleon - nucleon interaction potential. For consistency, the same effective potential has been used in the calculation of the transition form factors, as explained below.

5.1 Nuclear structure inputs: QRPA transition densities and nuclear interaction potential

Nuclear structure term, viz. the *reaction kernel* of eq. (3.20) is calculated, in coordinate space, according to the following formalism

$$K^{ST}_{\alpha\beta}(\mathbf{r},\omega) = \int \frac{d^3q}{(2\pi)^3}\, \rho^{ST}_{a\to b}(\mathbf{q},\omega) V^{ST}(\mathbf{q},\omega) \rho^{ST}_{A\to B}(\mathbf{q},\omega) e^{i\mathbf{q}\cdot\mathbf{r}} \tag{5.1}$$

where $V^{ST}(\mathbf{q},\omega)$ is the Fourier transform of the local effective nucleus - nucleus interaction potential, discussed in the previous chapters, and

$$\rho_{a\to b}(\mathbf{q},\omega) = \langle \phi_b | \sum_{j=1}^{A} \mathcal{O}_\lambda e^{i\mathbf{q}\cdot\mathbf{r}_j} | \phi_a \rangle \tag{5.2}$$

is nuclear transition density[1], i. e. the probability amplitude that the initial nucleus transforms, by means of the operator $\mathcal{O}_\lambda$, into the final nuclear system of interest; $\mathcal{O}_\lambda$ is a generic transition operator and ω is the total excitation energy of projectile - target system, encoded in nuclear wave functions ϕ_a/ϕ_A (ϕ_b/ϕ_B) of projectile/target (ejectile/product - nucleus); the operator $\mathcal{O}_\lambda$ for single charge exchange transition represents the spin and isospin components of the operator shown in the first column of tab. 3.1.

5.1.1 Transition densities

Transition densities are calculated according to the Green function formulation of the QRPA, in coordinate space, through the following expression

$$\rho_{a\to b}(r,\omega) = \frac{1}{\pi} Im \frac{\int dr' G_{RPA}(r,r',\omega) M^*_\lambda(r')}{\sqrt{\int d\omega R(\omega, P_\lambda)}} \tag{5.3}$$

[1] All quantities corresponding to the target are indicated by capital subscripts while that for projectile are indicated by lower - case subscripts.

where $\lambda = (S,T)$, as stated above, $G_{RPA}(r,r',\omega)$ is the many - body Green function; $R(\omega,P_\lambda)$ is the nuclear response function associated to the "probe" operator P_λ, that e. g. for Gamow - Teller transitions, corresponds to the multipole operator in eq. (3.27); $M^*_\lambda(r')$ is an auxiliary external field, used only for computational reasons and is chosen to account for (S,T) properties of the probe function P_λ.[2] The response function is calculated according to the expression

$$R(\omega,P_\lambda) = \frac{1}{\pi} Im\langle 0|P^\dagger_\lambda G_{RPA} P_\lambda|0\rangle \tag{5.4}$$

so that the poles of the RPA Green function lead to peaks in the response function, thus identifying resonances and other excited nuclear states populated by the transition.

The interacting many - body Green function can be derived from the Dyson equation,

$$G_{RPA}(\omega) = G_0(\omega) + G_0(\omega) V_{res} G_{RPA}(\omega) \tag{5.5}$$

involving the independent particle Green function, G_0, i. e. the Green function corresponding to the mean field (MF) hamiltonian $H_0 = -\sum_i \frac{\hbar^2\nabla^2_i}{2m_i} + U_{MF}$ and the residual potential, $V_{res} = V_{NN} - U_{MF}$, introduced in chapter 2, eqs. (2.70) and (2.71). For excitation energies near excited nuclear states, the full RPA Green function propagator, which tends to a Dirac delta, is approximated by a Lorentzian distribution, with a finite width due to the imaginary part of quasi-particle self - energy, accounting for the lifetime the quasi-particle[3].

For all other excitation energies, Dyson equation is solved recursively, once the free propagator G_0 is calculated. In order to evaluate the latter

[2]Since the response function in the denominator of (5.3) is calculated using the same auxiliary field, the dependence of the transition density on M_λ is neglegible.

[3]Possible non - Lorentzian trends in the response function, near excited nuclear states, are taken into account by using different methods to calculate the integral, in eq. (5.4), in the two energy intervals befor and after the given resonance; in particular, in one interval the integral is replaced by its analytical solution, while in the other interval is solved numerically by means of trapezoids method.

quantity, it is necessary to know nucleons single particle wave functions, which are obtained, separately for protons and neutrons, as eigenfunctions of a potential, given by the sum of a central nuclear (two Woods - Saxon functions shape), a spin - orbit (one Woods - Saxon derivative shape) and a Coulomb term, whose parameters are determined by fitting HFB nuclear energy levels.

According to the formalism shown above, the response functions, scilicet the square modulus of the Fourier transform of the radial transition densities (a part of a factor $2J + 1$, where J is the total angular momentum transfer), have been calculated for the nuclei ^{40}Ca, ^{40}Ar, ^{116}Sn, ^{116}Cd, ^{18}O, ^{18}Ne, ^{20}O and ^{20}Ne, chosen to investigate the experiments performed within the NUMEN collaboration [1, 80, 93, 142, 143], as shown in fig.s 5.1 − 5.8, respectively. The different curves represent nuclear charge exchange transitions, each one characterized by total angular momentum, J, and parity, π. Transitions can be of natural or unnatural parity: the former case is characterized by $\pi = (-1)^J$, while the latter refers to the processes with $\pi = (-1)^{J+1}$; both processes must fulfill the condition $\pi = (-1)^L$, so that natural parity transitions are characterized by $J = L$ and can be realized both for spin - flip ($S = 1$) and non - spin - flip ($S = 0$) processes, while unnatural parity transitions can occur for two values of total orbital angular momentum transfer L ($L = J \pm 1$) and thus they are characteristic of spin - flip ($S = 1$) processes only.

Response function peaks represent excited states of the final nucleus and the magnitude of each peak is related to the probability that such states are populated. QRPA calculations describe pretty well binding energies, density and charge root - mean - square radii and low lying energy states [6], despite some shift in the excitation energy and some spurious ("intruder") peak, which can be effects of the limited configuration space considered within QRPA calculations and of possible stable nuclear deformations which have not been taken into account (all nuclei

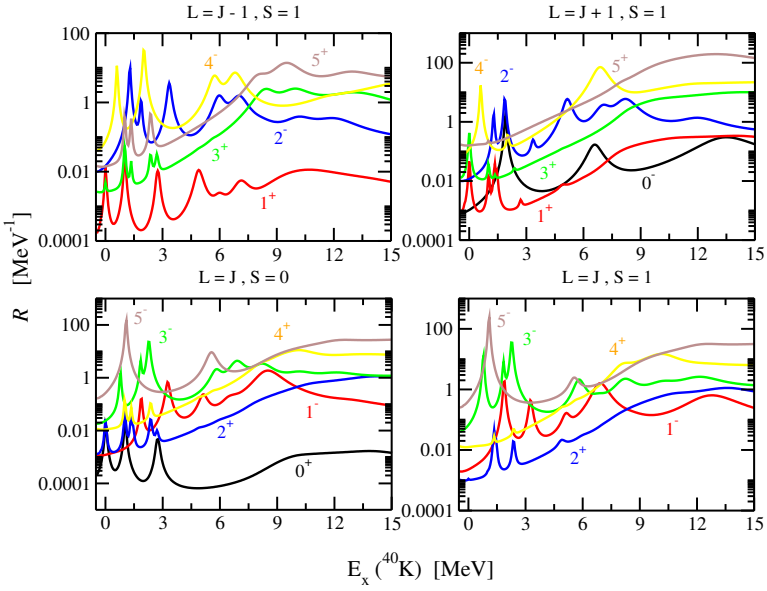

Figure 5.1: Response functions for ^{40}Ca nucleus subjected to the action of the $(p \to n)$ single charge exchange operator $\mathcal{O}_\lambda$, thus accounting for the transition ^{40}Ca $\to^{40}$ K. For details see the text.

are assumed to be spherically symmetric within the codes used). These nuclear structure calculations are customized for nuclei with $J^\pi = 0^+$ ground state.

Moreover, nuclear structure calculations, which refer only to SCE transitions, have been further constrained by performing a "general" and a "particular" check:

- the "general" check consists in verifying that both Fermi and Gamow-Teller numerical sum rules, for the particular transition under investigation, are in agreement with the corresponding analytical (and model - independet) values expected according to Ikeda's sum rules, eq. (2.90);

- the "particular" check is based on the comparison between experimental (if available) and numerical strength corresponding to the transition of the initial nucleus to a particular excited state (excitation energy, angular momenta and parity are fixed); in particular,

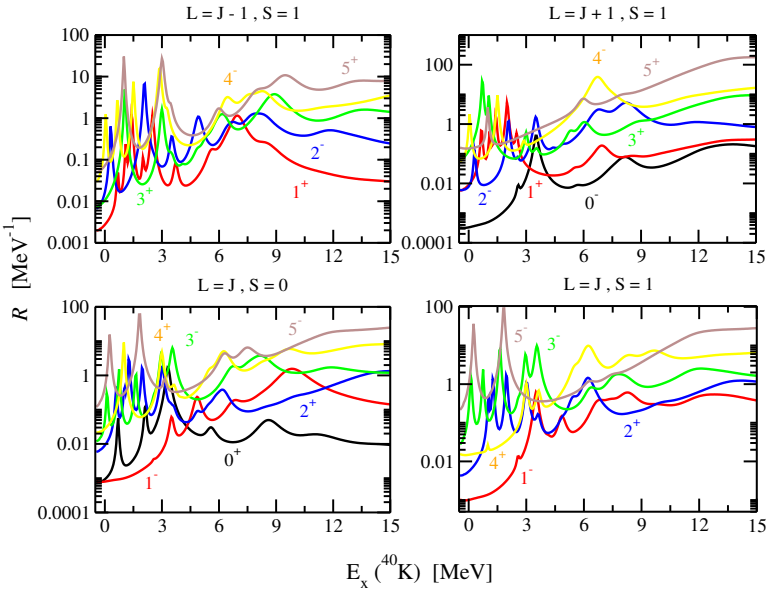

Figure 5.2: Response functions for ^{40}Ar nucleus subjected to the action of the $(n \rightarrow p)$ single charge exchange operator $\mathcal{O}_\lambda$, thus accounting for the transition ^{40}Ar $\rightarrow^{40}$ K. For details see the text.

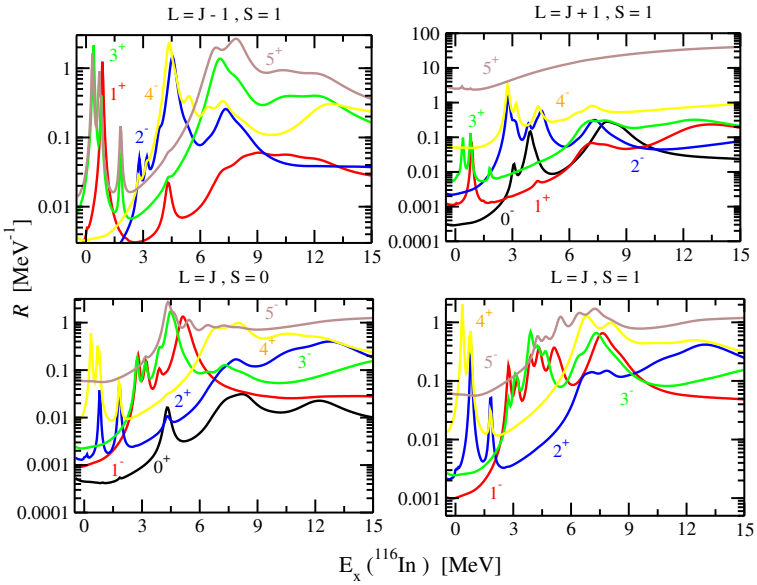

Figure 5.3: Response functions for ^{116}Sn nucleus subjected to the action of the $(p \rightarrow n)$ single charge exchange operator $\mathcal{O}_\lambda$, thus accounting for the transition ^{116}Sn $\rightarrow^{116}$ In. For details see the text.

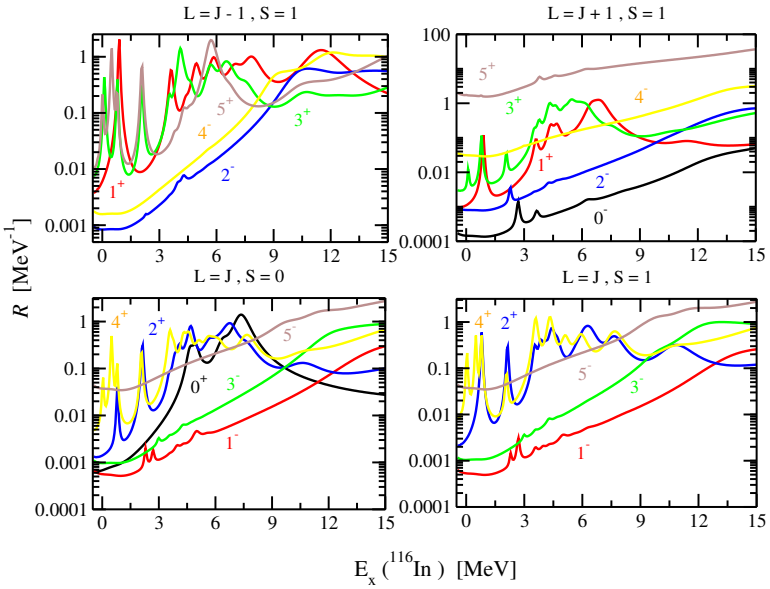

Figure 5.4: Response functions for ^{116}Cd nucleus subjected to the action of the $(n \rightarrow p)$ single charge exchange operator $\mathcal{O}_\lambda$, thus accounting for the transition ^{116}Cd $\rightarrow^{116}$ In. For details see the text.

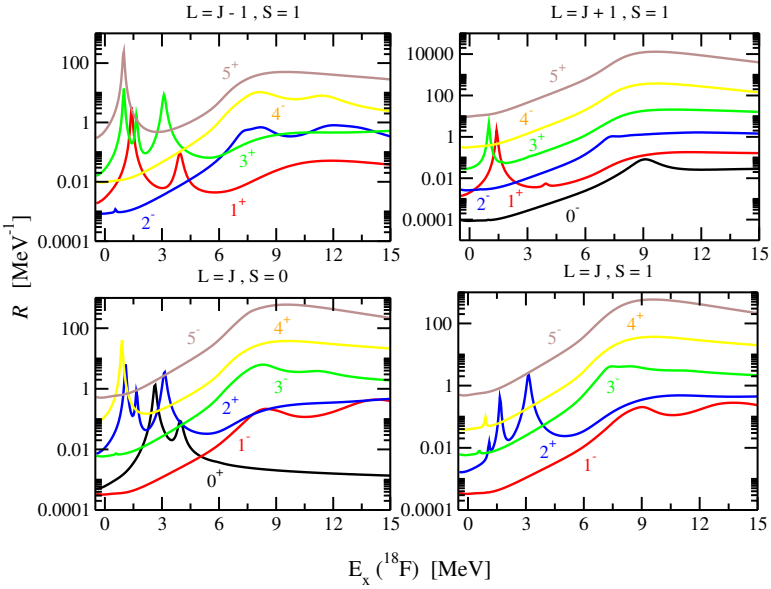

Figure 5.5: Response functions for ^{18}O nucleus subjected to the action of the $(n \rightarrow p)$ single charge exchange operator $\mathcal{O}_\lambda$, thus accounting for the transition ^{18}O $\rightarrow^{18}$ F. For details see the text.

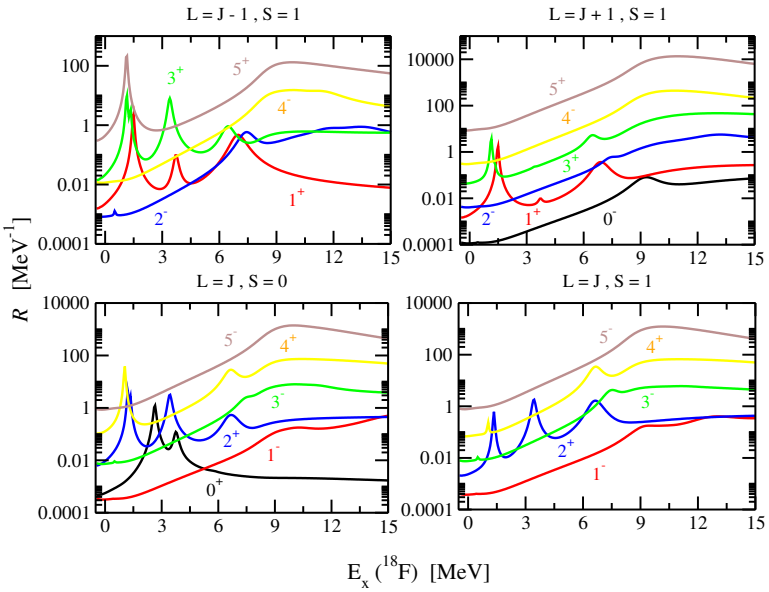

Figure 5.6: Response functions for ^{18}Ne nucleus subjected to the action of the $(p \to n)$ single charge exchange operator $\mathcal{O}_\lambda$, thus accounting for the transition ^{18}Ne $\to^{18}$ F. For details see the text.

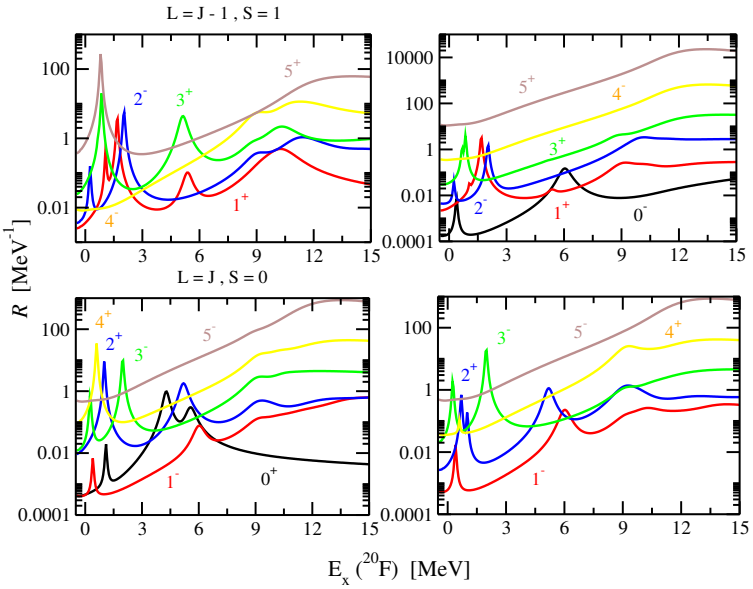

Figure 5.7: Response functions for ^{20}O nucleus subjected to the action of the $(n \to p)$ single charge exchange operator $\mathcal{O}_\lambda$, thus accounting for the transition ^{20}O $\to^{20}$ F. For details see the text.

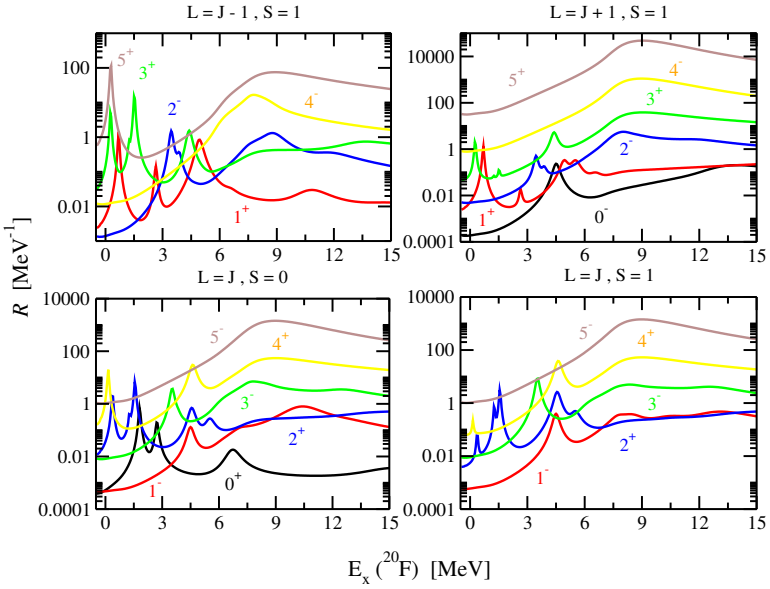

Figure 5.8: Response functions for ^{20}Ne nucleus subjected to the action of the $(p \rightarrow n)$ single charge exchange operator $\mathcal{O}_\lambda$, thus accounting for the transition ^{20}Ne $\rightarrow^{20}$ F. For details see the text.

this check has been performed compairing experimentally known Fermi and Gamow-Teller strengths, from beta decays, with the one obtained numerically by integrating the peak of the response function corresponding to the same transition (of course selecting $\Delta L = 0$ contributions only) and then evaluating the corresponding Fermi/Gamow-Teller strength according to the formula [147]

$$I_{E_x}(2J+1)\frac{g_A^2}{g_V^2} \tag{5.6}$$

where I_{E_x} represents the value of the integral of the response function peak of interest, the axial and vector coupling constants values used are $g_A = 1.26$ and $g_V = 1$, respectively.

Both the above checks have led to good agreement with Ikeda's sum rules and experimental strengths, respectively.

Table 5.1 lists the nuclear excited states populated through the SCE transitions considered in the present work, while table 5.2 illustrates the

projectile nucleus	J^π	E_x $[MeV]$	target nucleus	J^π	E_x $[MeV]$
^{18}O	0^+	0.0 (g.s.)	^{40}Ca	0^+	0.0 (g.s.)
^{18}F	1^+ 0^+	0.0 (g.s.) 1.042	^{40}K	4^- 2^- 5^- 0^+ 1^+	0.0 (g.s.) 0.80 0.89 1.64 2.29
^{18}Ne	0^+	0.0 (g.s.)	^{40}Ar	0^+	0.0 (g.s.)
^{20}O	0^+	0.0 (g.s.)	^{116}Sn	0^+	0.0 (g.s.)
^{20}F	1^+ 0^+	1.057 3.526	^{116}In	1^+ 5^+	0.0 (g.s.) 0.127
^{20}Ne	0^+	0.0 (g.s.)	^{116}Cd	0^+	0.0 (g.s.)

Table 5.1: Nuclei and corresponding excited states considered in both SCE and DCE simulations.

values of the strengths (only Gamow-Teller ones, $B(GT)$, are listed) deduced from beta decay or $(p,n)/(n,p)$ experiments and from the present calculation, for SCE nuclear transitions of interest (in view of DCE calculations).

5.1.2 Effective nuclear interaction potential

In order to take into account the "hard" (due to mesons exchange) nature of charge exchange nuclear interactions, nucleon - nucleon (NN) charge exchange reactions are described by means of an effective local

SCE transition	$B(GT)_{num.}$	$B(GT)_{exp}$
$^{40}\mathrm{Ca}_{0^+_{g.s.}} \rightarrow ^{40}\mathrm{K}_{1^+_{2.29}}$	0.015	0.014 [1]
$^{40}\mathrm{Ar}_{0^+_{g.s.}} \rightarrow ^{40}\mathrm{K}_{1^+_{2.29}}$	1.175	1.03 [1, 153]
$^{18}\mathrm{O}_{0^+_{g.s.}} \rightarrow ^{18}\mathrm{F}_{1^+_{g.s.}}$	2.86	3.27 [1]
$^{20}\mathrm{Ne}_{0^+_{g.s.}} \rightarrow ^{20}\mathrm{F}_{1^+_{1.057}}$	0.18	0.161 [150]
$^{20}\mathrm{O}_{0^+_{g.s.}} \rightarrow ^{20}\mathrm{F}_{1^+_{1.057}}$	0.98	1.124 [152]
$^{116}\mathrm{Sn}_{0^+_{g.s.}} \rightarrow ^{116}\mathrm{In}_{1^+_{g.s.}}$	0.263	0.256 [151]
$^{116}\mathrm{Cd}_{0^+_{g.s.}} \rightarrow ^{116}\mathrm{In}_{1^+_{g.s.}}$	0.27	0.28 [151]

Table 5.2: Gamow-Teller transition strengths from experiments and from the present calculations, for the nuclear SCE transitions indicated in the first column; the experimental Gamow-Teller strengths are shown in the second column, while the ones obtained through the present calculations are listed in the third column.

nuclear Michigan-3-Yukawa (M3Y) interaction potential, with strengths parameterized according to [146] and ranges chosen to represent the long - range tail ($1.414\,fm$) of the One Pion Exchange Potential (OPEP), corresponding to pion exchange, and medium and short - range parts, corresponding to σ ($0.40\,fm$), ω, ρ and δ ($0.25\,fm$) meson exchange. The nucleus - nucleus effective potential in the reaction kernel, eq. (5.1), is then obtained by multiplying the NN one by the kinematical correction factor $\frac{\epsilon_0^2}{\epsilon_p \epsilon_t}$, according to [122], where ϵ_0 is the total projectile energy, per nucleon, in NN center of mass system, while $\epsilon_{p/t}$ is the total projectile / target nucleus energy in nucleus - nucleus center of mass system.

Thus, once nuclear transition densities and effective nuclear interaction potential are determined, the reaction kernel can be calculated through the expression (5.1). For consistency, the same $M3Y$ effective nuclear interaction has been used both for QRPA and reaction kernel calculations. Fig. 5.9 show the radial nuclear reaction kernels for single charge exchange transitions in different nuclear systems, involving the nuclei listed in the above subsection, fixing excitation energy, total angular momentum and parity, J^π, of both target- and projectile-like final nuclear states, as indicated on the figures.

5.2 Initial and final state interaction inputs: optical potentials

Due to the lack of ion - ion elastic scattering data, both real and imaginary part of the optical potential can be calculated microscopically within the double folding approach:

$$U_{opt}(r,\omega) = \sum_{\tau=0,1} \int \frac{d^3q}{(2\pi)^3}\, \rho_a^\tau(\mathbf{q}) V_{NN}^\tau(\mathbf{q},\omega) \rho_A^\tau(\mathbf{q}) e^{i\mathbf{q}\cdot\mathbf{r}} \qquad (5.7)$$

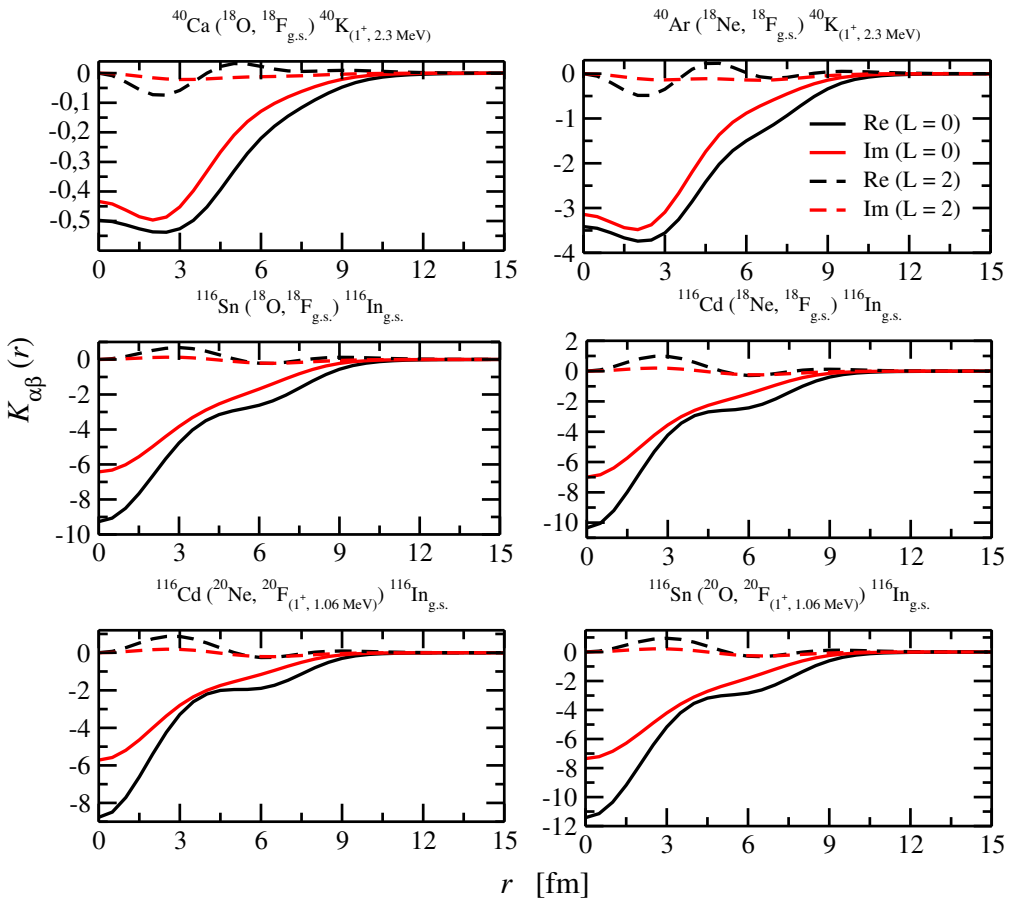

Figure 5.9: Radial reaction kernel as a function of the relative nucleus - nucleus distance, r, describing nuclear single charge exchange transitions for different nuclear systems.

scilicet the effective nucleon - nucleon interaction potential, $V_{NN}(\mathbf{q},\omega)$, parameterized according to [146], for $(0,0)$ and $(0,1)$ $(S,T)-$ channels[4], is folded with projectile and target HFB $1-$body ground state mass densities ($\rho_a^\tau(\mathbf{q})$ and $\rho_A^\tau(\mathbf{q})$, respectively)[5], parameterized by means of Fermi distributions, with proton and neutron density parameters from Skyrme systematics. In this way, smoothly- and slowly- energy dependent optical potentials are obtained.

Coulomb potential is calculated by folding the potential of a point - like charge with projectile and target nuclear charge density distributions. Both optical and Coulomb potentials are illustrated in fig. 5.10, for ^{40}Ca $+^{18}$ O and ^{116}Sn $+^{18}$ O nuclear systems.

At beam energies close to the Coulomb barrier, the double folding model fails in fitting the elastic scattering cross section data [148], overestimating the absorption effects, viz underestimating the probability of peripheral nuclear reactions.

5.3 Cross Section calculation: HIDEX, FRESCO and DCEx codes

The following subsections give a brief description of the main codes used in the SCE and DCE cross sections analysis performed during the PhD course, pointing out the importance of optical potentials and above all of nuclear structure inputs, described above.

All the results obtained by means of these codes (mainly HIDEX and DCEx) are shown in chapter 6, dedicated to the discussion of the results obtained.

[4]The spin - dependent parts of the optical potential are neglected, because an unpolarized heavy ion system is considered.

[5]For $(S,T) \equiv (0,0)$ channel isoscalar mass densities are used, while for $(S,T) \equiv (0,1)$ channel isovector mass densities are considered.

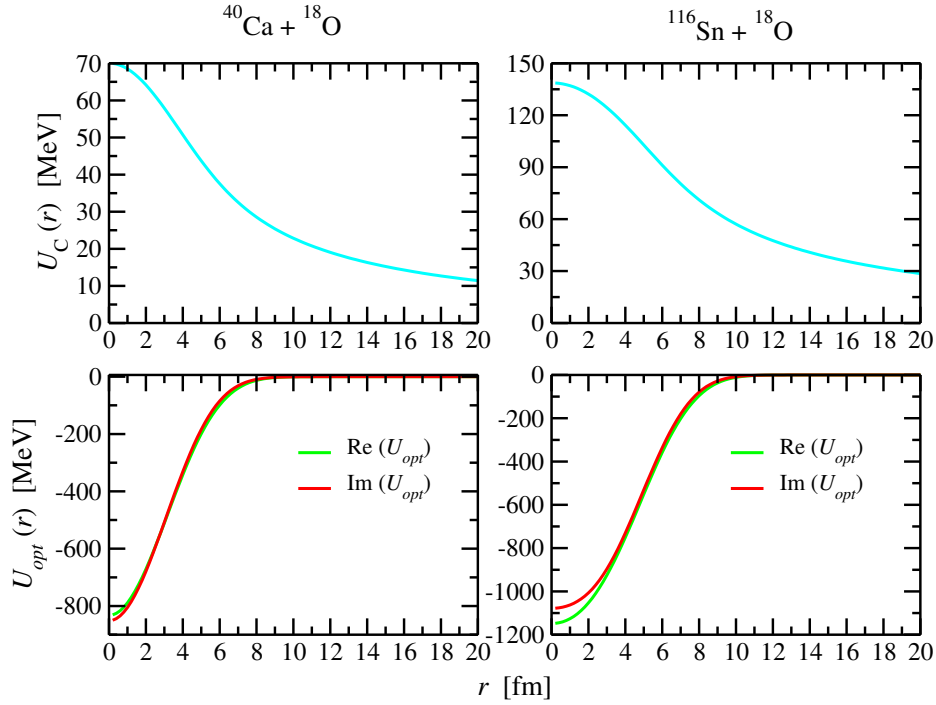

Figure 5.10: Potentials describing, as an example, initial state interactions for the two systems ^{40}Ca +^{18} O (left column) and ^{116}Sn +^{18} O (right column) at 15 $AMeV$. Coulomb potentials are displaied in the upper panels, while real (green line) and imaginary (red line) part of the optical potentials are shown in lower panels.

5.3.1 HIDEX code

HIDEX [101, 106] is a Fortran code, developed by H. Lenske in '80s, working within DWBA formalism. The code allows to calculate SCE reaction cross section (in the center of mass reference frame), as a function of the scattering angle, of projectile and target excitation energies[6] (or equivalentely as functions of momentum transfer, q), together with the angular integrated absorption cross section as a function of total excitation energy and the elastic angular distribution. All cross sections are obtained by means of the corresponding partial wave formalism shown in chapter 2.

[6]The energy of the projectile is fixed, so that faster numerical calculations can be performed.

To calculate these cross sections, initial and final state interactions must be taken into account; for this purpose, initial and final channel microscopic optical potentials, together with Coulomb potentials, described in the previous section, are used as input for solving the radial Schrödinger equation for partial distorted waves, by means of Numerov's numerical method and by linking up solutions to incoming/outcoming Coulomb wave functions, asymptotically behaving like spherical waves. Thus, once the radial component of partial distorted waves is determined, they are directly used to calculate elastic cross section, by a proper combination with Clebsch - Gordan coefficients and with Legendre polynomials, accounting for the dependence on the scattering angle, in the center of mass rest frame. The total absorption cross section, accounting for inelastic channels (including compound nucleus ones) other then the one under investigation, is calculated for each target and projectile excitation energy, according to the definition in the first line of eq. (2.69). To calculate reaction cross section, the radial partial distorted waves must be properly folded with the radial reaction kernel, discussed above, and with the factors accounting for the angular momentum and scattering angle dependeces. The radial reaction kernel is given as input to HIDEX code for each target and projectile excitation energy and for each value of the orbital angular momentum transfer involved in the transitions considered.

Calculations can be performed both for light and heavy nuclei and for a wide energy range.

5.3.2 FRESCO code

FRESCO code was developed by I. J. Thompson in the late '80s [108], employing coupled reaction channel formalism, within DWBA approach [105, 108].

The modified Numerov's method is used to numerically integrate the

Schrödinger equation, which is expressed in its coupled form [108, 149]. As a first step (*first, or initial, channel*), Schrödinger equation is calculated for each partial wave component of the initial channel distorted wave, χ_α,

$$\left[E_\alpha - U_{opt}^{(\alpha)} + \nabla_{\alpha,l}^2\right]\chi_{\alpha,l} = 0 \tag{5.8}$$

where the centrifugal barrier is encoded within $\nabla_{\alpha,l}^2$; in this way the elastic scattering of projectile off target nucleus is accounted for. As a second step (*second channel*), initial channel distorted waves thus found, are coupled to the distorted waves in the second channel (exit channel, for collisional SCE reactions) and to the matrix element of the interaction potential (i. e. the transition form factor), accounting for SCE transition,

$$\left[E_\beta - U_{opt}^{(\beta)} + \nabla_{\beta,l}^2\right]\chi_{\beta,l} = \langle\phi_b, \phi_B|\hat{\mathbb{V}}_{\alpha\beta}|\phi_a, \phi_A\rangle\chi_{\alpha,l} \tag{5.9}$$

thus enabling to describe inelastic scattering and its effect on the elastic channel [105]. To calculate two - step DCE nuclear reactions a third coupled equation must be solved, in the same way as for eq. (5.9) (replacing $\beta \rightarrow \gamma$ in the *second channel* and $\alpha \rightarrow \gamma$ in the *third channel*).

Hence, once partial wave components of the distorted waves are evaluated elastic angular distribution is calculated by properly combining partial waves, according with the formalism of chapter 2. Moreover, once the total wave functions are evaluated, the transition matrix element can be calculated and from this the corresponding reaction cross section, for fixed total excitation energy, as a function of the scattering angle, in center of mass rest frame.

For the purposes of this PhD work, results from FRESCO code, kindly provided by research-team Colleagues, has been used to check the dominance of collisional SCE and DCE mechanism over the multi - nucleon transfer processes, involving same initial and final nuclear states, and also to check the validity of the DCE formalism introduced in chapter 4 and the code DCEx, built on such formalism and described in the following

subsection.

5.3.3 DCEx code

DCEx is a Fortran code developed during the present PhD work and customized for light and heavy ion collisional SCE and DCE reactions, both in relativistic and non - relativistic regime. In particular, heavy ion DCE reactions are treated in the hypothesis of two uncorrelated SCE processes (dSCE), by means of the expression (4.21), in which the intermediate propagator is treated in pole approximation. Cross sections can be calculated as a function of the scattering angle, in the center of mass rest frame, and as a function of total excitation energy. This code simply performs the angular convolution of the two SCE transition matrix elements, i. e. the folding of the SCE reaction kernel with the distorted waves, according to eq. (4.21), taking care of referring all momenta involved in the two SCE processes to the same reference frame, chosen so that its z-axis coincides with the relative initial momentum, $\mathbf{k}_\alpha$. SCE transition matrix elements inputs are produced by HIDEX code and given to DCEx code separately for each excitation energy, for each orbital angular momentum transfer and for each of the corresponding z-projections.

DCEx code calculates dSCE cross section, with the possibility to introduce any projectile/target nuclear state in the intermediate channel, thus allowing to perform calculations within SSD, but also relaxing this approximation. In this sense the code can be used to provide a first check to assess the quality of SSD approximation.

CHAPTER 6

RESULTS

The present chapter shows the simulations performed for heavy ion collisional SCE and DCE reactions, focusing on the reactions under investigation within the NUMEN collaboration, as previously stated. The first studies of the present work have been performed, mainly for the SCE reaction ^{40}Ca(^{18}O,^{18} F)^{40}K at 15 $AMeV$; then, the corresponding DCE reaction, ^{40}Ca(^{18}O,^{18} Ne)^{40}Ar, and other DCE processes involving $A = 116$ nuclei, still for 15 $AMeV$ beam energies have been analyzed.

6.1 Single Charge Exchange simulations

In this section, all the results for heavy ion SCE reactions, at 15 $AMeV$, are illustrated.

First of all, the effect of the microscopically derived optical potentials have been checked by examining elastic, absorption and SCE reaction cross sections.

Fig. 6.1 shows the ratio between elastic and Rutherford cross sections for the entrance channel of the reaction ^{40}Ca(^{18}O,^{18} F)^{40}K, for different beam energies, exhibiting that at small momentum transfer the elastic scattering process is nearly purely Coulomb, while the higher the mo-

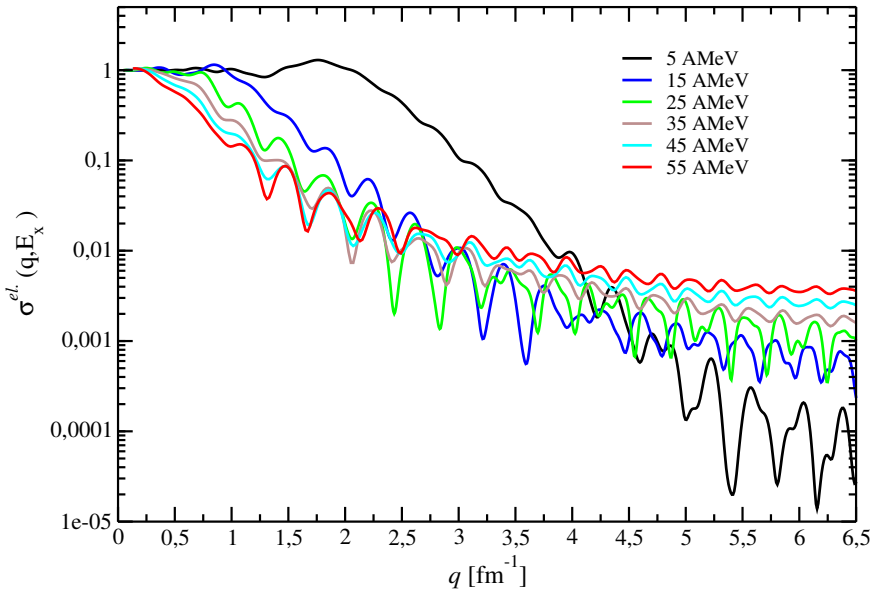

Figure 6.1: Elastic to Rutherford cross sections ratio for the system ^{40}Ca +^{18} O as a function of momentum transfer, in the center of mass reference frame; the different curves refer to different beam energies and are obtained through HIDEX simulations [6].

mentum transfer is, the smaller the ratio is, indicating that the short - ranged nuclear interaction takes over, thus leading to the increasingly dominance of channels other than the elastic one: the reaction channel of interest (e. g. SCE) and all the other possible (open) channels; the latter ones are accounted for by the imaginary part of the optical potential. Moreover, the higher beam energy is, the smaller is momentum transfer value at which this ratio decreases.

The absorption cross section, as a function of beam energy, exhibits a rapid increase for low energies and a flat behaviour for higher beam energies, as shown in fig. 6.2 for the two reactions ^{40}Ca(^{18}O,^{18} F)^{40}K and ^{116}Sn(^{18}O,^{18} F)^{116}In. The trend of the absorption cross section is in total agreement with that of the elastic cross section; moreover, the absorption cross section is higher for heavier nuclear systems, except for the value at very low energy, which however is not good because the double folding approach fails in describing nuclear reactions near

Coulomb barrier energies.

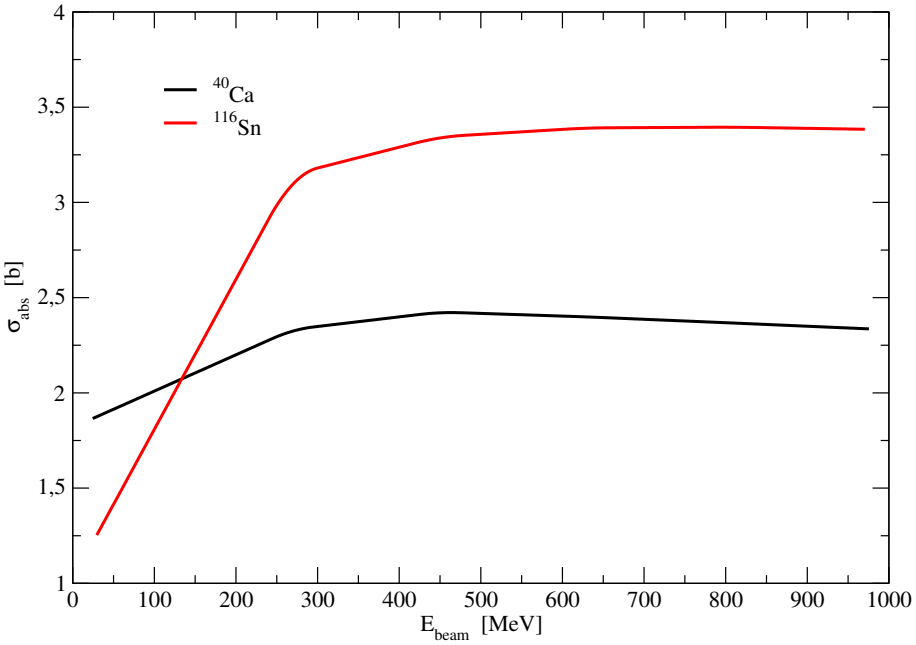

Figure 6.2: Absorption cross sections for the reactions ^{40}Ca(^{18}O,^{18} F)^{40}K and ^{116}Sn(^{18}O,^{18} F)^{116}In as a function of beam energy [6].

Most of the simulations shown in the following refer to the SCE reaction ^{40}Ca(^{18}O,^{18} F)^{40}K only, but the results that come out do not loose in generality, because they are aimed at providing global features of heavy ion collisional SCE processes. Moreover, compairing the absorption cross section and the "complementary" distortion factor as a function of beam energy, shown in the lower panel of fig. 3.8, the slow increase of the distortion factor (lowering of the absorption effects) for increasing beam energy and above all its lowering (stronger absorption) at low beam energies are in contrast with the behaviour of absorption cross section, as shown in fig. 6.2; these aspects reveal that black disk approximation, that only considers the effects of the imaginary part of the optical potential, is too strong for energies close to the Coulomb barrier [6].

According to the formalism illustrated in chapter 3 for heavy ion SCE reactions, the closest resemblance to nuclear beta decays is found in pure

Gamow-Teller (spin-isospin flipping $J^\pi = 1^+$) and pure Fermi (isospin flipping $J^\pi = 0^+$) excitations; but nuclear reactions via strong interactions allow to explore a wider multipolarity range of nuclear excitations, as stated in the previous chapters, thus giving the opportunity to investigate also the so called "$\beta-$decay forbidden" transitions, referred to as Gamow-Teller-like (spin-isospin flip) and Fermi-like (only isospin flip) excitations. Figs. 6.3 and 6.4 show DWBA cross sections for Fermi-like transitions, as a function of target-like excitation energy and as a function of scattering angle, respectively, while figs. 6.5 and 6.6 illustrate the corresponding observable for Gamow-Teller-like transitions. In both cases, simulations have been performed for the reaction ^{40}Ca(^{18}O,^{18} F)^{40}K, characterized by a $Q-$value of $Q_{val} = -2.967\, MeV$, while the complementary SCE reaction ^{40}Ca(^{18}O,^{18} N)^{40}Sc has not been treated here, in that it is kinematically suppressed, because of its $Q-$value, $Q_{val} = -28.22\, MeV$. Gamow-Teller (Fermi) transitions have been obtained by considering the transition leading to the 1^+ ground state (first 0^+ excited state) of the ejectile nucleus, ^{18}F, and Gamow-Teller-like (Fermi-like) transitions of different multipolarities, populating several excited states of ^{40}K, identifyed by total angular momentum J, parity π and excitation energy E_x. From figs. 6.3 - 6.6, it is straightforward to note that $J^\pi = 0^+$ and $J^\pi = 1^+$ target transitions contribute significantly to the cross section at low excitation energies and dominate at small scattering angles. Still for the global character of the present investigation on heavy ion SCE reactions, only pure Gamow-Teller transitions both in projectile and target nuclei have been focused; in fact the distortion effects, the relation between PWBA and DWBA cross sections together with the existence of a relation between the reaction kernel and beta decay strengths are nearly independent on the multipolarity of the transition, at least at small momentum transfer, as it transpires from SCE formalism, in chapter 3.

Another important feature emerging from the latter plots is that SCE

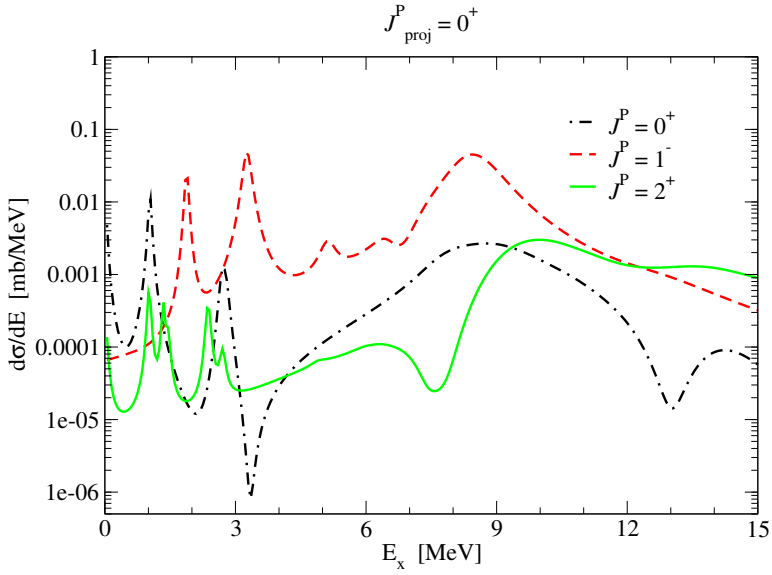

Figure 6.3: DWBA SCE cross section for the reaction ^{40}Ca(^{18}O,^{18}F)^{40}K at 15 $AMeV$, as a function of target-like excitation energy, integrated over the full angular range, for different target multipolarities and considering only (pure) Fermi transition, $J^\pi = 0^+$, for projectile nucleus [6].

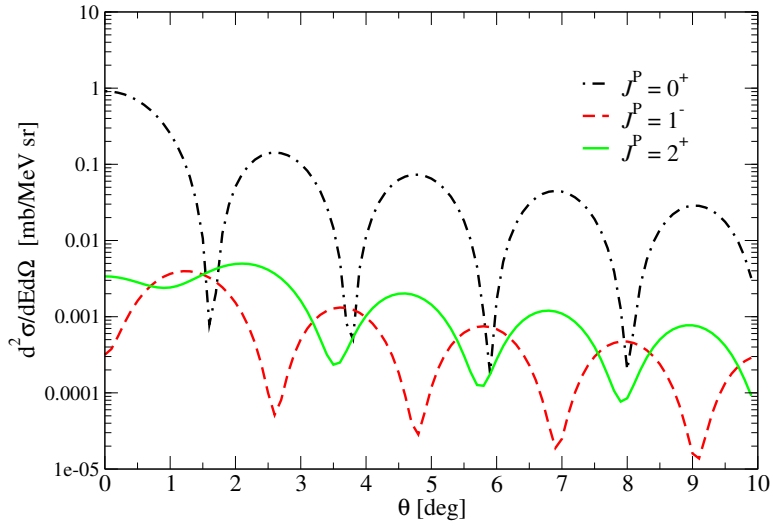

Figure 6.4: DWBA SCE angular distribution for the reaction ^{40}Ca(^{18}O,^{18}F)^{40}K at 15 $AMeV$, for fixed target-like and ejectile excitation energy $E_x = 0$, for different target multipolarities and considering only (pure) Fermi transition, $J^\pi = 0^+$, for projectile nucleus [6].

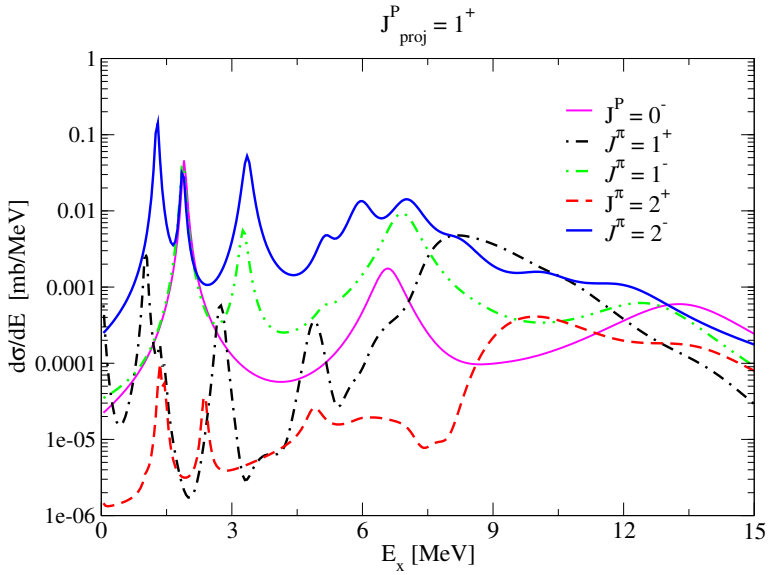

Figure 6.5: DWBA SCE cross section for the SCE reaction ^{40}Ca(^{18}O,^{18}F)^{40}K at 15 $AMeV$, as a function of target-like excitation energy, integrated over full angular range, for natural and unnatural parity transitions of different multipolarity in the target, considering only (pure) Gamow-Teller transitions, $J^\pi = 1^+$, for the projectile [6].

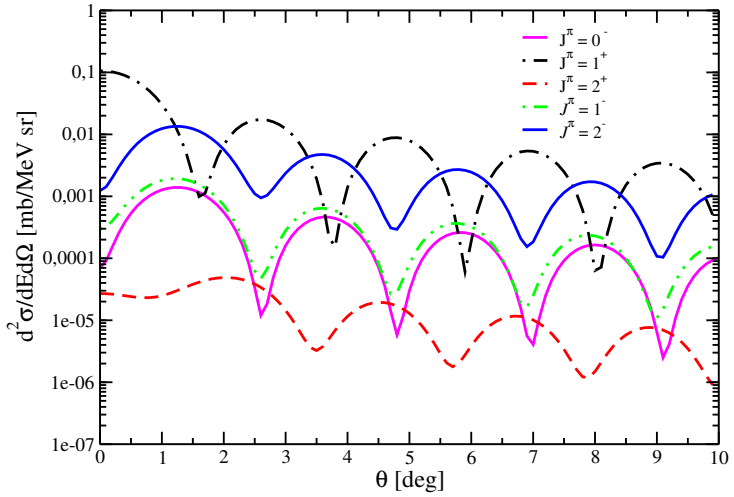

Figure 6.6: DWBA angular distribution for the SCE reaction ^{40}Ca(^{18}O,^{18}F)^{40}K at 15 $AMeV$, fixing $E_x = 0$ both for target-like and ejectile nuclei, for natural and unnatural parity transitions of different multipolarity in the target, considering only (pure) Gamow-Teller transitions, $J^\pi = 1^+$, for the projectile [6].

cross sections, whatever the multipolarity is, are very small (about $4-6$ order of magnitude) with respect to the absorption one, this signaling the strongly absorptive character of (low energy) heavy ion reactions, which in turn justifies the use of *black disk approximation* to get an "effective" simplification of the calculations.

In order to gain information on the contribution of the different ingredients flowing into the SCE reaction cross section, simulations have been performed by probing the effect of each component of the optical potentials. Fig. 6.7 illustrates SCE cross section for ^{40}Ca(^{18}O,^{18}F)^{40}K reaction, at $15\,AMeV$, as a function of target-like excitation energy, integrated over full solid angle; the different curves have been obtained first in PWBA, i. e. setting optical potential equal to zero, then turning on the components of the optical potential (real, $V(r)$, and imaginary, $W(r)$) and the Coulomb potential and finally in full DWBA. Already at the PWBA level, one can appreciate the main excitation peaks contributing to $J^\pi = 1^+$ transition in the target. Likewise, fig. 6.8 deals with the contribution of Coulomb potential, real and imaginary part of the optical potentials to the angular distribution for the same SCE reaction considered in fig. 6.7, fixing both ejectile and target-like excitation energies to their ground states[1].

Moreover, from the latter two figures, it is possible to observe that the cross section decreases when the effect of the Coulomb repulsion is taken into account or increases when considering the contribution of the (attractive) real part of the nuclear optical potential; however, the most striking feature is the strong suppression, by about a factor of $500-600$, obtained just taking into account the imaginary part of the optical potential, which essentially brings the cross section down to the value as-

[1]Note that the $J^\pi = 1^+$ peak in correspondence to target-like ground state, $E_x = 0$ in fig. 6.5, is an intruder peack, because experimentally the ground state of ^{40}K is a $J^\pi = 4^-$ one. But for the purpose of this first analysis, it is important just to select an excitation energy value corresponding to a peak in the SCE cross section.

sociated with the full DWBA calculation and also lead to a prominent diffraction pattern, reflecting the size of the absorbing region and above all strongly resembling the one of full DWBA case. These features indicate that the DWBA result is mainly explained in terms of strong absorption effects, as expected in heavy ion reactions, and justifies the strong absorption approach, viz. the black disk approximation, for modeling the ion-ion initial and final state interactions.

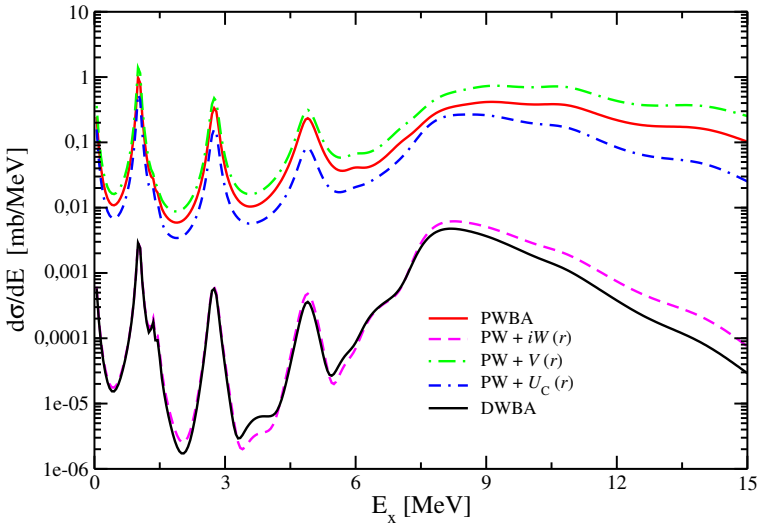

Figure 6.7: Cross sections for ^{40}Ca(^{18}O,^{18}F)^{40}K reaction, at 15 $AMeV$, as a function of target-like excitation energy, for $J^{\pi} = 1^{+}$ transition both in projectile and target nuclei, fixing ejectile excitation energy to its ground state. The red curve corresponds to PWBA calculations, the black one refers to full DWBA case, while the other curves are obtained by considering only the imaginary part of the optical potential (magenta curve), only the real part of the optical potential (green curve) and only Coulomb potential (blue curve) [6].

Then, the effect of central and tensor parts of the effective local nuclear interaction potential has been analyzed, together with the two orbital angular momentum contributions ($L = 0, 2$) leading to $J^{\pi} = 1^{+}$ transitions, as shown in figs. 6.9 and 6.10. The latter two plots illustrate that the central interaction contribution to the angle integrated cross section and the angular distribution, at small scattering angles, are dominated by the $L = 0$ transition. Considering the tensor component of the

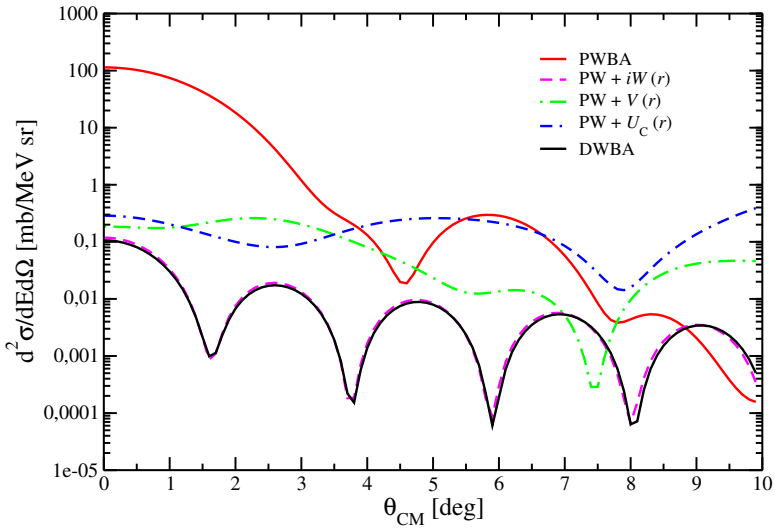

Figure 6.8: Angular distribution for ^{40}Ca(^{18}O,^{18}F)^{40}K reaction, at 15 $AMeV$, considering $J^{\pi} = 1^{+}$ transition both in projectile and target nuclei and fixing $E_x = 0$ both in ejectile and target-like nuclei. The red curve corresponds to PWBA calculations, the black one refers to full DWBA case, while the other curves are obtained by considering only the imaginary part of the optical potential (magenta curve), only the real part of the optical potential (green curve) and only Coulomb potential (blue curve) [6].

effective local nuclear interaction potential leads to a slight decrease of the magnitude of the whole PWBA cross section and of the main excitation peaks of DWBA cross section; moreover, tensor interaction causes a shift of PWBA and DWBA angular distribution towards larger scattering angles, particularly evident for PWBA calculations, owing to the dominant role of $L = 2$ (in this case).

The target mass dependence of the distortion factor provided by BDA, with black disk radius determined through the eikonal approximation (see chapter 3), has been tested by considering SCE reactions involving heavier target nuclei. As shown in fig. 3.7, for target mass numbers $A = 116$ it is expected a distortion factor smaller, by less than one order of magnitude, with respect to the one found for $A = 40$; in fact, this trend is in agreement with the distortion factor value obtained by performing the ratio between zero degree DWBA and PWBA cross sections

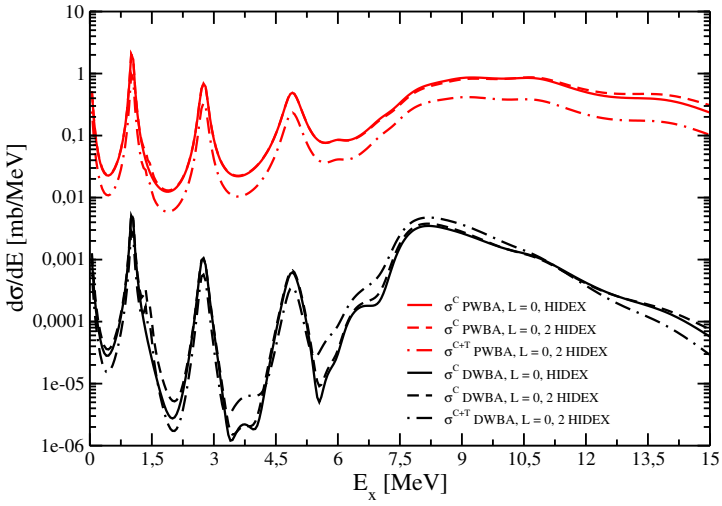

Figure 6.9: Cross section for ^{40}Ca(^{18}O,^{18} F)^{40}K reaction, at 15 $AMeV$, as a funciton of target-like excitation energy and integrated over full angular range. The results are obtained by considering $J^{\pi} = 1^{+}$ transition both in projectile and target nuclei, considering only central term of SCE effective nuclear interaction potential, for orbital momentum transfer $L = 0$ only (solid lines) and by adding $L = 0$ and $L = 2$ modes (dashed lines); dashed-dotted lines are obtained by considering central and tensor components of SCE effective nuclear interaction potential [6]. Red curves refers to PWBA calculations and the red ones to DWBA case.

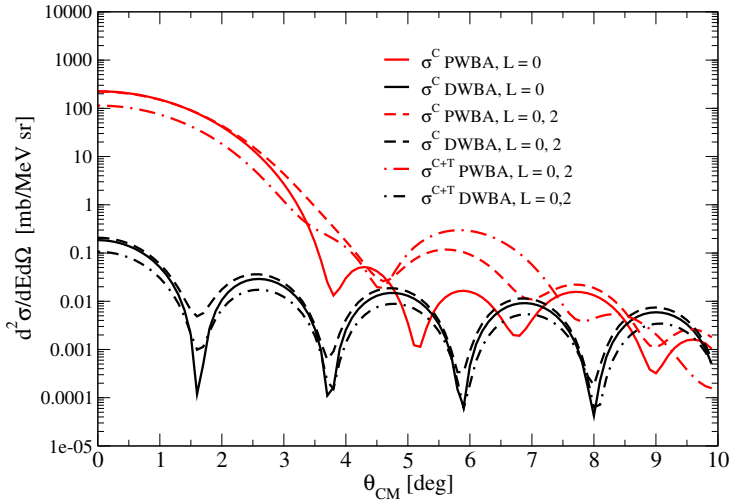

Figure 6.10: Angular distribution for the same nuclear reaction and the same conditions of fig. 6.9, fixing excitation energy $E_x = 0$ both for ejectile and target-like nuclei [6].

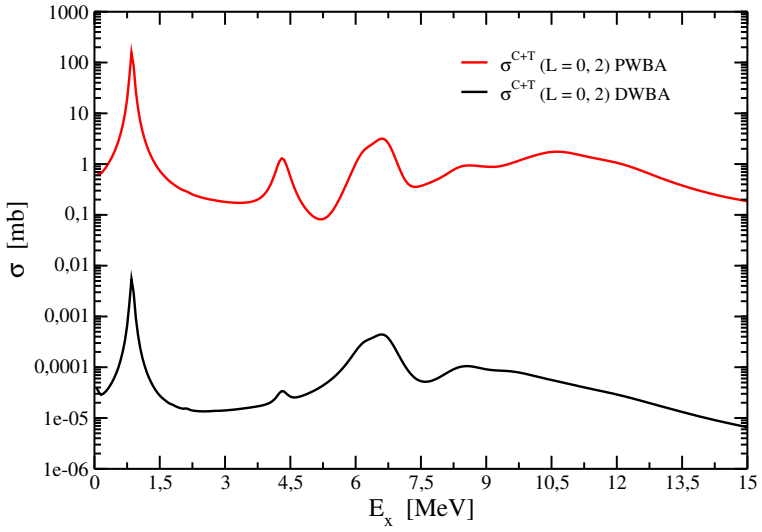

Figure 6.11: Cross section for ^{116}Sn(^{18}O,^{18}F)^{116}In SCE reaction, at 15 $AMeV$, as a function of target-like excitaiton energy, taking into account only zero degree contributions, considering the transition leading to ^{18}F ground state and to 1^+ states for ^{116}In. Red curve refers to PWBA calculation while the black one indicates DWBA case [6].

for ^{116}Sn(^{18}O,^{18}F)^{116}In reaction, at 15 $AMeV$, shown in fig. 6.11.

6.1.1 Testing SCE cross section factorization

The next step of the analysis of SCE reactions consists in a check to assess the quality of the factorized expression of SCE cross section al low beam energies. In light of the previous results, for the sake of simplicity, only central interactions and $L = 0$ transitions have been taken into account. Within the formailsm developed in chapter 3, the angular momentum dependence of the radial transition densities, eq. (3.24), implies that they can be interpreted as the multipole components of the corresponding reaction kernel, eqs. (3.20), (3.21); thus, by assuming gaussian transition densities and considering only their $L = 0$ components is equivalent to consider only the monopole term in the multipole expansion of the gaussian reaction kernel. Fig. 6.12 illustrates the comparison between the monopole component of the reaction kernel calculated within

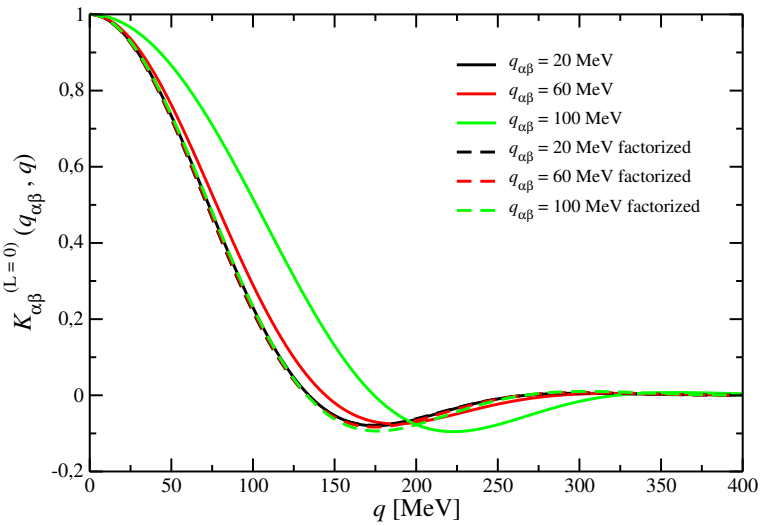

Figure 6.12: Monopole component of the reaction kernel, by using its factorized expression, eq. (3.32), (dashed lines) and without perfoming factorization (solid lines). The different colours refer to different values of momentum transfer, $q_{\alpha\beta}$, [6].

its factorized expression, eq. (3.32), where only the monopole term of the multipole decomposition of the separation function, eq. (3.43), has been taken into account, and its expression obtained relaxing any factorization hypothesis, just determined by performing the Fourier-Bessel transform of the corresponding gaussian in coordinate space (obtained by folding projectile and target radial transition densities, as illustrated in fig. 3.4). The different colours in fig. 6.12 refer to different values of momentum transfer, $q_{\alpha\beta}$: one can note that for small momentum transfer, $q_{\alpha\beta} \simeq 20\, MeV$, (black curves) the two curves overlap, i. e. the factorized expression for the reaction kernel works quite well; the curves start to separate, thus becoming distinguishable, for higher momentum transfer (red curves) and are very different for $q_{\alpha\beta} \gtrsim 100\, MeV$. A as a further check, the validity of the factorized expression for SCE cross section has been provided by analyzing the trend of the monopole component of the transition matrix element square modulus as a function of momentum transfer, $q_{\alpha\beta}$, in PWBA, DWBA and within factorized formulas,

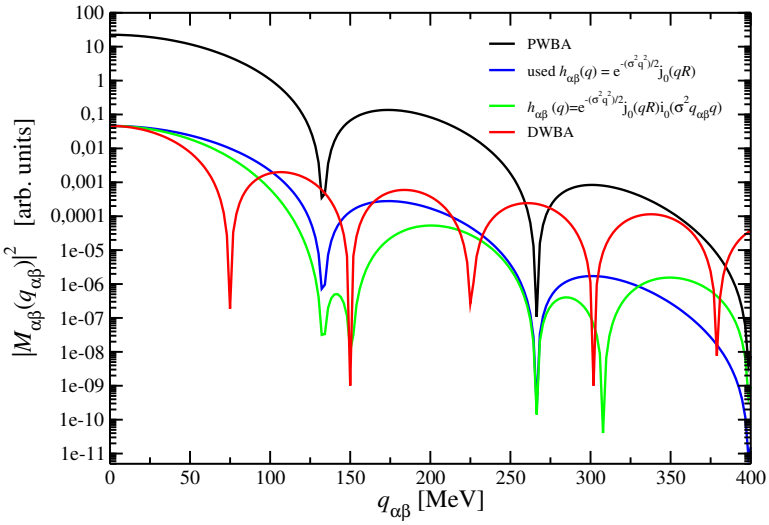

Figure 6.13: Comparison among SCE monopole component of the square modulus of transition matrix element, i. e. the cross section in arbitrary units, in PWBA (black line), full DWBA (red line) and Gaussian + BDA, for two different approximations of the reaction kernel [6].

adopting different degrees of approximation of the separation function (see fig. 6.13): the small momentum transfer limit, eq. (3.43), (green curve) and by assuming $h_{\alpha\beta}(q, R) = e^{-\frac{1}{2}\sigma^2 q^2} j_0(qR)$ (blue curve). As expected, the latter case leads to the same trend obtained in PWBA, just reduced by a multiplicative factor, while the dependence on the momentum transfer is evident in the narrower diffraction patterns of green and full DWBA curves; in particular, the changes in the diffraction pattern between PWBA and DWBA cases strongly resembles the ones observed in the complete HIDEX calculations. The main result emerging from fig. 6.13 is that blue, green and red curves coincide, scilicet the factorized expression for SCE cross section works, up to a momentum transfer $q_{\alpha\beta} \leqslant 25 - 30\, MeV$, as observed for the reaction kernel, in fig. 6.12. Simulations are illustrated in figs. 6.12 - 6.13 for ^{40}Ca(^{18}O,^{18}F)^{40}K (but the same results hold for heavier nuclear systems, by properly changing the parameters of the gaussian reaction kernel).

6.2 Double charge Exchange simulations

Once outlined the main features of low energy heavy ion SCE reactions, we have moved on to the study of heavy ion DCE reactions, within the same energy range as for SCE ones. As stated in the previous chapters, the focus has been placed on the formalism describing DCE processes as a tree - level convolution of two uncorrelated SCE reactions (dSCE).

6.2.1 Towards dSCE simulations: the two uncorrelated SCE reactions

In view of the study of heavy ion DCE reactions, within their interpretation in terms of two uncorrelated SCE processes, complete HIDEX calculations have been performed for six spin-isospin flipping $J^\pi = 1^+$ SCE transitions, relaxing the above simplifications, i. e. by considering both central and tensor components of the effective nuclear interaction potential and all orbital angular momentum contribution to the given transition. Fig.s 6.14 − 6.16 show HIDEX simulations of SCE cross sections at forward scattering angles, for the reactions under study within the NUMEN collaboration [80] ^{40}Ca(^{18}O,^{18} F)^{40}K($1^+_{2.29}$) and ^{40}K($1^+_{2.29}$)(^{18}F,^{18} Ne)^{40}Ar, ^{116}Sn(^{18}O,^{18} F)^{116}In and ^{116}In(^{18}F,^{18} Ne)^{116}Cd, ^{116}Cd(^{20}Ne,^{20} F($1^+_{1.057}$))^{116}In and ^{116}In(^{20}F($1^+_{1.057}$),^{20} O)^{116}Sn, where the subscripts refer to the experimental energy (MeV) of the excited state studied, while the absence of subscripts implies that ground state is considered.

In all the three latter plots, solid curves represent forward angular distributions for the SCE nuclear reactions constituting the first step of a DCE process, scilicet the exit channel of each of these SCE reactions acts as intermediate channel of the corresponding DCE process and is also used as the entrance channel of the second step SCE reactions, whose

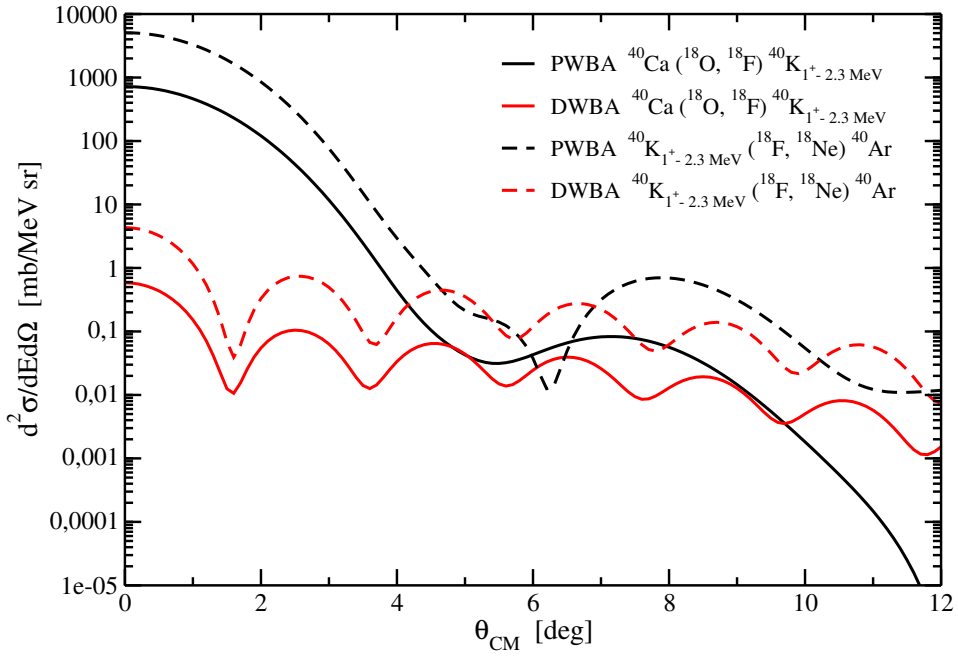

Figure 6.14: PWBA and DWBA SCE angular distributions, for the two reactions ^{40}Ca(^{18}O,^{18}F)^{40}K(1^+, $E_x = 2.29\,MeV$) and ^{40}K(1^+, $E_x = 2.29\,MeV$)(^{18}F,^{18}Ne)^{40}Ar, involved in the dSCE process ^{40}Ca(^{18}O,^{18}Ne)^{40}Ar. Simulations are performed by assuming a beam energy of 15 $AMeV$.

angular distributions are indicated by the dashed curves of figs. 6.14 - 6.16. Moreover, each of these plots contain PWBA and DWBA cross sections. The calculations of physical interest are the DWBA ones; PWBA simulations can be used to perform the ratio of DWBA to PWBA cross sections at $\theta = 0^\circ$, evaluating in this way the distortion factor, which is relevant for extracting the square modulus of nuclear matrix element from cross section measurements. The simulations in figs. 6.14 - 6.16 confirm the mass - dependent trend of the distortion factor, thus pointing out its general character. Referring to the latter figures, one can also note that SCE reaction cross section is smaller for heavier systems[2], according to the absorption cross section trend[3] and further confirming the

[2]This is consequentely true also for DCE reactions (see the sections below).

[3]Absorption cross section for ^{116}Cd(^{20}Ne,^{20}F)^{116}In have not been shown, because trend and magnitude are nearly the same of that for ^{116}Sn(^{18}O,^{18}F)^{116}In; similarly,

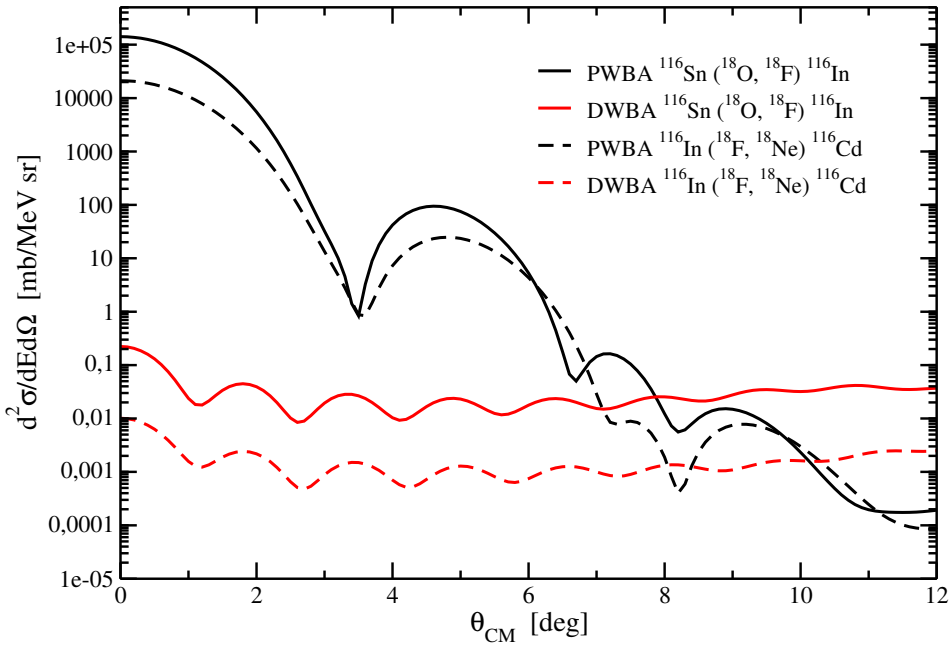

Figure 6.15: PWBA and DWBA SCE angular distributions, for the two reactions ^{116}Sn(^{18}O,^{18} F)^{116}In and ^{116}In(^{18}F,^{18} Ne)^{116}Cd, considering both nuclei in the exit channel in their ground states. This two processes have been exploited to determine dSCE cross section for the nuclear reaction ^{116}Sn(^{18}O,^{18} Ne)^{116}Cd. Simulations are performed by assuming a beam energy of 15 $AMeV$.

mass - dependence of the distortion factor. The magnitude of reaction cross sections is of course strongly influenced by the nuclear structure of the reacting ions, by means of the reaction kernel. For istance, for the reaction ^{40}Ca(^{18}O,^{18} F)^{40}K, starting from a doubly magic nucleus (^{40}Ca), the latter is lower than that for ^{40}K(^{18}F,^{18} Ne)^{40}Ar, involving no magic nuclei (see fig. 5.9, in chapter 5); the same considerations hold for the $Q-$value of the reaction, much more negative in the former case than in the latter. On the contrary, the radial reaction kernels of the heavier systems are of the same order of magnitude, because no doubly magic nucleus is involved in the reaction processes considered, so that the dif-

the absorption cross sections for the "second step" SCE reactions have not been shown too, because trends and magnitudes are nearly the same of the corresponding "first step" SCE processes.

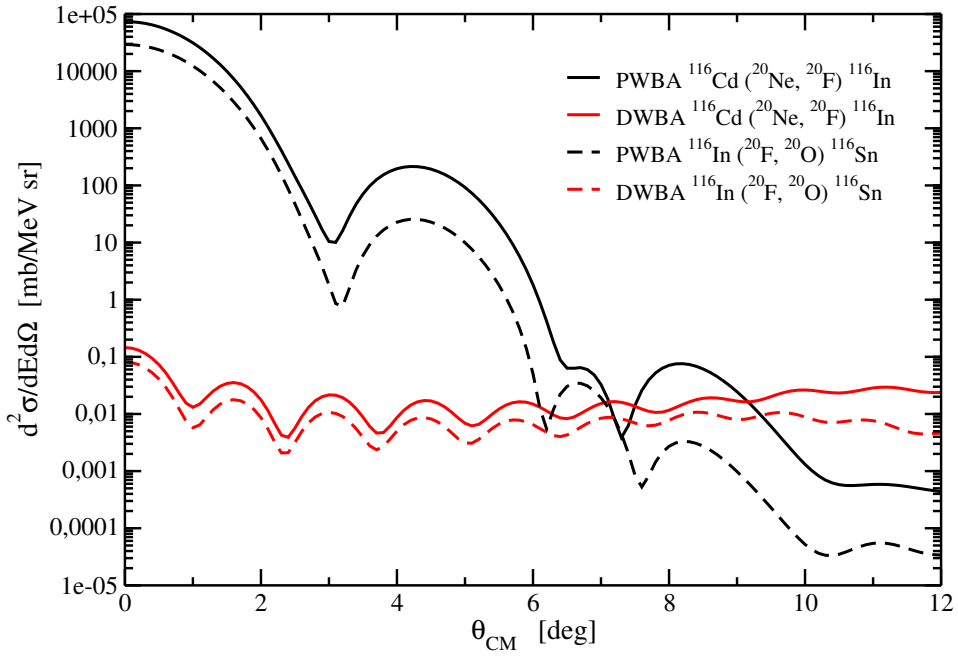

Figure 6.16: PWBA and DWBA SCE angular distributions, for the two reactions ^{116}Cd(^{20}Ne,^{20}F$_{1.057}$)^{116}In and ^{116}In(^{20}F$_{1.057}$,^{20}O)^{116}Sn, successively used to evaluate the cross section for the dSCE process ^{116}Cd(^{20}Ne,^{20}O)^{116}Sn. Simulations are performed by assuming a beam energy of 15 $AMeV$.

ferent magnitudes of the corresponding cross sections are mainly due to kinematics.

6.2.2 Heavy ion dSCE simulations

By means of the above SCE calculations, dSCE reaction cross sections have been determined, according to the formalism discussed in chapter 4. Figs. 6.17 - 6.19 show simulations performed by means of DCEx code, assuming SSD, for the low energy collisional DCE reactions ^{40}Ca(^{18}O,^{18}Ne)^{40}Ar, ^{116}Sn(^{18}O,^{18}Ne)^{116}Cd and ^{116}Cd(^{20}Ne,^{20}O)^{116}Sn, respectively. In particular, the first heavy ion DCE reaction has been obtained by convoluting the transition matrix elements relative e. g. to the

two $J^\pi = 1^+$ SCE reactions (Gamow-Teller-like)

$$^{40}\mathrm{Ca}(^{18}\mathrm{O},^{18}\,\mathrm{F})^{40}\mathrm{K}_{1^+_{2.29}} \quad \text{(I step)}$$

$$^{40}\mathrm{K}_{1^+_{2.29}}(^{18}\mathrm{F},^{18}\,\mathrm{Ne})^{40}\mathrm{Ar} \quad \text{(II step)}$$

considering only the SCE transition leading to the ground state of ^{18}F and the first 1^+ excited state of ^{40}K, at $E_x = 2.29\,MeV$, in the intermediate channel; the latter nuclear state has been chosen, instead of that at $2.7\,MeV$, characterized by an experimental higher Gamow-Teller strength, because QRPA calculations give a response function, associated to $J^\pi = 1^+$ and $L = 0$ transitions, with only one peak in the region between these two energies and this is also the first "true" (i. e. not intruder) peak, so that it has been identified with the first 1^+ excited state. Similarly, fig. 6.18 show DCEx simulations for the reaction ^{116}Sn(^{18}O,^{18} Ne)^{116}Cd obtained by folding the SCE processes

$$^{116}\mathrm{Sn}(^{18}\mathrm{O},^{18}\,\mathrm{F})^{116}\mathrm{In} \quad \text{(I step)}$$

$$^{116}\mathrm{In}(^{18}\mathrm{F},^{18}\,\mathrm{Ne})^{116}\mathrm{Cd} \quad \text{(II step)}$$

considering the 1^+ transition leading to the ground state both in ejectile and target-like nuclei in both SCE processes. In the same way, fig. 6.19 illustrates simulations for ^{116}Cd(^{20}Ne,^{20} O)^{116}Sn DCE reaction involving

$$^{116}\mathrm{Cd}(^{20}\mathrm{Ne},^{20}\,\mathrm{F})^{116}\mathrm{In} \quad \text{(I step)}$$

$$^{116}\mathrm{In}(^{20}\mathrm{F},^{20}\,\mathrm{Ne})^{116}\mathrm{Sn} \quad \text{(II step)}$$

1^+ SCE transitions leading to ^{116}In ground state and to the first excited state of ^{20}F, at $1.057\,MeV$, in the first step, and to ejectile and target-like ground states, in the II SCE step.

All these three heavy ion DCE reactions have been performed considering projectile nuclei with a kinetic energy of $15\,AMeV$ (according to NUMEN experiments). The quality of the above dSCE calculations obtained through DCEx code has been confirmed by simulations performed with FRESCO code[4] [108], represented by solid curves in fig. 6.17 for the pilot reaction ^{40}Ca(^{18}O,^{18} Ne)^{40}Ar, for PWBA and DWBA cases.

[4]Courtesy of Dr. S. Burrello and Dr. J. A. Lay.

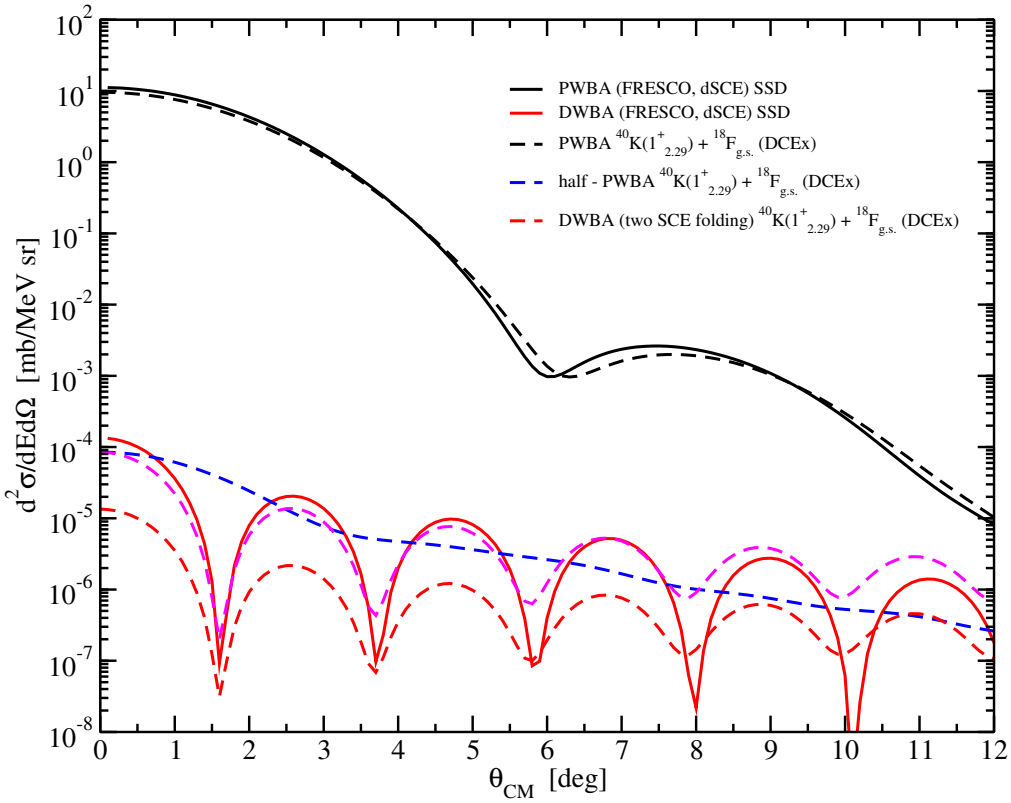

Figure 6.17: DCE cross section for ^{40}Ca(^{18}O,^{18} Ne)^{40}Ar at $E_{lab} = 15\,AMeV$, obtained within the framework of two uncorrelated SCE processes (dSCE). The solid curves are obtained by performing FRESCO simulations, while the dashed ones are obtained through the new DCE code; in particular, black curves refers to PWBA case, the solid red line refers to the complete, DWBA, case, while the dashed red curve refers to the folding of the two DWBA SCE cross sections (i. e. in the intermediate channel, $W(r)$ appears always negative); finally, the dashed blue curve is obtained by using plane waves in the intermediate channel and the magenta one is obtained by scaling the dashed red curve for reproducing the order of magnitude of the dashed blue curve.

Referring to the latter three figures, one can note that the distortion factor in the DCE processes, described through the dSCE reaction mechanism within SSD, is higher than the product of the distortion factors of the two SCE events, so that the absorption effects do not act twice, i. e. the effects of the absorption potentials partially compensate each other, due to the constructive interference among distorted waves in the intermediate channel. The compensating effect is not fully achieved, as

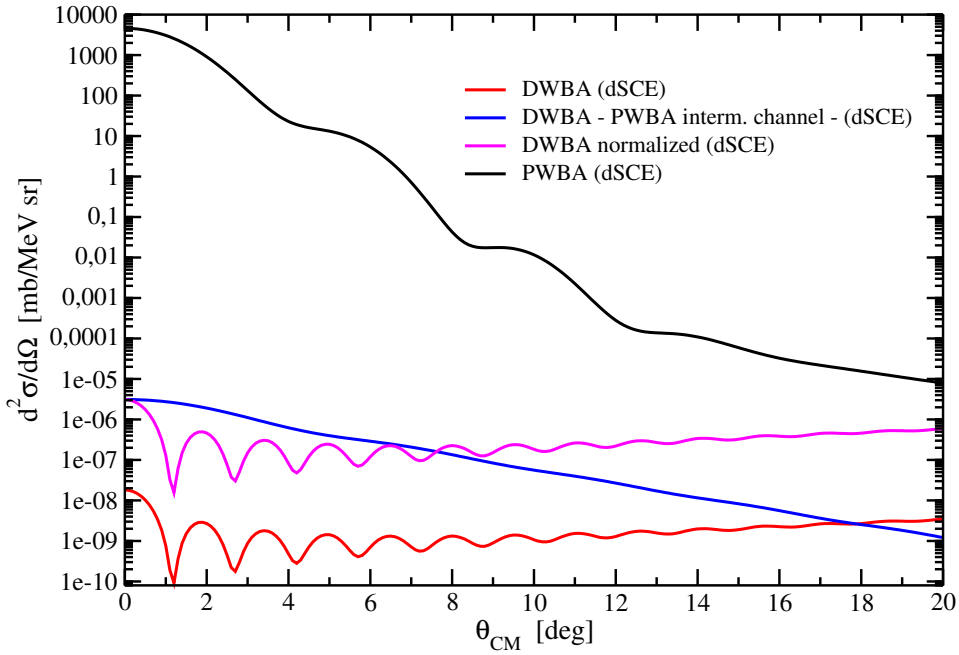

Figure 6.18: dSCE cross sections for ^{116}Sn(^{18}O,^{18}Ne)^{116}Cd DCE reaction. Black curve refers to PWBA case, the red one to DWBA calculations, obtained simply by folding two SCE transition matrix elements (from HIDEX code), the blue one to calculations performed by assuming plane waves in the intermediate channel and, finally, the magenta curve represents the DWBA cross section normalized to the blue curve, scilicet obtained through eq. (4.21).

one can see comparing the calculations obtained by assuming plane waves in the intermediate channel (thus mimicking a perfect compensation of distortion effects) with the full DWBA ones (FRESCO and DCEx codes).

Moreover, in fig. 6.17 it is shown that the DCE cross section obtained by using plane waves in the intermediate channel (dashed blue line) allows to recover the order of magnitude of the complete (DWBA) case, represented by the solid red curve.

As expected, dSCE cross section magnitude is smaller than SCE one, showing that a dSCE process is rarer than a SCE one, because the former is a process of higher order (in transition matrix element) with respect to the latter. Of course, this argument is anything but straightforward

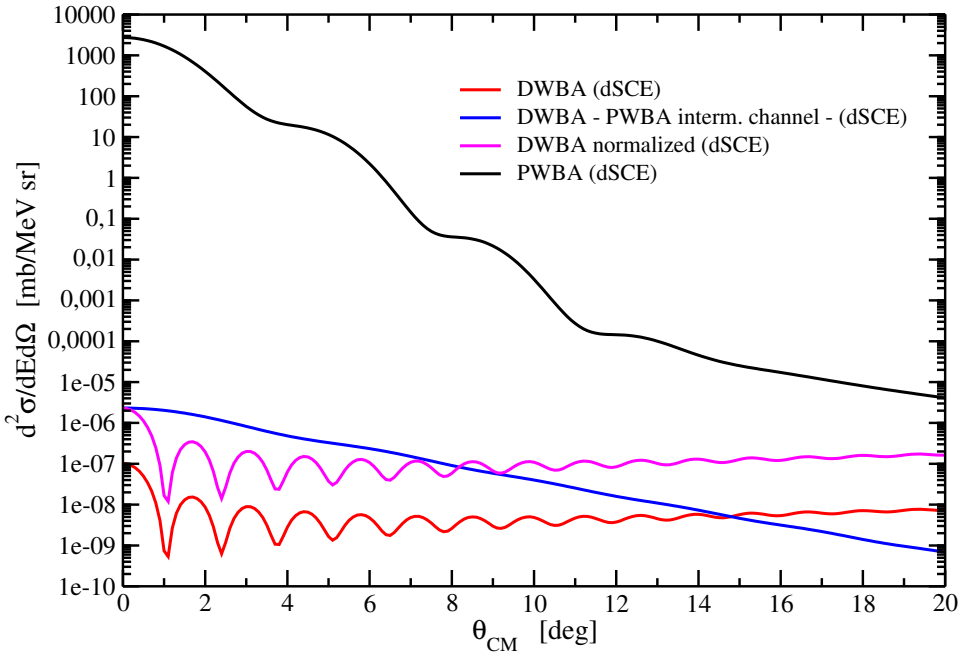

Figure 6.19: dSCE cross sections for ^{116}Cd(^{20}Ne,^{20}O)^{116}Sn DCE reaction. Black curve refers to PWBA case, the red one to DWBA calculations, obtained simply by folding two SCE transition matrix elements (from HIDEX code), the blue one to calculations performed by assuming plane waves in the intermediate channel and, finally, the magenta curve represents the DWBA cross section normalized to the blue curve, scilicet obtained through eq. (4.21).

for DCE processes described in terms of two correlated SCE reactions, which are still under study [5].

In order to improve DCE calculations, SSD hypothesis has been relaxed and more than one state has been considered in the intermediate channel, this leading to increasingly large dSCE cross sections, as can be seen e. g. for ^{40}Ca(^{18}O,^{18}Ne)^{40}Ar, in fig. 6.20, with diffraction patterns arising from the coherent superposition of transition matrix elements for the different multipolarity transitions. The nuclear states in the intermediate channel have been chosen according to the value of the corresponding cross sections, strongly influenced by the $Q-$value of the SCE processes populating that intermediate channel and by shape and

magnitude of the transition form factors involved, so that the magnitude of dSCE cross section turns out to be very sensitive to nuclear structure calculations, as expected. In particular, adding more than one intermediate state shows that only few nuclear states really contribute to the reaction cross section.

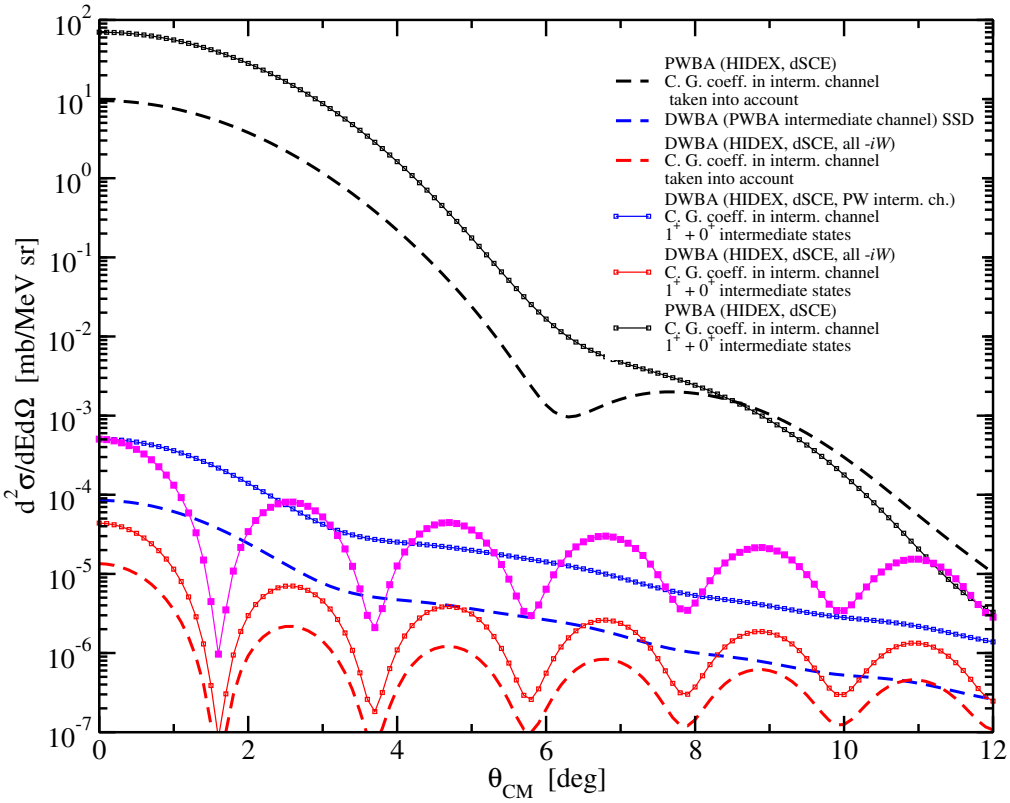

Figure 6.20: Comparison between DCE cross sections, for ^{40}Ca(^{18}O,^{18}Ne)^{40}Ar reaction, at $15\,AMeV$, obtained by considering only $^{40}\mathrm{K}(1^+, 2.3\,MeV)$ $+^{18}\mathrm{F}(1^+, g.s.)$ (dashed lines) and adding $^{40}\mathrm{K}(0^+, 1.64\,MeV)$ $+^{18}\mathrm{F}(0^+, 1.04\,MeV)$ to the former state (squares + solid line), in full PWBA (black lines), DWBA obtained without considering the normalization matrix element, $\tilde{S}^{\dagger}_{\delta}$, (red curves) and by considering plane waves in the intermediate channel (blue lines). Magenta curve fefers to the complete DWBA case, obtained by normalizing the red curve (squares + solid line) to the magnitude of the blue one (squares + solid line).

The introduction of the 5^+ excited state of ^{116}In at $0.1273\,MeV$, interesting because experimentally decaying β^- [154], in the intermediate

channel of the reactions ^{116}Sn(^{18}O,^{18} Ne)^{116}Cd and ^{116}Cd(^{20}Ne,^{20} O)^{116}Sn, does not lead to any significant contribution to the corresponding dSCE reaction cross sections and for this reason these results are not shown here.

Finally, fig. 6.21 shows preliminary calculations performed for all the DCE reactions, previously treated in SSD, by assuming closure approximation, so that all possible intermediate nuclear states are taken into account, in opposition to the SSD hypothesis. These preliminary results are obtained through HIDEX code, assuming the 2 - body reaction kernel as given by the product of the propagator, evaluated at a constant intermediate energy of about $4\,MeV$, and two 1 - body reaction kernels, properly weighted through Clebsch - Gordan coefficients, in order to account for angular momentum combinations, matching the angular momenta of the final channel; in particular, the total energy of the intermediate channel (closure energy) has been selected as the one corresponding to the mean value of the integrand of the off - shell relative momentum integral in eq. (4.8), which is in turn roughly given by the energy allowing to recover half of the transition strength.

The dSCE mechanism in closure approximation is the most interesting case, in that it resembles the Majorana, one - step mechanism, even if in Majorana - like one - step processes other contributions can occur, which can enhance or lower the DCE reaction cross section. Comparing the above preliminary closure approximation results with the ones obtained assuming SSD, one can note that the trend of all the above three DCE angular distributions is nearly the same; moreover, the distortion factor for the nuclear reaction ^{40}Ca(^{18}O,^{18} Ne)^{40}Ar, treated within SSD (dSCE), is of the same order of magnitude as the one from closure approximation calculations, while for the other two reactions, involving heavier nuclei, SSD calculations give a distortion factor smaller than the one obtained from simulations within closure approximation. Furthermore, the closure

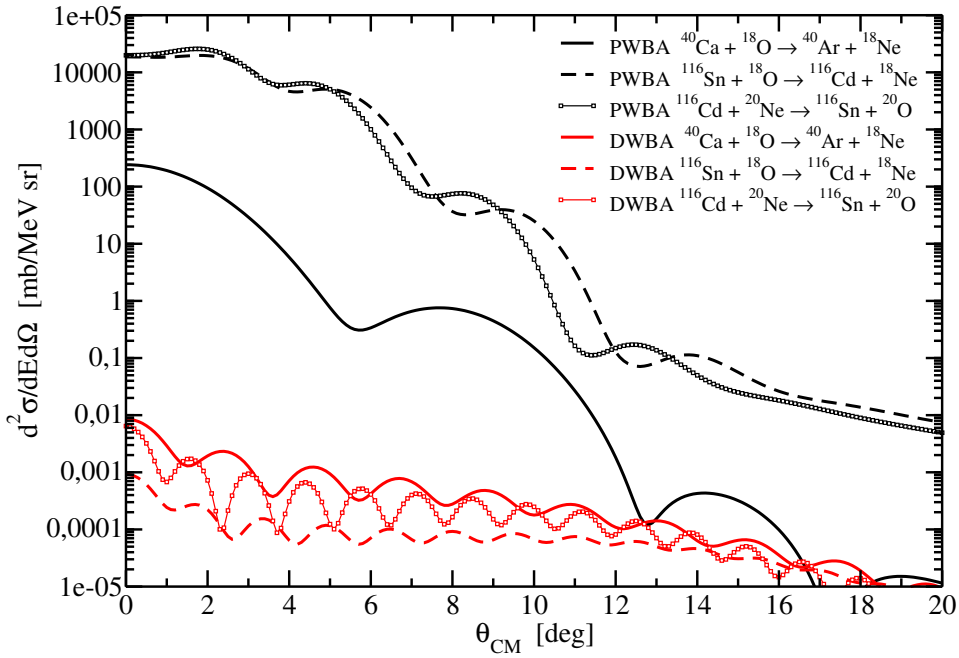

Figure 6.21: DCE cross sections, for ^{40}Ca(^{18}O,^{18} Ne)^{40}Ar reaction, at 15 $AMeV$, obtained within the closure approximation, both in full PWBA (black line) and full DWBA (red curves). For details, see the text.

approximation (cDCE) cross sections are from 2 to 3 orders of magnitude greater than the corresponding dSCE ones, depending on the Q-value and on projectile and target masses and transition densities characterizing the reaction, thus bringing hope to neglect the competing dSCE mechanism in favor of the one mimicking Majorana - like processes.

6.2.3 Some insight on possible full dSCE cross section factorization

The dSCE mechanism makes heavy ion DCE reactions very close to $2\nu\beta\beta$ decays, even though different intermediate nuclear states and momenta can be involved in the two processes. As stated in the previous chapters, to extract the nuclear matrix element (embedded into the reaction kernel) it is necessary to factorize heavy ion DCE reaction cross

section into the product of a nuclear reaction term and a nuclear structure term, with the aim to provide a proportionality relation between the latter observable and the nuclear matrix element. In chapter 4, we have shown that it is anything but straightforward to provide such proportionality relation, because of the integral over the off - shell relative momentum involved in the intermediate channel, which is not completely removed even assuming Gaussian SCE reaction kernels, pole approximation and SSD, thus leaving a partially - factorized expression for dSCE cross section.

To assess the quality of the partially - factorized dSCE formalism thus developed, simulations have been performed by naïvely describing dSCE reaction kernel as simply given by the product of the only monopole component of the two SCE Gaussian reaction kernels and fixing their intermediate channel - angular dependence, so that a fully - factorized expression for dSCE cross section has been in fact implemented. In the same vein of SCE simulations shown in fig. 6.13, the square modulus of the dSCE transition matrix element, thus obtained, has been studied as a function of momentum transfer, as illustrated in fig. 6.22, for the DCE reaction ^{40}Ca(^{18}O,^{18} Ne)^{40}Ar, interpreted as combination of the same two SCE nuclear reactions considered in the calculations performed in SSD. The different curves in fig. 6.22 refer to DCE transition matrix elements calculated by using the same approximations displayed in fig. 6.13 for each of the two SCE reaction kernels. These simplified dSCE calculations well reproduce the diffraction pattern of the angular distribution, which presents narrower minima passing from PWBA to DWBA calculations, and the ratio between DWBA and PWBA cross section at zero degrees, i. e. the distortion factor, as compared to DCEx and FRESCO simulations (fig. 6.17).

Comparing dSCE simulations in fig. 6.22 with the analogous SCE ones (fig. 6.13), one can also note that the former are characterized by

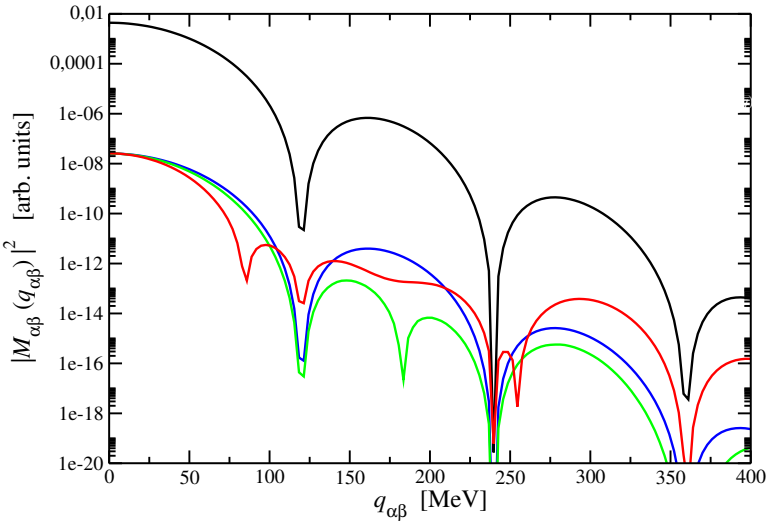

Figure 6.22: Comparison among dSCE monopole component of the square modulus of transition matrix element, i. e. the cross section in arbitrary units, in PWBA (black line), full DWBA (red line) and for two different approximations of the gaussian reaction kernel, within BDA, corresponding (same colours are used) to the product of the SCE transition matrix elements obtained in the cases illustrated in fig. 6.13.

a distortion factor greater (stronger absorption[5]) than the one of each SCE reaction, even if smaller than the product of the distortion factors of the two SCE component processes; for this simplified calculations the latter effect is merely related to the reaction kernels used, in that the intermediate channel has been neglected, so that it does not affect the dSCE distortion factor for this simple simulations; of course, the absence of the intermediate angular integration in the DWBA dSCE curve of fig. 6.22 leads to a trend different from the one of DWBA dSCE complete calculations (fig. 6.17).

Moreover, similarly to SCE calculations, comparing the red curve with the green and blue curves, one can note that these three functions overlap up to $q_{\alpha\beta} \simeq 25 - 30\, MeV$, thus defining a range of values of (DCE) momentum transfer within which the above naïvely fully factorized calculation for heavy ion dSCE cross section (and a fortiori the partially -

[5]More processes that remove the probability flux from the elastic channel.

factorized one, implemented in DCEx code) works quite well. In this way, an approximate proportionality relation is provided between dSCE reaction cross section and the corresponding nuclear matrix element, which in turn can only approximately be expressed as the product of two SCE ones.

6.3 Preliminary comparison with data

In order to perform a (preliminary) comparison with experimental data, it is important to stress that for SCE processes the collisional mechanism dominates the sequential one for high beam energies, $E_{beam} \gtrsim 100\,AMeV$, as provided by Lenske et al. for the nuclear reaction ^{12}C(^{12}C,^{12} N)^{12}B [101], whatever the angular momentum transfer is, while for heavier systems at intermediate and low energies[6] SCE reactions dominate for small angular momentum transfer [81], while sequential mechanisms are suppressed with respect to direct DCE ones, because the former represent higher order processes, since their contributions are at least of the 4th order in transition matrix element.

Once checked the quality of the formalism developed to describe heavy ion SCE and dSCE reactions, at low energies, together with approximations used to factorize charge exchange cross sections, one can move to perform a comparison with the experimetal data, in order to extract SCE and dSCE nuclear matrix elements. It is important to stress that such factorization is independent of the nuclear structure model adopted, because it lays down its basis simply on the direct nature of charge exchange processes; what changes is the value of the parameters in the gaussian reaction kernel together with the magnitude of the transition densities, and thus of the cross section.

Hence, both SCE and DCE cross sections can be influenced by the

[6] This is the range of interest for the experiments performed within the NUMEN collaboration.

nuclear structure peculiarities of the nuclei involved in the transition; the diffraction pattern is also influenced by the imaginary part of the optical potential used, so that the availability of elastic cross section data plays a crucial role in the comparison of charge exchange reaction calcultations with the experimental charge exchange cross sections.

Fig. 6.23 shows a preliminary comparison with the data, obtained from experiments performed by the NUMEN collaboration, for the pilot SCE reaction ^{40}Ca(^{18}O,^{18}F)^{40}K. The energy range [0.7, 1.4] MeV has been set, because in this interval the experimental energy spectrum [80] presents two peaks that can be identified with the transitions to the 2^- and 5^- excited states of ^{40}K at 0.8 and 0.891 MeV, respectively, indicated in the legend.

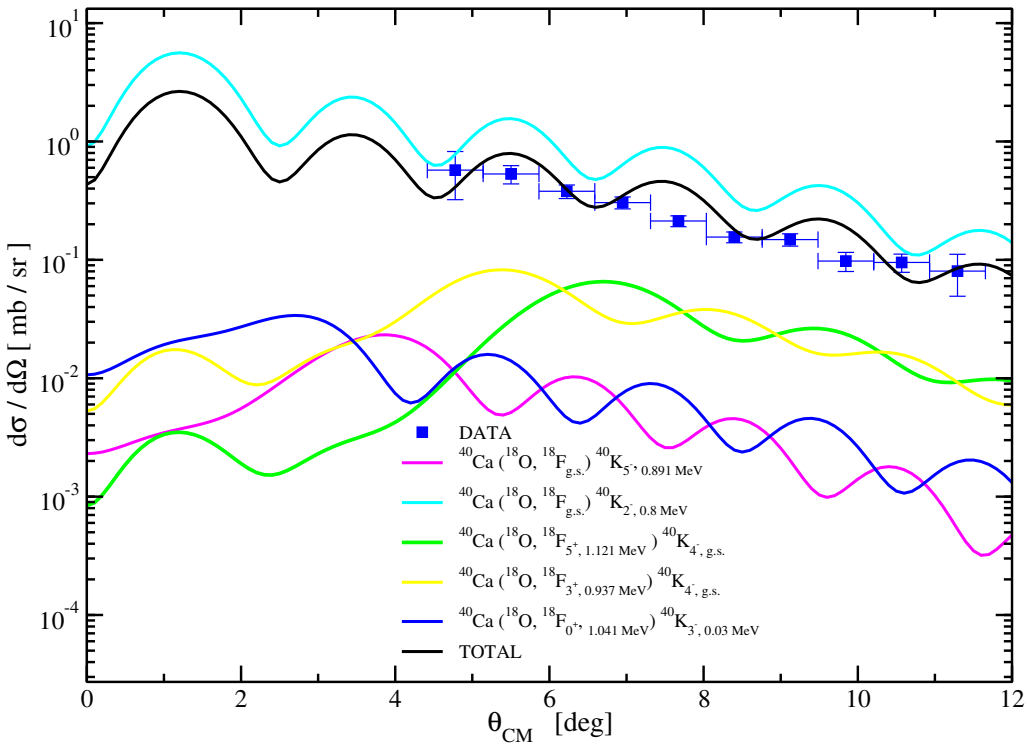

Figure 6.23: Angular distribution within [2°, 4°] range, for the SCE reaction ^{40}Ca(^{18}O,^{18}F)^{40}K, integrated over the total excitation energy range [0.7, 1.4] MeV, compared to the experimental data [155]. Calculations include some of the excited states of both ^{18}F and ^{40}K populated within such energy range.

The plot also shows other transitions characterized by a total (projectile + target) excitation energy falling within the interval of interest. One can immediately note that the main contribution within this energy interval comes from the lowest multipolarity transition involved, i. e. the one populating the 2^- excited state of ^{40}K. All these angular distributions are obtained by integrating each HIDEX SCE reaction cross section with respect to the proper target - like excitation energy range. In order to take into account the different ejectile excitation energies involved in these transitions, the sum of the above cross sections have been properly weighted by ejectile excitation energy range, thus getting the black curve in fig. 6.23. The latter shows a clear diffraction pattern, in contrast to the quite smooth trend of data. This reveals that some interference with other competing transitions may attenuate the diffraction pattern of the angular distribution at forward angles. Possible sources of discrepancy are represented by the optical model potentials, coming from microscopic calculations, and by the limitations of the nuclear structure model used. In this sense calculations must be improved, by fitting optical potential parameters with the experimental elastic cross section, once available, and checking the effect of different nuclear structure models on shape and magnitude of the cross section. Considering the state - of -art of the calculations we consider satisfactory that SCE simulations already allow to reproduce the magnitude of the data.

DCE cross section data [1] also show a smooth trend, which is steeper for $\theta_{CM} \lesssim 6\,\mathrm{deg}$ than for larger scattering angles; this behaviour could indicate the dominance of a given DCE mechanism at small angles and of another one for higher angular values or one low multipolarity (because of the peak at small scattering angles) transition at forward angles and higher multipolarity transitions for larger scattering angles. Unfortunately, the state - of - art of the theoretical framework of DCE reactions is still in its infancy, so that the above interpretations of DCE data are

merely speculative.

A very preliminary comparison with DCE experimental results is shown in fig. 6.24, where one can see that the dSCE angular distribution obtained by considering two low momentum transfer nuclear states in the intermediate channel, $^{18}\mathrm{F}_{g.s.} + ^{40}\mathrm{K}(1^+, 2.29MeV)$ and $^{18}\mathrm{F}_{g.s.} + ^{40}\mathrm{K}(0^+, 1.64MeV)$, that should be the ones giving the main contributions in the intermediate channel of dSCE processes, underestimates experimental results by about a factor of 100, while the magenta curve obtained within closure approximation allows to recover the order of magnitude of the data, but not the trend.

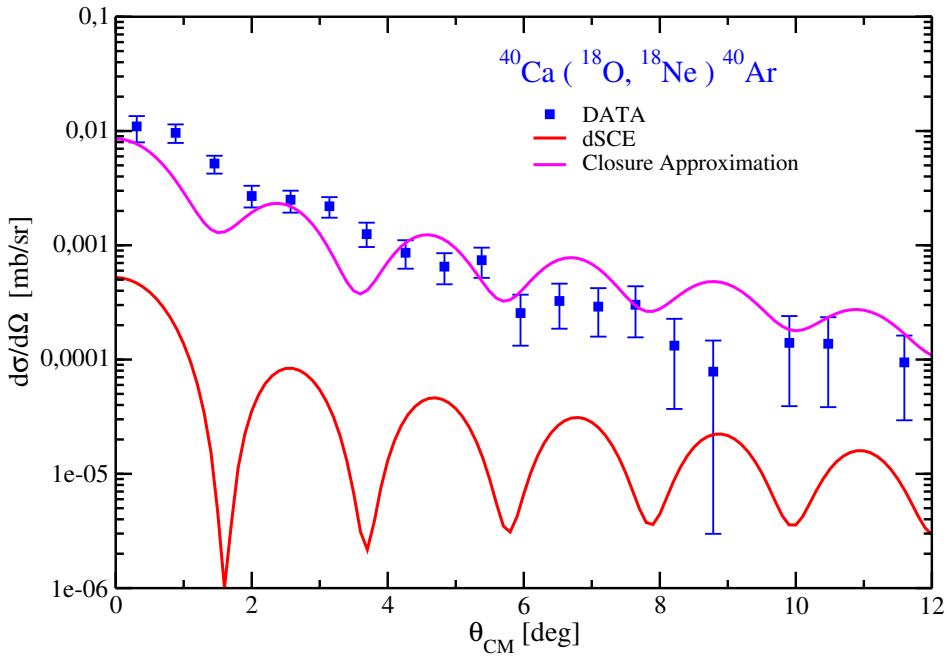

Figure 6.24: DCE angular distribution data [1] for the pilot reaction, compared with dSCE calculations including two dominant states in the intermediate channel (red line) and with a preliminary calculation of DCE cross section in closure approximation (magenta curve).

As in the case of the SCE cross section, the differences in the diffraction pattern may be caused by the choice of the optical potentials (now considering also that involved in the intermediate reaction channel), still derived microscopically because of the absence of DCE elastic scattering

data. A further complication is related to the two possible mechanisms describing a DCE nuclear reaction: calculations within SSD underestimate the data by about a factor of 100, which could be recovered by considering the contributions of different excited states of both projectile - like and target - like nuclei in the intermediate channel, but this is still under study; closure approximation simulations need also further improvement in the calculation of the corresponding cDCE reaction kernel, hoping to reproduce also the trend of the experimental results.

CONCLUSIONS

Summarizing, the present PhD work has been dedicated to the study of heavy ion charge exchange reactions, focusing in particular on the range of low energies, which up to now lacks of a theoretical framework.

The main goal of the present thesis is just represented by the formulation of a theory describing both single and double charge exchange heavy ion reactions in the energy range mentioned above. This target has been reached by providing an elegant and simple extension of the '80s and '90s formalism developed by Taddeucci for (p, n) reactions to heavy ion single and double charge exchange processes, at low and intermediate energies; moreover, factorization of both single and double charge exchange cross sections into the product of a reaction and a nuclear structure term has been reached, starting from the simple assumption of nuclear surface peaked gaussian reaction kernels, that is supported by the direct nature of charge exchange nuclear reactions. All calculations have been performed within the DWBA formalism.

First of all, a study of the influence of the different optical potential components to the single charge exchange heavy ion cross section has been checked, together with the role of central and tensor components of the effective nuclear interaction potential [6], in order to have under con-

trol single charge exchange reactions. This is particularly important also because SCE rections constitute the basic processes in terms of which heavy ion double charge exchange reactions can be explained. In this way, we noted that at low and intermediate energies, heavy ion reactions are dominated by central interactions and low angular momentum transfer at forward scattering angles while higher angular momenta and tensor interaction start to give significant contribution at larger scattering angles, as expected. Finally, the dominant role of the absorption effects has been confirmed.

Once got deeper insight into the different elements taking part to the single charge exchange reaction cross section, a study of low energy heavy ion DCE reactions has been performed within the hypothesis of two - step process. Then a code has been developed, DCEx, through which it has been possible to simulate dSCE reactions proceeding via SSD and then considering more than one nuclear state in the intermediate channel in order to assess the quality of SSD assumption; in this way, it has been evidenced how dSCE reactions strongly depend on the nuclear structure features.

Moreover, very preliminary calculations have been performed for low energy heavy ion DCE reactions within closure approximation, by means of HIDEX simulations by employing naive 2-body operators.

Finally, once noted that the radial SCE transition densities can be nicely fitted by gaussians peaked at the nuclear surface, as expected for direct reactions, it has been developed a simple model of cross section factorization, depending on parameters related to the features of the optical potential (reaction part) and to magnitude and shape of the transition densities (nuclear structure part), the latter being proportional to β (single charge exchange) and $2\nu\beta\beta$ decay strengths. The factorization procedure thus obtained is valid indipendentely of the nuclear structure model adopted, in that changes in nuclear structure only lead to varia-

tions of the values of the parameters of the gaussian reaction kernel. The factorization framework developed can be extended to dSCE processes, because they are still direct reactions, simply tuning the value of the parameters appearing in the gaussian reaction kernel.

An analytical expression of the whole reaction cross section has been derived within the black disk approximation, justified by the dominance of absoption effects in heavy ion reactions.

Within such a context, cross section factorization procedure, provided in the present work, is exact for zero linear momentum transfer, but it has been tested that it works pretty well for momentum transfer values less than $25 - 30\, MeV$, both for single and double charge exchange reactions.

Simulations have been perfomed for nuclear systems investigated by the NUMEN collaboration, by using HIDEX and DCEx codes. It should be noticed that the latter code, fully developed within the present thesis work, has been tested by comparisons with FRESCO simulations, kindly provided by Seville University collegues, who moreover have provided the conditions under which the contribution from transfer reactions, mimicking the channel under study, can be neglected.

The validity of the black disk hypothesis has been tested for different beam energies, finding that such approximation takes into account pretty well the strong absorption effects in heavy ion nuclear reactions for energies greater than about $10\, AMeV$, while starts to fail for beam energies close to the Coulomb barrier, overestimating absorption effects. Through this approximation it has been obtained a distortion factor strongly descreasing with the target mass and mildly increasing with the beam energy (both for single and double charge exchange processes).

A preliminary comparison with experimental results (NUMEN, [1]) for ^{40}Ca(^{18}O,^{18}F)^{40}K single charge exchange reaction turned out to be quite satisfactory, providing the correct order of magnitude of the cross section, even if the trend of the data is not correctly reproduced.

Double charge exchange reactions can proceed via two main mechanisms [80, 144]: sequence of two uncorrelated single charge exchange processes (dSCE) and combination of two correlated single charge exchange reactions (cDCE). In the present work, main attention has been focused on the former mechanism, which can give information on $2\nu\beta\beta$, thus representing a mechanism competing with the second one, which is still under study and should allow to gain information on the desired $0\nu\beta\beta$ decay strength.

A preliminary comparison with double charge exchange data has been performed, indicating that the dSCE mechanism underestimates experimental data, thus leaving some hope that the "golden" cDCE mechanism dominates, getting closer to the possibility of gaining information on the wanted $0\nu\beta\beta$ decay strength, but the work in this direction is still too long and tricky.

Concluding, the factorizaton procedure formulated in this PhD thesis represents a nice "trick" to gain information on double charge exchange nuclear matrix elements, in the perspective to get a deeper insight on the different mechanisms realizing double charge exchange processes and on the possible analogy with 0 and $2\nu\beta\beta$ nuclear matrix elements. Work is in progress along this direction, in the hope to be able to understand which one of the two "strong-analogous" processes dominates and possibly gain information on $0\nu\beta\beta$ nuclear matrix elements.

BIBLIOGRAPHY

[1] F. Cappuzzello, M. Cavallaro, C. Agodi, M. Bondì, D. Carbone, A. Cunsolo, A. Foti, Eur. Phys. J. A (2015), 51.

[2] T. N. Taddeucci et al., Nucl. Phys. A 469 (1987) 125-172.

[3] N. Shimizu, J. Menéndez and K. Yako, Phys. Rev. Lett. 120 (2018) 142502.

[4] E. Santopinto, H. Garcìa - Tecocoatzi, R. I. Magaña - Vsevolodovna and J. Ferretti, "Heavy-ion double-charge-exchange and its relation to neutrinoless double beta decay", available on arXiv: 1806.03069v2 [nucl-th] 27 Jun 2018.

[5] H. Lenske, "Probing Double Beta - Decay by Heavy Ion Charge Exchange Reactions", IOP Conf. Series: Journal of Physics: Conf. Series 1056 (2018) 012030.

[6] H. Lenske, J. I. Bellone, M. Colonna, J. A. Lay, Phys. Rev. C 98 (2018) 044620.

[7] C. D. Goodman et al., Phys. Rev. Lett. 44 (1980) 1755.

[8] Y. Fujita et al., PPNP 66 (2011) 549-606.

[9] F. Osterfeld, Rev. Mod. Phys., Vol. 64, 2 (1992) 491-550.

[10] M. Ichimura, H. Sakai, and T. Wakasa, Prog. Part. Nucl. Phys., 56, 446 (2006).

[11] G. Martínez-Pinedo, J. Phys. G: Nucl. Part. Phys. 35, 014057 (2008).

[12] O. Cremonesi and M. Pavan, Adv. High Energy Physics 2014, 951432 (2014).

[13] W. P. Alford and B. M. Spicer, Adv. Nucl. Phys. 24, 1 (1998).

[14] E. Fermi, Z. Phys. 88, (1934) 161.

[15] P.Christmas et al., Nuclear Instruments and Methods in Physics Research 215 (1983) 397 - 408.

[16] Y. Fukuda et al., Phys. Rev. Lett., 81 (1998), 1562-1567.

[17] Q. R. Ahmad et al., Phys. Rev. Lett., 89 (2002) 011301.

[18] C. Giunti, C.W. Kim, Fundamentals of Neutrino Physics and Astrophysics, (2007).

[19] E. Holzschuh, Rept. Prog. Phys., 55, 1035-1091, 1992.

[20] C. Kraus et al., Eur. Phys. J., 40 (2005) 447.

[21] V. M. Lobashev et al., Phys. Lett. B 460 (1999) 227-235.

[22] L.Bornschein, the KATRIN-Collaboration, Nucl. Phys. A, 752 (2005), 14-23.

[23] E. Majorana, Nuovo Cimento 14, 171 (1937).

[24] Maggiore M., A modern introduction to quantum field theory, Oxford University Press (2005). Peskin M. E., Schroeder D. V., An Introduction to Quantum Field Theory, Westview Press (1995).

[25] G. Racah, Nuovo Cimento 14, 322 (1937).

[26] M. Jezabek, Y. Sumino, Phys. Lett. B 440 (1998) 327-331.

[27] S. Antusch, S. F. King, New J. Phys. 6 110 (2004).

[28] S. F. King, Phys. Lett. B 718 (2012) 136-142.

[29] S. F. King, J. Phys. G: Nucl. Part. Phys. 42 (2015) 123001.

[30] R. N. Mohapatra and G. Senjanovic, Phys. Rev. Lett. 44, 912 (1980).

[31] A. Abada and M. Lucente, Nucl. Phys. B 885 (2014) 651 - 678.

[32] A. G. Dias et al. Phys. Rev. D 86 (2012) 035007.

[33] M. Mitra *et al.*, Phys.Rev. D95 (2017) 3, 035042.

[34] F. R. Joaquim and A. Rossi, AIP Conf. Proc. 1078, 372 (2009) [arXiv:0809.2859 [hep-ph]]. A. de Gouvêa and P. Vogel [arXiv:1303.4097v2[hep-ph](2013)].

[35] M. Lindner, T. Ohlsson, G. Seidl, Phys. Rev. D65 (2002) 053014.

[36] D. A. Dwyer, Physics of the Dark Universe 4 (2014)31-35.

[37] A. D. Sakharov, Pisma Zh. Eksp. Teor. Fiz.5, 32 (1967) [JETP Lett. 5, 24 (1967 SOPUA,34,392-393.1991 UFNAA,161,61-64.1991)].

[38] M. Fukugita and T. Yanagida, Phys. Lett. B 174, 45 (1986).

[39] W. Buchmuller, R. D. Peccei, T. Yanagida, Ann. Rev. Nucl. Part. Sci. 55: 311-355, 2005.

[40] S. Dell'Oro, S. Marcocci and F. Vissani, Phys. Rev. D 90, 033005 (2014).

[41] W. H. Furry Phys. Rev. 56 (1939) 1184.

[42] Primakoff and Rosen, Rep. Prog. Phys. 22 (1959) 121.

[43] M. Doi et al, Prog. Theor. Phys. 66, 1739 (1981); 69, 602 (1983).

[44] T.Tomoda, Rep. Prog. Phys. 54, 53 (1991).

[45] F. Šimkovic et al., Phys. Rev. C60, 055502 (1999).

[46] J. Barea, J. Kotila, F. Iachello, Phys. Rev. C 87, 014315 (2013).

[47] M. R. Schindler and S. Scherer, Eur. Phys. J. A 32, 429 (2007).

[48] O. Dumbrajs et al., Nucl. Phys. B 216, 277 (1983).

[49] M. Kortelainen and J. Suhonen, Phys. Rev. C 75, 051303 (2007).

[50] J. Menéndez, A. Poves, E. Caurier, and F. Nowacki, Nucl. Phys. A 818, 139 (2009).

[51] J. D. Holt, J. Engel, Phys. Rev. C 87, 064315 (2013).

[52] J. Barea, J. Kotila, F. Iachello, Phys. Rev. C 91 034304 (2015).

[53] R. A. Sen'kov and M. Horoi, Phys. Rev. C 88, 064312 (2013).

[54] J. Engel and J. Menéndez, Rep. Prog. Phys. 80, 046301 (2017).

[55] J. Alster and J. Warszawski, Phys. Rep.52, 2 (1979) 87-132.

[56] W. R. Gibbs, M. Elghossain, W. B. Kaufmann, Phys. Rev. C 48 (1993) 1546.

[57] D. S. Koltun and M. K. Singham, Phys. Rev. C 39, (1989) 704.

[58] M. Goeppert-Meyer, Phys. Rev. 48, (1935) 512.

[59] M. G. Inghram, J. H. Reynolds, Phys. Rev. 78 (1950) 822.

[60] T. Kirsten, W. Gentner, O. A. Schaeffer, Z. Phys. A 202 (1967) 273.

[61] S. R. Elliott, A.A. Hahn, and M.K. Moe, Phys. Rev. Lett. 59 (1987) 2020.

[62] A. Barabash, Phys. Part. Nucl. 42, 613 (2011).

[63] A.S. Barabash, Nucl. Phys. A 935, 52 (2015).

[64] A. L. Turkevich, T. E. Economou, G. A. Cowan, Phys. Rev. Lett. 67 (1991) 3211.

[65] J. Abad, A. Morales, R. Nuñez Lagos, and A. F. Pacheco, Anales de física: Serie A: Fenómenos e interacciones 80, 9 (1984); J. Phys. (Paris) 45, 147 (1984).

[66] A. Griffiths and P. Vogel, Phys. Rev. C 46, 181 (1992).

[67] O. Civitarese and J. Suhonen, Phys. Rev. C 58, 1535 (1998).

[68] F. Šimkovic, P. Domin, and S. V. Semenov, J. Phys. G 27, 2233 (2001).

[69] P. Domin, S. Kovalenko, F. Šimkovic and S. V. Semenov, Nucl. Phys. A 753, 337 (2005).

[70] F. Šimkovic, G. Panits and A. Faessler, Prog. in Part. and Nucl. Phys. 40 (1998) 285 - 294.

[71] F. Šimkovic et al., Phys. Rev. C 83 (2011) 015502.

[72] W.M. Visscher, R.A. Ferrell, Phys. Rev. 107, 781 (1957).

[73] S. Bloom, N. Glendenning, S. Moszkowski, Phys. Rev. Lett. 3, 98 (1959).

[74] A. Klein, E. R. Siciliano and N. Auerbach, Phys. Rev. C 32 (1985) 1998.

[75] E. Oset and D. Strottman, Nucl. Phys. A 355 (1981) 437 - 476.

[76] C. Wong, J.D. Anderson, S.D. Bloom, J.W. McClure, B.D. Walker, Phys. Rev. 123, 598 (1961).

[77] J.D. Anderson, C. Wong, I.W. McClure, Phys. Rev. 126, 2170 (1962).

[78] J. S. Blair and E. M. Henley, Phys. Rev. 112 2029 (1958).

[79] J. S. Blair, Phys. Rev. 115 (1959) 928.

[80] F. Cappuzzello et al. Eur. Phys. J. A (2018) 54: 72.

[81] J. A. Lay, S. Burrello, J. I. Bellone, M. Colonna and H. Lenske, within the NUMEN project, "Double Charge-Exchange Reactions and the effect of transfer", IOP Conf. Series: Journal of Physics: Conf. Series 1056 (2018) 012029.

[82] K. Kisamori et al., Phys. Rev. Lett. 116, 052501 (2016).

[83] N. Auerbach et al., Ann. Phys. 192, 77 (1989).

[84] H. Clement, Prog. Part. Nucl. Phys., Vol. 29, (1992) 175-250.

[85] J. D. Vergados, Phys. Rev. D 25, 914 (1982).

[86] A. Fazely, L.C. Liu, Phys. Rev. Lett. 57, 968 (1986).

[87] S. Mordechai et al., Phys. Rev. Lett. 61, 531 (1988).

[88] Report to the Nuclear Science Advisory Committee, Neutrinoless Double Beta Decay (2014).

[89] F. Naulin et al., Phys. Rev. C 25, 1074 (1982).

[90] J. Blomgren et al., Phys. Lett. B 362, 34 (1995).

[91] D.M. Drake et al., Phys. Rev. Lett. 45, 1765 (1980).

[92] C.H. Dasso, A. Vitturi, Phys. Rev. C 34 (1986) 743.

[93] F. Cappuzzello e al., AIP Conference Proceedings 1894, 020004 (2017).

[94] M. Takaki et al., CNS Ann. Rep. 94, 9 (2014).

[95] T. Uesaka et al., RIKEN RIBF NP-PAC, NP1512- RIBF141 (2015).

[96] G. R. Satchler, Nuclear Physics 55 (1964) 1 - 33.

[97] W. G. Love and G. R. Satchler, Nucl. Phys. A 159 (1970) 1 - 44.

[98] D.R. Bes, O. Dragun, E.E. Maqueda, Nucl. Phys. A 405 (1983) 313.

[99] W. Von Oertzen, et al., Nucl. Phys. A 588 (1995) 129c.

[100] D. M. Brink, Phys. Lett. B 40 (1972) 37.

[101] H. Lenske, H. H. Wolter, and H. G. Bohlen, Phys. Rev. Lett. 62, 1457 (1989).

[102] S. Burrello, J. I. Bellone, M. Colonna, J. A. Lay, H. Lenske, "Charge-exchange reactions and role of competing transfer channels", contribution to ECT^* workshop 2018.

[103] J. J. Sakurai, "Modern Quantum Mechanics. Revised Edition", Zanichelli, 1996.

[104] J. R. Taylor, "Scattering Theory: The Quantum Theory on Non-relativistic Collisions", John Wiley & Sons, Inc., 1972.

[105] G. R. Satchler, "Introduction to Nuclear Reactions", second edition, Macmillan Education UK (1990).

[106] F. Cappuzzello *et al.*, Nuclear Physics A 739 (2004) 30 - 56.

[107] T. Tamura, Annual Review of Nuclear Science 1969 19:1, 99-138.

[108] I. J. Thompson, Computer Physics Reports 7 (1988) 167-212.

[109] P. Ring and P. Schuck,"The Nuclear Many-Body Problem", Springer-Verlag (1980).

[110] C. A. Bertulani, arXiv:0908.3275v2 [nucl-th] 14 Jul 2010.

[111] S. N. Ghoshal, Phys. Rev. 80, 939 (1950).

[112] F. Petrovich, in The (p, n) reaction and the nucleon - nucleon force, ed. C. D. Goodman et al. (Plenum, New York, 1980), p. 115.

[113] N. Austern, "Direct reaction theories" (Wiley, New York, 1970).

[114] W. Greiner and J. A. Maruhn, "Nuclear Models" (Springer - Verlag, Berlin Heidelberg, 1996).

[115] G. F. Bertsch, "The Nuclear Response Funciton", Supplement of the Progress of Theoretical Physics, 74 - 75 (1983).

[116] A. L. Fetter and J. D. Walecka, "Quantum Theory of Many - particle Systems" (McGraw - Hill Book Company, 1971).

[117] K.Ikeda, Prog. Theor. Phys. 31 (1964) 434.

[118] A. Bohr and B. Mottelson, "Nuclear Structure" (Benjamin, New York, 1969), Vol. 1, pp. 345, 349, 411.

[119] J. D. Anderson, C. Wong, and V. A. Madsen, Phys. Rev. Lett. 24, 1074 (1970).

[120] S. M. Austin, "The Two Body Force in Nuclei", edited by S. M. Austin and G. M. Crawley (Plenum, New York, 1972).

[121] M. Bondí, PhD thesis (2014).

[122] A. K. Kerman, H. McManus, R. M. Thaler, Ann. Phys. 8 (1959) 551-635.

[123] F. Petrovich, W. G. Love and R. J. McCarthy, Phys. Rev. C 21 (1980) 1718.

[124] P. E. Hodgson, The Optica/ Model of Elastic Scattering, Clarendon Press, New York, 1962.

[125] P. E. Hodgson, Nuclear Heavy Ion Reactions, Clarendon Press, Oxford, 1978.

[126] J. H. Thies et al., Phys. Rev. C 86, 044309 (2012).

[127] D. Frekers, Progr. Part. Nucl. Phys. 57, 217 (2006).

[128] S. Rakers et al., Nucl. Instrum. Methods A 481, 253 (2002).

[129] H. Dohmann et al., Phys. Rev. C 78, 041602(R) (2008).

[130] E. W. Grewe et al., Phys. Rev. C 78, 044301 (2008).

[131] H. Okamura et al., Phys. Lett. B 345, 1 (1995).

[132] H. Ohnuma et al., Phys. Rev. C 47, 648 (1993).

[133] W. G. Love, A. Scott, F. Todd Baker, W. P. Jones and J. D. Wiggins, Jr. , Phys. Lett. 73B, 277 (1978).

[134] G. Potel et al., Nucl.Phys.News. 24 (2014) n.1, 19 - 25.

[135] T. Tamura, T. Udagawa and H. Lenske, Phys. Rev. C 26 (1982) 379.

[136] H. Lenske, S. Landowne, H. H. Wolter, T. Tamura and T. Udagawa, Phys. Lett. B 122 (1983) 333.

[137] H. Lenske, H. H. Wolter and A. Weigel, Nucl. Phys. A 690 (2001) 267.

[138] J. Cerny, 3rd International Conference on Nuclei Far from Stability, Cargese, France, 19 - 26 May 1976, pp.225-34 (CERN-1976-013).

[139] H. Matsubara and et al., CNS Annual Report (2011).

[140] H. Matsubara and et al., Few-Body System 54, 1433 (2013).

[141] G.R. Satchler, International Series Of Monographs On Physics, Vol. 68 (Clarendon, Oxford, UK, 1983).

[142] F. Cappuzzello *et al.*, J. Phys.: Conf. Ser. **630** (2015) 12018.

[143] C. Agodi *et al.*, Nuclear and Particle Physics Proceedings **265-266** (2015) 28-30.

[144] H. Lenske, private communication (unpublished).

[145] F. Hofmann and H. Lenske, Phys. Rev. C 57 (1998) 2281.

[146] M. A. Franey and W. G. Love, Phys. Rev. C 31 (1985) 488.

[147] D. J. Mercer et al., Phys. Rev. C 49 (1994) 3104.

[148] J. S. Lilley, B. R. Fulton, M. A. Nagarajan and I. J. Thompson, Phys. Rev. B 151 (1985) 181.

[149] B. Buck, A.P. Stamp and P.E. Hodgson, Phil. Mag., 8 (1963) 1805.

[150] B.W. Pointon et al., Phys. Rev. C 44 (1991) 2430.

[151] M. Sasano et al., Phys. Rev. C 85, 061301(R) (2012).

[152] D. E. Alburger, G. Wang and E. K. Warburton, Phys. Rev. C 35 (1987) 1479.

[153] M. Bhattacharya, C.D. Goodman, A. Garcia, Phys. Rev. C 80, 055501 (2009).

[154] NNDC Interactive Nuclear Chart; URL: https://www.nndc.bnl.gov/chart/

[155] Courtesy of MAGNEX experiment research team, within the NUMEN collaboration.